Inaugural dissertation

for

obtaining the doctoral degree

of the

Combined Faculty of Mathematics, Engineering and Natural Sciences

of the

Ruprecht - Karls - University

Heidelberg

Presented by

Catalina Rivera Krstulovic

Born in: Santiago, Chile

Oral-examination: 27.10.2023

Role of vascular Dnmt3a during adult homeostasis and disease-associated vascular re-activation

Referees:

Prof. Dr. Frank Lyko

Prof. Dr. Hellmut G. Augustin

Die vorliegende Arbeit wurde in der Abteilung „Vaskuläre Onkologie und Metastasierung“ am Deutschen Krebsforschungszentrum (DKFZ) in Heidelberg zwischen April 2019 und Juli 2023 durchgeführt.

“Las experiencias de hoy son los recuerdos del mañana” – Isabel Allende

Acknowledgments

This PhD was not the easiest journey, but it was certainly one of the experiences that have helped me grow the most, both as a person and as a professional. It was a journey full of ups and downs but what I have learned is invaluable! I'm very grateful to all the people that were part of this PhD and made it possible.

First, I would like to thank **Prof. Dr. Hellmut Augustin** for giving me the opportunity to come to work in his lab and on this exciting project. Thank you for your guidance and supervision during my PhD time, and for all scientific and non-scientific discussions.

I would like to express my gratitude to **Dr. Katharina Schlereth** for her mentorship and constant guidance during the first 3 years of my PhD. Thank you for the scientific and personal support, you were an important part of my formation as a scientist and I will take all the advice with me in my next journey.

I express my sincere gratitude to **Prof. Dr. Frank Lyko** for giving me the opportunity to accomplish my doctoral thesis at the Combined Faculty of Natural Sciences and Mathematics of the Ruperto Carola University of Heidelberg and the German Cancer Research Center. Thank you for being part of Thesis Advisory Committee together with **Prof. Dr. Gergana Dobreva** and for their advice and the constructive feedback over the past years. Additionally, I would like to thank **Prof. Dr. Ilse Hoffmann** and **Dr. Julieta Alfonso** for being part of my Defense Committee.

I am also thankful to the **CRC1366 graduate school** for the financial support and for providing a collaborative and exciting research environment. I would like to thank the "Helmholtz International Graduate School for Cancer Research" for giving me the opportunity to work in a highly international institution. And a big thank you to the DKFZ Flow Cytometry, Light Microscopy, Genomics and Proteomics, and Laboratory Animal Core Facilities for their assistance and technical support.

Special thanks to **Dimi**, **Robert** and **Paula** for the amazing time and their friendship! I wouldn't have survived this experience without you! Thanks for all the jokes, talks, dinners, trips, parties and picnics, the discussions and the experimental help during all these years. I really love you guys and I hope we keep in touch when we move to the next chapter of our lives ♡

I would also like to thank the **A190** people for their scientific input, experimental support and fun life discussions during lunch and parties. I really enjoyed your company! Mil gracias Denise, Stephi P., Stephi G, Guanxiong, Xiaowen, Ki, Michi, Ashik, Mahak, Miki, Shubhada, Divya, Ywen, Biblap, Anja G, Anja R, Donato, Eva G, Jingjing, Laura, Nico, Niklas, Till, Sandra, Petra, Monika, Clara, Eva B, Luisa, Alina, Maria, Carleen, Claudine. And especially **Moritz** who helped me with my thesis and **Benny** for all the experimental support!

No pueden faltar mis **Amikas**, que a pesar de la distancia nunca las sentí lejos. Me encanta como cada vez que nos vemos es como si el tiempo no hubiera pasado, las amo un montón y gracias por estar para mi aunque estemos repartidas por el mundo ♡!

Quiero agradecer a mi **Mamá** por todo el apoyo y el amor en este proceso. No sería la persona que soy hoy sin ti, gracias por cuidarme y ponerme como tu prioridad toda tú vida. Fuiste la mejor mamá y papá que podría haber tenido! Sé que el camino fue duro, pero quiero que sepas que estoy muy orgullosa de ser tu hija y que todo lo que soy hoy es gracias a ti ♡ Te amo un montón y gracias por tu apoyo incondicional en todas las decisiones que tomo, aunque impliquen irme al otro lado del mundo ♡

And finally I want to thank **Tim**, gracias por todo el apoyo y el amor que me has dado. Por soportar mis mañas, mi estrés, y por nunca dejar de amarme. No habría podido vivir esta experiencia sin ti ♡ gracias por empujarme a tomar la decisión de moverme y poder construir esta vida contigo. Eres una de las personas más lindas que he conocido y estoy muy feliz que el destino nos juntó y permitió que todo saliera perfecto ♡ Espero con ansias todas las aventuras que vamos a vivir. Ik hou van jou pollo rico ♡

Table of Contents

List of Figures

List of Tables

Summary

Vascular remodeling represents an adaptive mechanism to physiological alterations. However, when this mechanism is dysregulated, it results in pathological vascular re-activation. Pathological vascular re-activation is involved in tumor progression, cardiovascular diseases and chronic inflammatory conditions, and it may lead to impaired vascular function, formation of an aberrant vascular network and disease progression. Cancer is one of the leading causes of death worldwide. Similarly, obesity is a prominent risk factor for the development of cardiovascular diseases, which corresponds to a leading cause of mortality and morbidity worldwide as well. Since both pathological conditions are highly dependent on angiogenesis, the study of modulators of vascular re-activation and their particular role in tumor progression and obesity-derived cardiovascular impairment is crucial. During the last years, epigenetic modifications have emerged as critical regulators in the development and progression of various diseases including cancer, cardiovascular diseases, and neurological disorders. Consequently, epigenetic therapies have gone through clinical trials as potential treatments for cancer and other diseases, particularly those targeting DNA methylation.

Previous studies from our group identified Dnmt3a as an epigenetic modifier in angiogenic neonatal endothelial cells. In neonates, the loss of Dnmt3a led to impaired vascular growth, suggesting Dnmt3a as a candidate to target in order to interfere with angiogenesis. DNMT3A contributes to the establishment, maintenance and remodeling of the DNA methylation landscape, but its role in endothelial cell disease-associated vascular re-activation has not been addressed so far. Therefore, by using a conditional mutant mouse that lacks Dnmt3a specifically in the endothelium ($Dnmt3a^{iECKO}$), the present thesis was aimed at deciphering if the interference with Dnmt3a-dependent DNA methylation halts vascular re-activation during primary tumor development and obesity-induced inflammation, and if this interference would then impair vascular quiescence during health. The determination of the expression level of Dnmt3a in the disease-associated reactivated lung and heart endothelium revealed an induction of Dnmt3a expression after tumor growth and diet-induced obesity. Primary tumor experiments using the LLC tumor model in $Dnmt3a^{iECKO}$ mice revealed that Dnmt3a loss in the endothelium impairs tumor angiogenesis without affecting overall tumor development. In order to achieve obesity-induced inflammation, endothelial Dnmt3a deficient mice were fed a high fat diet for 8 weeks. The lack of Dnmt3a in the endothelium led to an alleviation of obesity-induced cardiac hypertrophy and a reduced vascular density. Moreover, increased cardiac fibrosis incidence and apoptosis, which impairs cardiac

relaxation, led to diastolic dysfunction in Dnmt3a^{iECKO} mice. In summary, the lack of endothelial Dnmt3a has a morphological and functional impact on the obese heart and Dnmt3a is required for obesity-induced cardiac hypertrophy. Lastly, I studied if the loss of Dnmt3a has an effect on the healthy quiescent endothelium. No major organ morphological changes in lung and liver were derived from the lack of Dnmt3a in the healthy endothelium. However, an enlarged heart was observed though there was no impact on cardiac function. A change in the expression of genes related to cell division in the heart, in addition to an up-regulation of aerocyte markers in the lung endothelium was observed after the loss of Dnmt3a in the homeostatic endothelium.

In conclusion, this study demonstrated that the activity of endothelial Dnmt3a plays an important role in angiogenesis during pathological vascular re-activation, yet the healthy quiescent endothelium remains unaffected.

Zusammenfassung

Der vaskuläre Umbauprozess stellt einen adaptiven Mechanismus dar, der für den Aufbau des Blutgefäßsystems verantwortlich ist. Die Dysfunktion dieses Mechanismus führt zu einer pathologischen Aktivierung der Blutgefäße. Die pathologische Aktivierung der Blutgefäße ist an der Tumorprogression, kardiovaskulären Erkrankungen und chronisch entzündlichen Zuständen beteiligt und kann zu einer Beeinträchtigung der Gefäßfunktion, der Bildung eines fehlerhaften Gefäßnetzwerks und dem Fortschreiten von Krankheiten führen. Krebs ist eine der führenden Todesursachen weltweit. Ebenso ist Fettleibigkeit ein bedeutender Risikofaktor für die Entwicklung von kardiovaskulären Erkrankungen, die weltweit eine führende Ursache für Sterblichkeit und Morbidität darstellen. Da beide pathologische Zustände stark von Angiogenese abhängig sind, sind die Untersuchung von Modulatoren der Gefäßreaktivierung und ihre spezielle Rolle bei der Tumorprogression und der durch Fettleibigkeit verursachten Beeinträchtigung des Herz-Kreislauf-Systems entscheidend. In den letzten Jahren wurden epigenetische Modifikationen als wichtige Regulatoren in der Entwicklung und Progression verschiedener Krankheiten, einschließlich Krebs, kardiovaskulärer Erkrankungen und neurologischer Störungen, entdeckt. Infolgedessen wurden epigenetische Therapien in klinischen Studien als potenzielle Behandlungen für Krebs und andere Krankheiten, insbesondere solche, die die DNA-Methylierung beeinflussen, untersucht. Da epigenetische Veränderungen dynamisch sind, wächst das Interesse, Wirkstoffe zu identifizieren, die das Epigenom beeinflussen, um Zellen umzuprogrammieren und gesunde Genexpressionsmuster wiederherzustellen. Unsere Gruppe hat vor kurzem Dnmt3a als einen epigenetischen Modulator in angiogenen neonatalen Endothelzellen identifiziert. Bei Neugeborenen führte der Verlust von Dnmt3a zu einer Beeinträchtigung des Gefäßwachstums. Insgesamt legen diese Daten nahe, dass Dnmt3a ein Kandidat ist der die Gefäßaktivierung reguliert. DNMT3A trägt zur Etablierung, Aufrechterhaltung und der dynamischen Umgestaltung der DNA-Methylierungslandschaft bei, aber seine Rolle in der durch Gefäßerkrankungen verursachten Aktivierung der Endothelzellen wurde bisher noch nicht untersucht. Die vorliegende Arbeit soll mithilfe von konditional mutierten Mäusen (Dnmt3a^{iECKO}), untersuchen, welchen Einfluss Dnmt3a auf die pathologische Gefäßaktivierung in Primärtumoren und in durch Fettleibigkeit verursachter systemischer Entzündung hat. Außerdem soll untersucht werden, ob der Eingriff in Dnmt3a-bedingte Methylierungsmuster den Ruhezustand der Gefäße während der Gesundheit beeinträchtigt. Die Dnmt3a Expression wurde im reaktivierten Herz- und Lungenendothel nach der Injektion von Tumorzellen und durch diätbedingte Fettleibigkeit induziert. Experimente im Primärtumor unter Verwendung des LLC-Tumor-Modells bei Dnmt3aiECKO-Mäusen zeigten, dass

der Verlust von Dnmt3a im Endothel die Tumorangiogenese beeinträchtigt, ohne die allgemeine Tumorentwicklung zu beeinflussen. Um eine durch Fettleibigkeit verursachte systemische Entzündung hervorzurufen, wurden Dnmt3a-defiziente Mäuse im Endothel 8 Wochen lang fettreiches Futter verabreicht. Der Mangel an Dnmt3a im Endothel führte zu einer Linderung der durch Fettleibigkeit verursachten Herzhypertrophie und einer verringerten Gefäßdichte. Darüber hinaus führten erhöhte kardiale Fibrose und Apoptose, die die Herzentspannung beeinträchtigen, zu einer diastolischen Dysfunktion. Zusammenfassend hat das Fehlen von endothelialem Dnmt3a eine morphologische und funktionelle Auswirkung auf das fettleibige Herz und ist für die durch Fettleibigkeit verursachte Herzhypertrophie verantwortlich. Schließlich haben wir untersucht, ob der Verlust von Dnmt3a Auswirkungen auf das gesunde, ruhende Endothel hat. Durch den Mangel an Dnmt3a im gesunden Endothel traten keine größeren organmorphologischen Veränderungen in Lunge und Leber auf. Es wurde jedoch ein vergrößertes Herz beobachtet, das allerdings keine Auswirkungen auf die Herzfunktion hatte. Es wurde aber eine Veränderung in der Expression von Genen, die mit Zellteilung im Herzen zusammenhängen, sowie eine Hochregulierung von Aerozyten-Markern im homöostatischen Lungen-Endothel nach dem Verlust von Dnmt3a beobachtet.

Zusammenfassend hat diese Studie gezeigt, dass die Aktivität des endothelialen Dnmt3a eine wichtige Rolle bei der Angiogenese während der pathologischen vaskulären Reaktivierung spielt, das gesunde, ruhende Endothel jedoch unbeeinflusst bleibt.

1. Introduction

1.1 The vascular system

The vascular system is a complex network of blood vessels that transport oxygen and nutrients throughout the body[1]. Endothelial cells (ECs), pericytes, smooth muscle cells (SMC) and fibroblasts are the major cell types that comprise blood vessels[2]. ECs form the inner lining of blood vessels, and through regulation of blood flow and blood pressure, are responsible for the maintenance of vascular homeostasis[1-5]. Blood vessels can be generated via two processes: vasculogenesis and angiogenesis. Vasculogenesis corresponds to the process of de novo blood vessel formation that happens during embryogenesis, and includes the differentiation and aggregation of mesodermal cells into hemangioblasts[6]. On the other hand, angiogenesis corresponds to the process of the expansion of an existing vascular network, meaning the formation of new blood vessels from pre-existing ECs[4,5]. During angiogenesis, ECs are in an active and proliferative state. However, when reaching vascular homeostasis these cells enter a quiescent and non-proliferative state, that can be switched back to an active state by pro-angiogenic stimuli such as inflammatory signals and hypoxia[5,3,7].

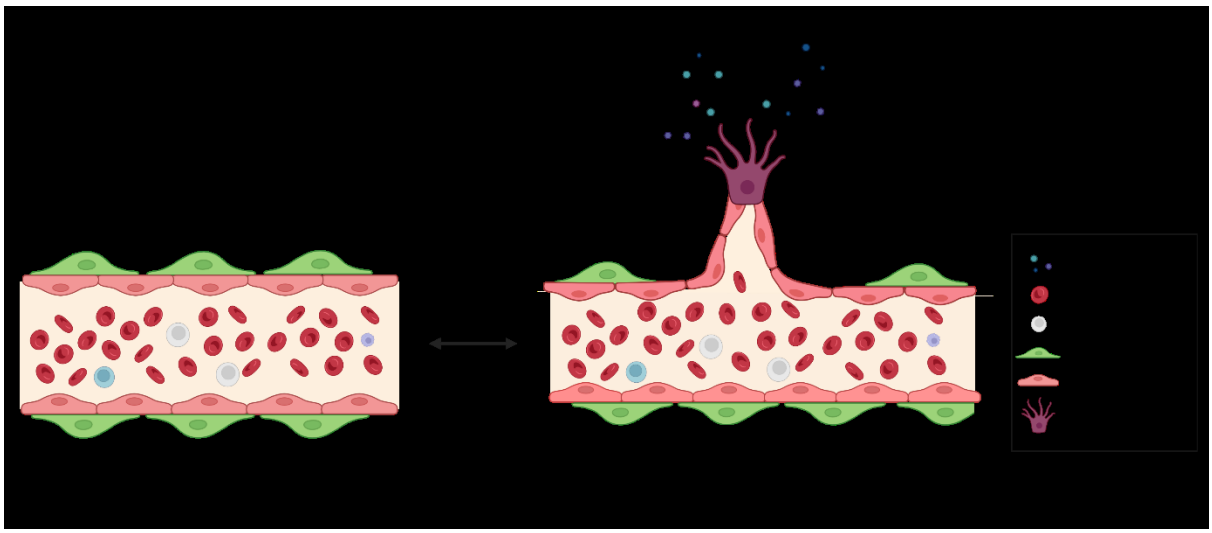

Figure 1: Quiescent and activated endothelium

Under homeostasis, endothelial cells are in a quiescent and non-proliferative state. When exposed to pro-angiogenic growth factors, endothelial cells can transition into an angiogenic state, becoming active and proliferative to form new blood vessels[4].

1.1.1 Endothelial quiescence

Quiescence is a state of cellular dormancy. In this state, cells are in a non-proliferative state but they can resume the cell cycle when stimulated. This protective state helps to prevent cellular

damage[8]. In the context of the vascular system, endothelial quiescence is critical for maintaining vascular homeostasis. This state protects the cells from molecular damage, exhaustion and senescence. Quiescent ECs exhibit low levels of oxidative stress, vascular leakage and expression of leukocyte adhesion molecules[9]. Endothelial quiescence is a critical aspect of vascular homeostasis, and its disruption can lead to endothelial re-activation and disease-associated angiogenesis.

In order to maintain a non-proliferative state, the regulation of different growth factors and cytokines is necessary. One of the crucial pathways in healthy quiescent endothelium is the transforming growth factor-beta (TGFβ) pathway. Activation of TGFβ signaling promotes an inflammatory phenotype in EC, in addition to the loss of normal endothelial cell fate via endothelial to mesenchymal transition (EndMT), leading to the development of different vascular diseases, such as atherosclerosis[10]. The vascular endothelial growth factor (VEGF) pathway is one of the most-studied pro-angiogenic growth factors. It has been proven that constitutive endothelial deletion of VEGFA in mice results in multi-organ hemorrhage, myocardial infraction and lethality due to endothelial apoptosis[11], demonstrating its importance in the maintenance of a healthy endothelium. Other extracellular factors that have been shown to promote endothelial quiescence include the angiopoietin/Tie2 pathway. The Ang1-Tie2 signaling axis maintains vascular quiescence, yet the loss of Tie2 signaling due to the binding of Ang2, an antagonist of Ang1, destabilizes blood vessels facilitating sprouting angiogenesis[12,13]. Ang2 is expressed mainly by EC and mediates the response of the endothelium to inflammatory stimuli[9,14,15]. Conditions such as oxidative stress, inflammation, and disturbed blood flow can promote endothelial re-activation and vascular remodeling. Endothelial activation is characterized by increased expression of adhesion molecules and pro-inflammatory cytokines, which promote leukocyte adhesion and infiltration into the vascular wall[7,9].

1.1.2 Vascular remodeling

Vascular remodeling is a complex process that plays a critical role in the maintenance of vascular homeostasis and adaptation to physiological changes. This process involves structural and functional changes in the blood vessels and is necessary for the growth and development of organs, and the regulation of intravascular pressure[16]. Vascular remodeling involves cell death, proliferation and migration, and matrix destruction, synthesis and reorganization[17]. Endothelial cell activation and angiogenesis are the first steps in vascular remodeling. This process is mediated by growth factors such as VEGF, fibroblast growth factor (FGF) and TGFβ[4,9-11]. Endothelial cell activation induces the expression of adhesion molecules such as intercellular adhesion molecule-1 (ICAM-1) and vascular cell adhesion molecule-1 (VCAM-1) which promote leukocyte recruitment and

inflammation, and further contribute to vascular remodeling. Inflammatory cells infiltrate the vessel wall and release pro-inflammatory cytokines and matrix metalloproteinases (MMPs), contributing to the degradation of the extracellular matrix, and promoting migration and proliferation[18].

Recent studies have highlighted the importance of endothelial-derived extracellular vesicles (EVs) in the regulation of vascular remodeling. Endothelial-derived EVs are released as a response to EC injury and activation. They contain bioactive molecules such as proteins, cytokines, microRNAs (miRNAs), and lipids to target cells[19]. Endothelial-derived EVs can modulate SMC function, angiogenesis and inflammation, modulating vascular remodeling[19-21].

Another key mechanism of vascular remodeling is SMC remodeling, which involves changes in proliferation, migration and differentiation. This process is regulated by growth factors, cytokines and extracellular matrix (ECM) proteins, such as platelet-derived growth factor (PDGF)[22], TGFβ and collagen[23]. SMC remodeling can result in the thickening or thinning of the arterial wall, which is essential for maintaining the regulation of vascular tone and blood pressure[17,18,22,23].

Vascular remodeling is an adaptive response to physiological alterations, however, it can become abnormal and pathological leading to impaired vascular function and dysregulation of apoptosis and proliferation of ECs. Endothelial dysfunction is associated with the development of cardiovascular diseases and cancer, two of the leading causes of death worldwide[24,25], among other diseases[16,26]. Understanding the molecular and cellular mechanisms underlying endothelial pathological re-activation is crucial for developing effective therapeutic strategies against these life-threatening diseases. Numerous studies have shed light on the regulation of these mechanisms, but further research is needed to develop novel interventions that can effectively modulate pathological vascular remodeling[27,28].

1.1.2.1 Tumor vascularization

Tumor angiogenesis plays a crucial role in tumor growth and metastasis since new blood vessels are needed to provide oxygen and nutrients to the growing tumor[29]. Over the years, several studies have focused on understanding the molecular and cellular mechanisms involved in tumor vascularization, aiming to identify potential therapeutic targets for cancer treatment[26,30,31].

Tumor vascularization is driven by an angiogenic switch. This process is initiated by tumor cells that start to express pro-angiogenic factors such as VEGF, FGF and PDGF, among others[32]. The rapid proliferation of tumor cells results in a hypoxic core of the primary tumor. In order to relieve hypoxia, cancer cells start expressing high levels of VEGF to attract EC and promote angiogenesis[26,33]. Hypoxia-inducible factor-1 alpha (HIF-1α) has been identified as a transcriptional activator of VEGF, along with a positive correlation between HIF-1α levels and tumor

progression[30,34]. The tumor microenvironment plays a critical role in regulating tumor vascularization. As part of the tumor microenvironment, tumor-associated macrophages (TAMs) secrete various pro-angiogenic factors, including VEGF[35]. Cancer-associated fibroblasts (CAFs), on the other hand, produce extracellular matrix components and growth factors that support the formation of new blood vessels[36]. However, the results of these therapies in clinics have not been exceedingly successful therefore new methods to stop tumor angiogenesis continue to be studied[26,37].

1.1.2.2 Cardiovascular diseases

Cardiovascular diseases (CVDs) comprise a wide range of conditions affecting the heart and blood vessels, including coronary artery disease, myocardial infarction, heart failure, and atherosclerosis. According to the World Health Organization, CVDs are one of the leading causes of mortality and morbidity worldwide[24,38]. Obesity, smoking, physical inactivity, hypertension and diabetes, among others are part of the main risk factors for the development of CVDs[39,40]. The inflammatory response that is activated due to the prevalent exposure to the previously mentioned cardiovascular risk factors, drives the re-activation of ECs[7,40]. Due to this prolonged exposure to inflammation, the endothelium can lose integrity and become dysfunctional, resulting in an aberrant vascular structure[41,42]. Endothelial dysfunction leads to reduced nitric oxide (NO) bioavailability, increased oxidative stress and inflammation, all of which contribute to the progression of CVDs[43,44].

It has been described that the activation of immune cells, such as macrophages and T cells, is involved in the progression of different cardiovascular diseases[45-47]. Immune cell-derived cytokines can promote the progression of atherosclerosis and myocardial infarction, affecting cellular proliferation and promoting extracellular matrix synthesis, resulting in fibrosis and subsequent organ dysfunction[48]. The development of cardiac fibrosis occurs due to the excessive deposition of ECM, primarily driven by activated fibroblasts which are the main cellular source of ECM proteins. However, immune cells, EC and cardiomyocytes (CM) can secrete different growth factors and induce fibroblast activation[49]. While cardiac fibrosis is generally associated with poor prognosis in most CVDs, due to increased myocardial stiffness, it can also serve as a reparative mechanism. In the adult heart, healing takes place through the formation of a collagen-based scar that replaces dead CM. Although scar tissue lacks contractile ability, it plays a crucial role in preserving the heart's structural integrity[49]. The risk of developing CVDs is influenced by both genetic and epigenetic factors. Through genome-wide association studies, a large number of genetic variations associated with CVDs have been discovered[50,51]. These variations play a role in various biological processes, including lipid metabolism, inflammation, and endothelial function. Additionally, epigenetic

changes, such as DNA methylation and histone acetylation, have been identified as factors involved in the control of gene expression and the development of CVDs[52].

Therefore, understanding the complex molecular mechanisms underlying the correlation between endothelial dysfunction and the progress of CVDs is crucial for developing effective strategies for prevention, diagnosis, and treatment.

1.1.3 Endothelial response to inflammatory signals

Another function of the endothelium corresponds to the regulation of the infiltration of immune cells during the inflammatory process[18,53]. Activation of the endothelium in response to inflammatory stimuli is initiated by the stimulation of pattern recognition receptors, such as Toll-like receptors (TLRs). TLR stimulation leads to the upregulation of adhesion molecules, such as ICAM-1, VCAM-1 and P-selectin facilitating immune cell trafficking[54,55] (Fig 2). The pro-inflammatory cytokines and chemokines secreted by activated ECs are key mediators of leukocyte recruitment. These cytokines and chemokines include interleukin-6 (IL-6), interleukin-8 (IL-8), monocyte chemoattractant protein-1 (MCP-1), chemokine ligand 2 (CCL2), colony-stimulating factor 1 (CSF1) and type I interferon[56-58].

During inflammatory responses, endothelial cells play a crucial role in regulating vascular permeability. Inflammatory stimuli trigger the upregulation of VEGF and Ang2, which modulate the endothelial barrier function and in consequence leukocyte transmigration. Moreover, the formation of endothelial gaps and the reorganization of junctional proteins, such as vascular endothelial-cadherin (VE-cadherin) and occludin, are critical events in the disruption of the endothelial barrier[9,59,60].

To prevent excessive inflammation and tissue damage, the endothelial response to inflammatory stimuli is tightly regulated through several negative feedback mechanisms. Upon exposure to such stimuli, endothelial cells secrete anti-inflammatory cytokines, including interleukin-10 (IL-10) and TGF-β. These cytokines inhibit the expression of adhesion molecules, suppress the production of pro-inflammatory cytokines, and promote the differentiation of regulatory T cells, thereby facilitating the rapid return of ECs to a homeostatic state[61,62].

The response of ECs to inflammatory stimuli is not only influenced by intrinsic cellular processes, but also by the surrounding cellular and extracellular matrix components. For example, interactions between ECs and pericytes play a role in regulating vascular stability and permeability. Similarly, fibroblasts contribute to the control of endothelial activation and leukocyte recruitment during inflammation. ECs can produce pro-fibrotic mediators that stimulate the growth, differentiation and collagen production of fibroblasts. Furthermore, ECs can undergo EndMT and differentiate into

fibroblast-like cells that secret collagen. The accumulation of extracellular matrix or fibrosis can ultimately result in organ failure[63,64].

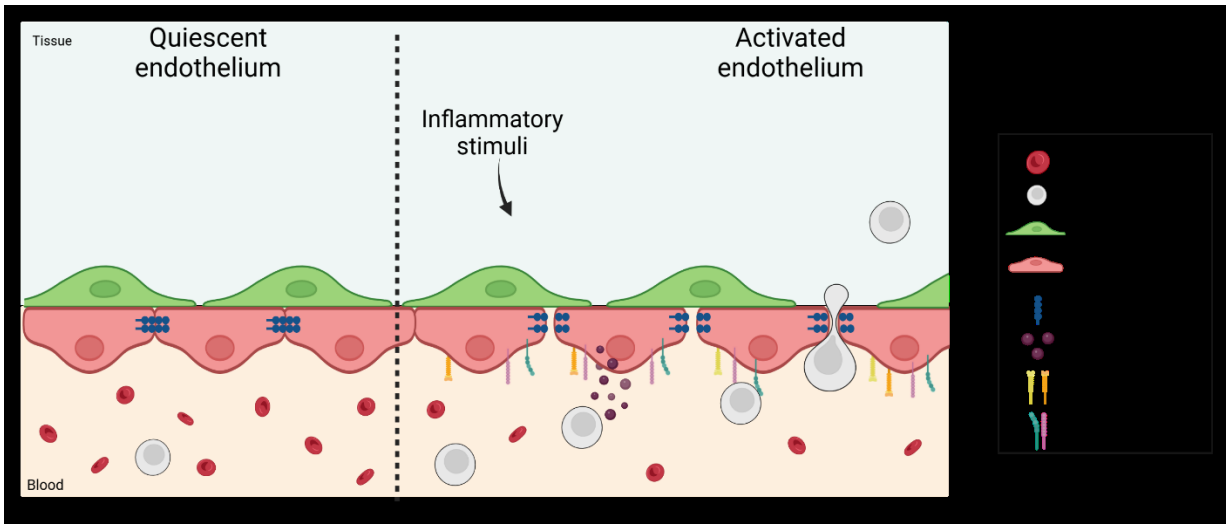

Figure 2: Endothelial response to inflammatory signals

Upon inflammatory stimuli the quiescent endothelium become activated. Upregulation of adhesion molecules, such as ICAM-1, VCAM-1, E-selectin and P-selectin, and reorganization of junctional proteins to form endothelial gaps and increase vascular permeability takes place. Subsequently, EC secrete pro-inflammatory cytokines, triggering the recruitment and activation of immune cells, leading to immune infiltration into the damage tissue[58,60].

1.1.4 Obesity as an inflammatory setting

Obesity is associated with the development of different disorders including CVD, type 2 diabetes, metabolic syndrome and hypertension. The excess of nutrients in the organism generates a state of chronic inflammation due to the release of inflammatory mediators by the adipose tissue, liver, pancreas and skeletal muscle[65].

The adipose tissue is formed by ECs, immune cells and adipocytes. During obesity, it undergoes dynamic remodeling, which generates adipocyte hypertrophy and hyperplasia[66]. Due to adipose tissue remodeling, fibrosis, hypoxia and altered extracellular matrix composition can occur[65]. Adipocytes secrete cytokines and adipokines, such as leptin and adiponectin, IL-6 and tumor necrosis factor alpha (TNFα), which can regulate the inflammatory response and endothelial remodeling[65,67,68]. These cytokines secreted by the adipocytes can affect multiple organs, including the liver and the heart. During obesity, cardiac function and structure are altered resulting in cardiac hypertrophy, increased cardiac wall thickness, myocardial lipid accumulation, atrial enlargement, impaired myocardial contractility due to fibrosis, and cardiac dysfunction[69,70].

It has been described that during obesity there is a dysregulation of adipokine production, with an increased level of leptin, a pro-inflammatory adipokine, and a reduction of adiponectin, an anti-inflammatory adipokine[67,68,71,72]. The recruitment, infiltration and activation of immune cells in the adipose tissue due to the secretion of inflammatory cytokines by hypertrophic adipocytes leads to an increased inflammatory response in obesity[68,73]. Macrophages and T cells are part of the immune cells recruited and activated during obesity-induced inflammation. Adipose tissue macrophages upon free fatty acid exposure are polarized into a pro-inflammatory M1 phenotype, and secrete pro-inflammatory cytokines such as TNFα and IL-6, and subsequently disruption of insulin signaling[73-75]. Besides adipose tissue, the liver plays a role in obesity-associated inflammation. The infiltration of immune cells into the liver and the subsequent release of pro-inflammatory cytokines are key features of non-alcoholic fatty liver disease, which is a common comorbidity of obesity[76].

The increase in fat intake promotes vascular remodeling through inflammation, endothelial dysfunction, dysregulated lipid metabolism and altered angiogenesis. Increased fat intake leads to the accumulation of free fatty acids (FFA) in the blood vessels due to dysregulated lipid metabolism. FFA can trigger inflammation, oxidative stress and apoptosis in the endothelium promoting endothelial dysfunction[67,77]. Obesity disrupts endothelial NO signaling, reducing NO bioavailability, increasing oxidative stress and impairing endothelium-dependent vasodilation. This promotes vasoconstriction and contributes to the remodeling of the vessel wall[78,79]. Furthermore, an increase in fat intake has been shown to dysregulate the expression of angiogenic factors, such as VEGF and angiopoietins, in ECs contributing to vascular remodeling[80].

1.2 Epigenetic remodeling

Epigenetic remodeling corresponds to the dynamic modifications of DNA and histones that regulate gene expression without affecting the underlying DNA sequence (Fig. 3). These modifications influence chromatin structure and accessibility for the transcriptional machinery. Epigenetic remodeling plays a key role in development, cellular differentiation and disease development[81].

DNA methylation is one of the principal epigenetic modifications that involves the addition of a methyl group by DNA methyltransferases (DNMT) commonly to the C5' position of cytosine residues within the context of a CpG dinucleotide to form 5-methylcytosine (5-mC). This 5-mC can be oxidized by TET proteins and form 5-Hydroxymethylcytosine (5-HmC) [82]. DNA methylation can be reversed through different processes. There are two frequently occurring ones which are passive and active DNA demethylation. Passive DNA demethylation occurs with the absence of DNA methylation during successive replication rounds of newly synthesized DNA strands. Active DNA demethylation, on the other hand, takes place through the oxidation of 5-mC by TET proteins,

followed by its removal through excision mechanisms or replication-dependent dilution, resulting in the loss of methylation[83].

Epigenetic remodeling is not only involved in normal development but also contributes to the progression of various diseases. In the context of cancer, global hypomethylation, along with localized hypermethylation of specific gene promoters are frequently observed[81,84]. These epigenetic alterations contribute to the silencing of tumor suppressor genes and the activation of oncogenes, thereby driving the development and progression of tumors. Understanding the mechanisms underlying epigenetic remodeling has significant implications for therapeutic interventions, as epigenetic modifications are reversible and can be targeted pharmacologically[84].

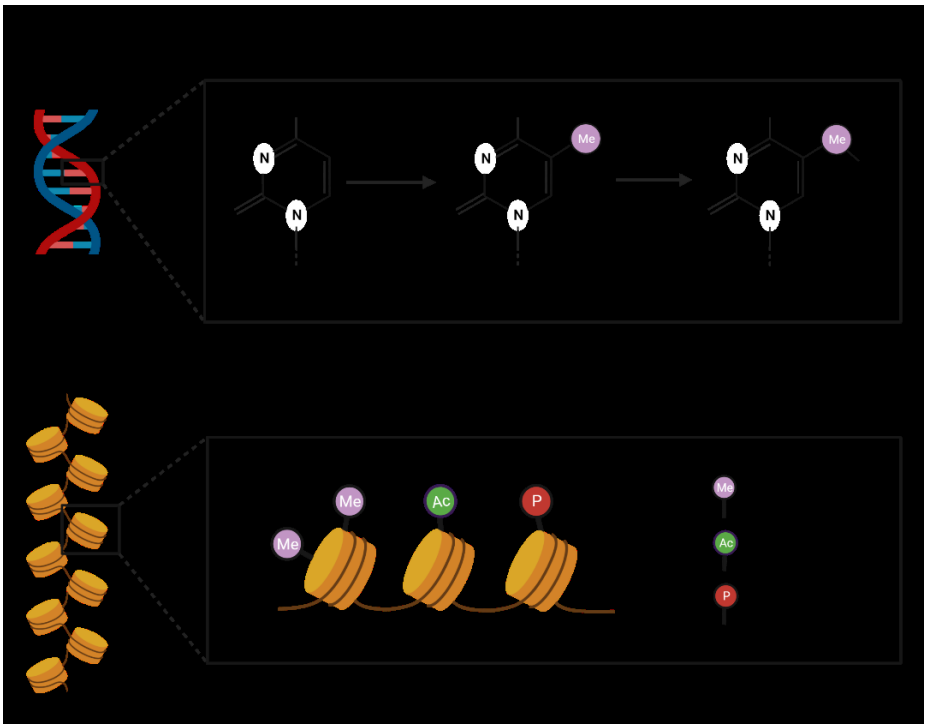

Figure 3: Epigenetic remodeling

Epigenetic remodeling mechanisms include DNA methylation and Histone modifications. DNA methylation corresponds to the addition of a methyl group to the C5' position of cytosine to form 5-mC. This can be transformed in 5-HmC by TET proteins. Histone modifications include methylation, acetylation and phosphorylation. These modifications can alter chromatin structure, regulating gene expression[81,83]. Definitions of acronyms can be found under section 7.

1.2.1 Epigenetics and vasculature

Epigenetic modifications play a fundamental role in the development, maintenance, and function of blood vessels. The dynamic interplay between DNA methylation, histone modifications and non-

coding RNAs is an important part of the regulatory mechanism for endothelial function and angiogenesis[85].

DNA methylation, catalyzed by DNA methyltransferases, is a well-studied epigenetic modification that influences ECs function. Aberrant DNA methylation can lead to altered expression of genes associated with vascular activity and angiogenesis. For instance, DNA hypermethylation of the promoter of endothelial nitric oxide synthase (eNOS) results in reduced eNOS expression and impaired NO production, leading to endothelial dysfunction[86,87]. Additionally, promoter hypermethylation of anti-angiogenic genes such as thrombospondin-1 (THBS1) and tissue inhibitor of metalloproteinase-3 (TIMP3), and hypomethylation of pro-angiogenic genes, such as VEGF, can regulate their expression, promoting angiogenesis[88-90].

Dysregulation of histone modifiers, such as acetylases and methylases, have been implicated in vascular diseases like atherosclerosis and hypertension[91]. These modifications play a crucial role in altering the chromatin structure, influencing gene transcription[92]. It has been shown that increased histone deacetylase activity and consequent reduced histone acetylation is associated with endothelial dysfunction, repression of pro-angiogenic genes and vascular inflammation[93]. On the other hand, the demethylation of lysine 27 on histone H3 (H3K27me3) facilitates the expression of pro-angiogenic genes[94].

Emerging evidence suggests that environmental factors can influence vascular epigenetic modifications. Diet, physical activity, stress, and exposure to toxins or pollutants can modulate the epigenome of endothelial cells and affect cardiovascular health[95]. A study from our group identified that 10% of the chromatin-modifying enzymes were differentially expressed during the acquisition of vascular quiescence in the lung compared to the postnatal development state. The majority of these differentially expressed chromatin-modifying enzymes were repressed in lung EC isolated from adult mice, including Dnmt3a. This study suggests that the DNA methylation patterns in EC are more dynamic during postnatal development compared to quiescence[96].

1.2.2 Epigenetics and disease

In recent years, there has been a growing recognition of the significant role that epigenetic modifications play in the development and progression of various diseases including cancer, CVDs and neurological disorders[84,97-99]. The interplay between DNA methylation, histone modifications, and non-coding RNAs orchestrates complex gene regulatory networks that can be dysregulated in pathological conditions[99].

Inflammatory stimuli can induce epigenetic modifications, leading to altered gene expression patterns and contributing to the development and progression of inflammatory diseases[99]. The

dynamic changes in DNA methylation patterns, histone modifications and non-coding RNA expression play a key role in modulating the immune response and shaping the pathogenesis of inflammation-related disorders[100]. For instance, the DNA methylation status of TNFα has an impact on the development of heart and liver failure[101-103]. The hypomethylation of the Toll-like receptor 2 (TLR2) promoter is correlated with an increased pro-inflammatory response to bacterial peptidoglycan[104]. Similarly, the transcription of pro- and anti-inflammatory cytokines is regulated by histone deacetylases via the recruitment of co-repressor complexes and transcription factors[105]. Such as the recruitment of NF-κB at the promoter region of several cytokines after inflammatory stimuli due to the acetylation of histone H3[106].

Epigenetic modifications have been observed in numerous types of cancers. These aberrant epigenetic patterns are responsible for mutational events and for the silencing of tumor suppressor genes, disrupting the normal function of cell proliferation and leading to full malignant status. It has been demonstrated that aberrant DNA methylation patterns in genes involved in cell proliferation, such as CDKN2A or p16[107,108], estrogen receptor[109,110] and MLH1[111,112], lead to the progression of cancer. DNA methylases can also interact with other epigenetic modifiers to regulate gene expression in cancer cells. For instance, DNMTs have been found to physically interact with histone deacetylases to promote gene silencing in lung cancer[113,114]. This crosstalk between DNA methylation and histone modifications highlights the intricate interplay of epigenetic mechanisms in cancer.

Regarding CVDs, epigenetic remodeling has emerged as one of the mechanisms involved in disease progression. For example, global DNA hypomethylation has been associated with atherosclerosis, hypertension and obesity[98,115], while site-specific hypermethylation has been linked to cardiac hypertrophy and heart failure[98,116]. Furthermore, epigenetic alterations in CVDs are not only influenced by genetic factors but also by environmental and lifestyle factors. The exposure to risk factors such as smoking, diet, and pollution have the potential to induce epigenetic modifications that contribute to the development and progression of cardiovascular disease[117].

1.2.3 DNMT3A

DNMT3A is a de novo DNA methyltransferase involved in the establishment and maintenance of DNA methylation patterns. This enzyme is highly expressed in early mammalian embryos, yet the expression is reduced over the course of cell differentiation[113,118]. DNMT3A comprises several functional domains, including a catalytic domain responsible for the DNA methylation activity and several regulatory domains involved in protein-protein interactions and targeting. Through its

catalytic domain, DNMT3A recognizes unmethylated CpG dinucleotides and transfers a methyl group from S-adenosylmethionine to the cytosine residue, resulting in DNA methylation[119-121].

DNMT3A has been implicated in various biological and pathological processes, particularly in the context of hematopoiesis and tumorigenesis. In hematopoietic stem cells (HSCs), DNMT3A plays a crucial role in regulating lineage specification and differentiation. Studies have shown that loss of DNMT3A function in HSCs leads to impaired differentiation and an increased risk of myeloid malignancies[122,123]. In the context of cancer, DNMT3A mutations have been frequently observed in acute myeloid leukemia (AML) and myelodysplastic syndromes (MDS). These mutations often result in the production of a truncated DNMT3A protein lacking the catalytic domain, leading to disrupted DNA methylation patterns and altered gene expression. The presence of DNMT3A mutations is associated with poor prognosis and disease progression[122,124,125]. In addition, DNMT3A mutations have been detected in solid tumors such as colorectal cancer, glioblastoma and gastric cancer. These mutations may contribute to tumorigenesis by dysregulating DNA methylation patterns and affecting the expression of genes involved in cell proliferation, DNA repair, and apoptosis[126-128]. However, Dnmt3a plays a complex role in cancer due to its function in both tumor suppressor and oncogenic pathways[113].

Understanding the molecular mechanisms underlying DNMT3A function is crucial for developing targeted therapeutic approaches. Several studies have focused on unraveling the complex regulation of DNMT3A, including its interaction with other epigenetic regulators and the identification of specific target genes[113,129-131]. Targeting DNMT3A mutations and aberrant DNA methylation patterns holds promise for personalized therapeutic interventions in cancer and other diseases.

1.3 Cardiac structures in health and disease

1.3.1 Cardiac morphology

The heart is the organ responsible for pumping blood throughout the body, ensuring the delivery of oxygen and nutrients to tissues and organs. The structure of the heart consists of the cardiac wall, formed by the epicardium, the myocardium, the endocardium and the connective tissue, the atrioventricular and semilunar valves, and the internal cavity that contains the ventricles and atriums[132].

The epicardium is a thin layer of mesothelial cells, adipose and connective tissue. It is adjacent to the myocardium and during embryonic development contributes as a source of progenitor cells, becoming dormant after birth[133]. The myocardium corresponds to the layer of cardiac muscle cells

or cardiomyocytes, and is responsible for the contractile function of the heart. In health, the myocardium exhibits a well-organized arrangement of CM, allowing for efficient pumping action. Nevertheless, CM can undergo physiological hypertrophy in response to exercise or pregnancy, allowing the heart to adapt to increased demand[134].

Between the myocardium and the endocardium is the impulse-conductive system that ensures the coordinated electrical impulses that regulate the rhythmic contraction of CM[135]. The endocardium is composed of specialized ECs that form a physical barrier between the inner cardiac tissue and the circulation. In addition, they participate in cellular signaling[136].

Congenital and acquired structural abnormalities can influence cardiac function. For example, hypertension or prolonged exposure to high blood pressure causes myocardial hypertrophy, fibrosis, and impaired relaxation, leading to diastolic dysfunction and, eventually, heart failure[137].

Intercellular communication is essential for the coordinated function of the heart. The different cardiac cell types communicate through a network of signaling mechanisms allowing synchronized contraction, electrical signaling, tissue repair and maintenance of cardiac homeostasis. Dysregulation of this communication can contribute to cardiac dysfunction and the progress of pathological states[138].

CM can communicate with each other through coupling between adjacent cells or gap junctions, and paracrine signaling[138-140]. Gap junctions allow the propagation of electrical signals and coordination of cell contraction. Disruption of their function can lead to arrhythmias and impaired contractility[139]. In addition, CM can secrete growth factors, cytokines and extracellular vesicles that can act on neighboring cells in a paracrine or endocrine manner and regulate cardiac hypertrophy and fibrosis[138,140].

Fibroblasts in intercellular communication, is particularly important in cardiac remodeling and fibrosis. Fibroblasts can communicate with CM via direct cell-cell interactions and through the secretion of various soluble factors. These cells can produce extracellular matrix components, growth factors, and cytokines that influence CM function and tissue remodeling[141].

Importantly, ECs can communicate with CM through paracrine signaling, modulating myocardial function, immune cell recruitment and neovascularization in response to ischemic stimuli[4,138]. For example, ECs release NO with diffuses to adjacent CM and regulate their contractility and oxygen supply[142].

Lastly, intercellular communication in the heart also involves immune cells. Macrophages and lymphocytes release pro-inflammatory cytokines and chemokines in response to tissue injury, these molecules interact with CM and fibroblast, affecting cardiac remodeling and fibrosis. Dysregulated

immune cell-cardiac cell communication is associated with various cardiac pathologies, including myocarditis and heart failure[134,143].

1.3.2 Cardiac response to inflammation

The cardiac response to inflammation is a complex process involving the activation of immune cells, modulation of cardiomyocytes, activation and fibrotic transformation of fibroblasts, and endothelial cell dysfunction (Fig. 4). This process leads to the activation of signaling pathways that regulate inflammation and tissue repair. Macrophages are the primary immune cells involved in the early response to cardiac inflammation, they are recruited to the site of injury or infection and release pro-inflammatory cytokines contributing to tissue damage[69,143]. CM respond to inflammatory stimuli by upregulating the expression of various inflammatory mediators such as MCP-1 and IL-8, which recruit immune cells to the site of inflammation[144]. The activation of inflammatory signaling pathways, such as NF-κB and mitogen-activated protein kinases (MAPKs), further amplifies the inflammatory response in CM[144]. Upon exposure to inflammatory stimuli, fibroblasts become activated and undergo a phenotypic transition known as myofibroblast transformation. Activated fibroblasts secrete pro-inflammatory cytokines promoting inflammation, immune cell recruitment and fibrosis. Myofibroblasts can express paracrine factors that regulate angiogenesis as well, indicating a potential contribution to the control of revascularization in the damaged heart[145].

Inflammation can lead to cardiac remodeling, where CM become hypertrophic and a remodeling of the extracellular matrix occurs. CM hypertrophy is initially an adaptive response to increased workload, aiming to normalize wall stress and maintain cardiac output. However, sustained hypertrophic signaling can lead to maladaptive remodeling, characterized by CM elongation, disarray, and impaired contractility[134]. In addition, in response to inflammation, an imbalance between matrix MMPs and tissue inhibitors of metalloproteinases (TIMPs) can take place. This results in excessive matrix deposition and fibrosis, disrupting normal myocardial architecture, impairing contractility, and promoting arrhythmogenesis[49].

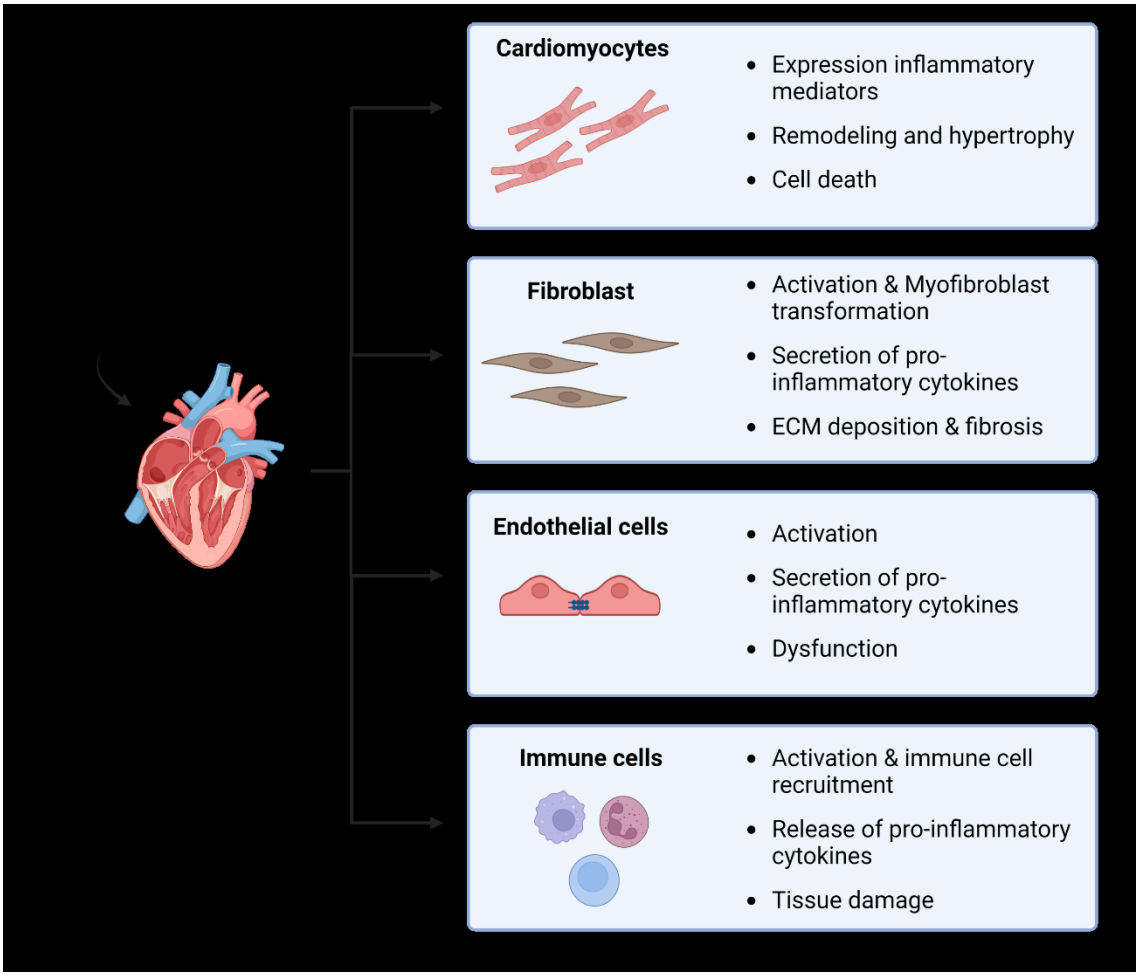

Figure 4: Cardiac response to inflammation

Upon inflammatory stimuli, cardiac cells initiate a complex response. This response leads to the activation of signaling pathways that modulate both inflammation and the restoration of tissue integrity[49,58,60,69,143-145]. Definitions of acronyms can be found under section 7.

2. Aims of the thesis

According to the World Health Organization, cancer is one of the leading causes of death worldwide and obesity corresponds to one of the leading risk factors for early death and development of CVDs[24,25,38]. Since both pathological conditions are highly dependent on angiogenesis, the study of modulators of vascular re-activation and their particular role in tumor progression and obesity-derived cardiovascular impairment is crucial. Previous studies from our group identified Dnmt3a as an epigenetic modifier in angiogenic neonatal endothelial cells. In neonates, the loss of Dnmt3a leads to impaired vascular growth. Based on these findings, I hypothesized that the modulation of Dnmt3a may disrupt pathological vascular re-activation as well. Therefore, this thesis aimed to further study if the interference with Dnmt3a-dependent DNA methylation halts vascular re-activation during disease, and whether this interference impairs vascular quiescence during health. In order to study vascular re-activation during disease, two relevant disease models were selected, primary tumor development and high fat diet-induced inflammation. Specifically, the aims of this thesis were to i) investigate the role of endothelial Dnmt3a in the context of tumor development and vascularization, ii) investigate the role of endothelial Dnmt3a in the context of high fat diet-induced chronic inflammation, and iii) identify the effect of endothelial Dnmt3a loss in the maintenance of vascular quiescence.

3. Results

3.1 Dnmt3a expression is induced in re-activated endothelium

To investigate the role of Dnmt3a in vascular re-activation during disease, an in vivo model for endothelial cell-specific deletion of Dnmt3a was established. For this purpose, Dnmt3a floxed mice were bred with the endothelial-specific Cre-line Cdhe-cre to generate an inducible EC-specific Dnmt3a knock-out mouse line ($Dnmt3a^{iECKO}$). Since Dnmt3a global knock-out mice die at maximum at 4 weeks of age[118], $Dnmt3a^{flox/flox}$ mice were obtained from RIKEN BioResource Center (No. RBRC03731). These mice express a floxed Exon 19 that encodes for the conserved PC motif of the catalytic domain of Dnmt3a[146]. In order to obtain a time-controlled endothelial-specific Dnmt3a deletion following tamoxifen administration, these $Dnmt3a^{flox/flox}$ mice were crossed with Tg(Cdh5-cre/ERT2)1Rha($Cdh5Cre^{ERT2}$) mice[147]. These transgenic mice express the Cre recombinase under the Cdh5-promoter and upon tamoxifen (TAM) induction the Cre recombinase performs a site-specific deletion of the DNA sequence between the two flanked *loxP* sites (floxed sites). $Dnmt3a^{flox/flox}$ mice were used as controls (from now on referred to as $Dnmt3a^{WT}$).

In order to validate the mouse model, endothelial deletion of Dnmt3a was induced with intraperitoneal (i.p) injections of TAM in 6-8 weeks old mice. After 21 days from the last injection of TAM, mice were sacrificed and EC from lung and heart were isolated via FACS (Fig. 5A). Viable $CD45^{-}LYVE1^{-}PDPN^{-}TER119^{-}CD31^{+}CD34^{+}$ EC were selected and isolated, and subsequently, the deletion efficiency of Dnmt3a was evaluated by qPCR. This analysis showed an 85-95% of deletion in both heart and lung EC from $Dnmt3a^{iECKO}$ mice (Fig. 5B-C). To determine the stability of the Dnmt3a deletion over time, $Dnmt3a^{iECKO}$ mice were sacrificed 1 year after the last injection of TAM (Fig. 6A) and qPCR analysis of Dnmt3a expression in sorted lung and heart EC was performed. I observed that the deletion efficiency was maintained at 85-95% one year after knockout induction (Fig. 6B-C), validating the stability of the mouse model.

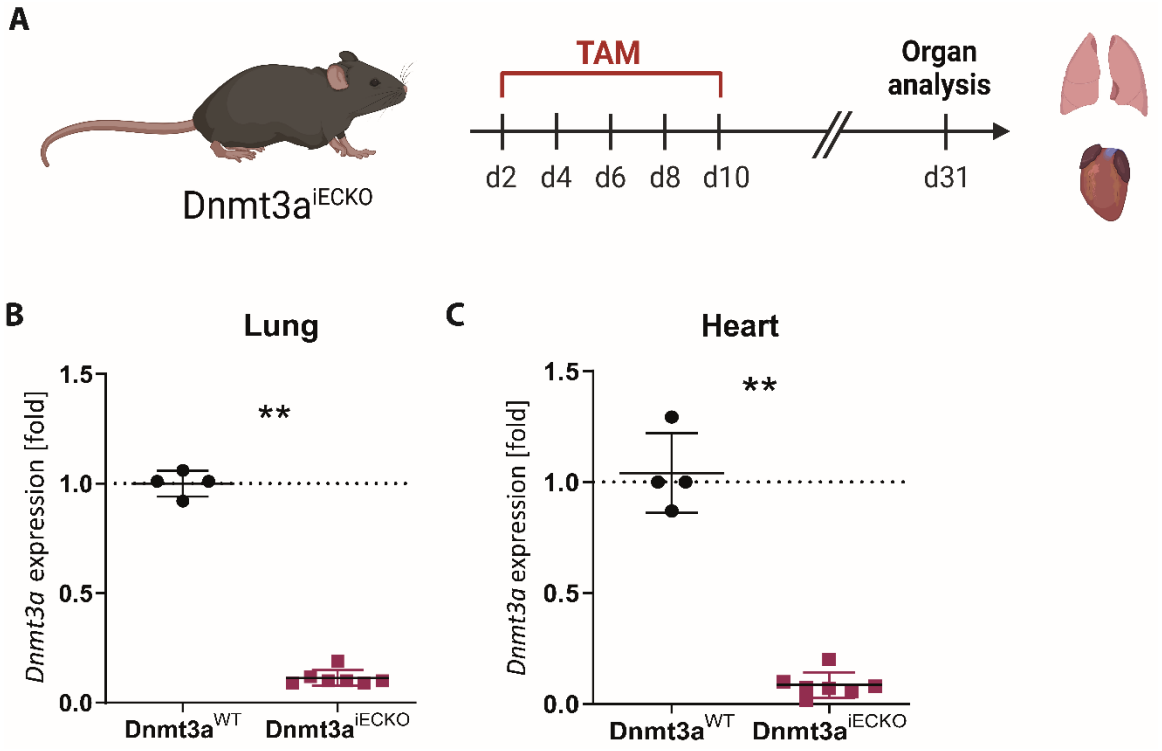

Figure 5: Validation of Dnmt3a^{iECKO} mouse model

(A) Schematic representation of experimental model. Dnmt3a^{iECKO} mice were treated with 5 doses of tamoxifen (TAM) and after 3 weeks of wash-out period the organ analysis was performed. **(B-C)** Dnmt3a expression in sorted lung **(B)** and heart **(C)** EC from Dnmt3a^{iECKO} and Dnmt3a^{WT} mice. Gene expression is normalized to *βActin* expression and to WT. Data are shown as mean±sd. (n=4-7; Mann-Whitney test).

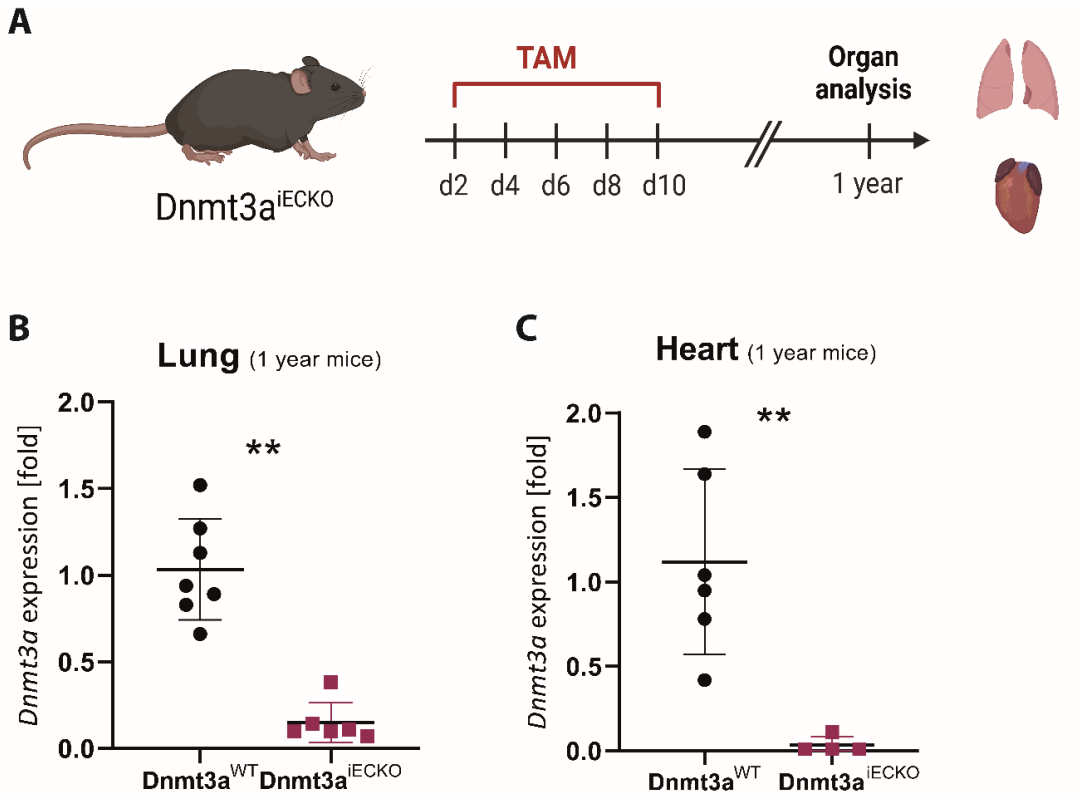

Figure 6: Stability of Dnmt3a^{iECKO} mouse model in time.

(A) Schematic representation of experimental model. Dnmt3a^{iECKO} mice were treated with 5 shots of tam and sacrificed 1 year after the last shot of tamoxifen. **(B-C)** *Dnmt3a* expression in sorted lung **(B)** and heart **(C)** EC from Dnmt3a^{iECKO} and Dnmt3a^{WT} 1 year after the last shot of tamoxifen. Gene expression is normalized to *βActin* expression and to WT. Data are shown as mean±sd.

Next, the effect of endothelial Dnmt3a deletion on DNA methylation was assessed. For this purpose, global DNA 5-mC and 5-HmC of isolated lung and heart ECs from Dnmt3a^{iECKO} and Dnmt3a^{WT} mice 21 days after TAM administration was measured via ELISA (Fig. 7A-B). No major effect due to the deletion of endothelial Dnmt3a in the percentage of 5-mC and 5-HmC DNA in heart and lung ECs was observed. As the measurement of the levels of global DNA methylation does not provide information regarding specific methylation changes in distinct regions of the genome, a DNA methylation array from isolated Dnmt3a^{iECKO} and Dnmt3a^{WT} lung EC was performed. This analysis yielded a comparable proportion of hyper- and hypo-methylated CpGs (Fig. 8A) and comparable distribution of methylation difference on single significantly differentiated methylated CpGs (Fig. 8B) when comparing Dnmt3a^{iECKO} vs Dnmt3a^{WT} mice. Further analysis identified 2756 differentially methylated CpGs between Dnmt3a^{iECKO} and Dnmt3a^{WT} lung EC. However, 90% of these differentially methylated CpGs presented less than a 10% difference in methylation. In addition, gene set enrichment analysis (GSEA) gene ontology analysis of the differentially hyper- and hypo-methylated genes between Dnmt3a^{iECKO} vs Dnmt3a^{WT} mice did not show significantly regulated gene

sets (data not shown). Altogether, these data suggests that there was no major methylation changes in EC due to Dnmt3a loss.

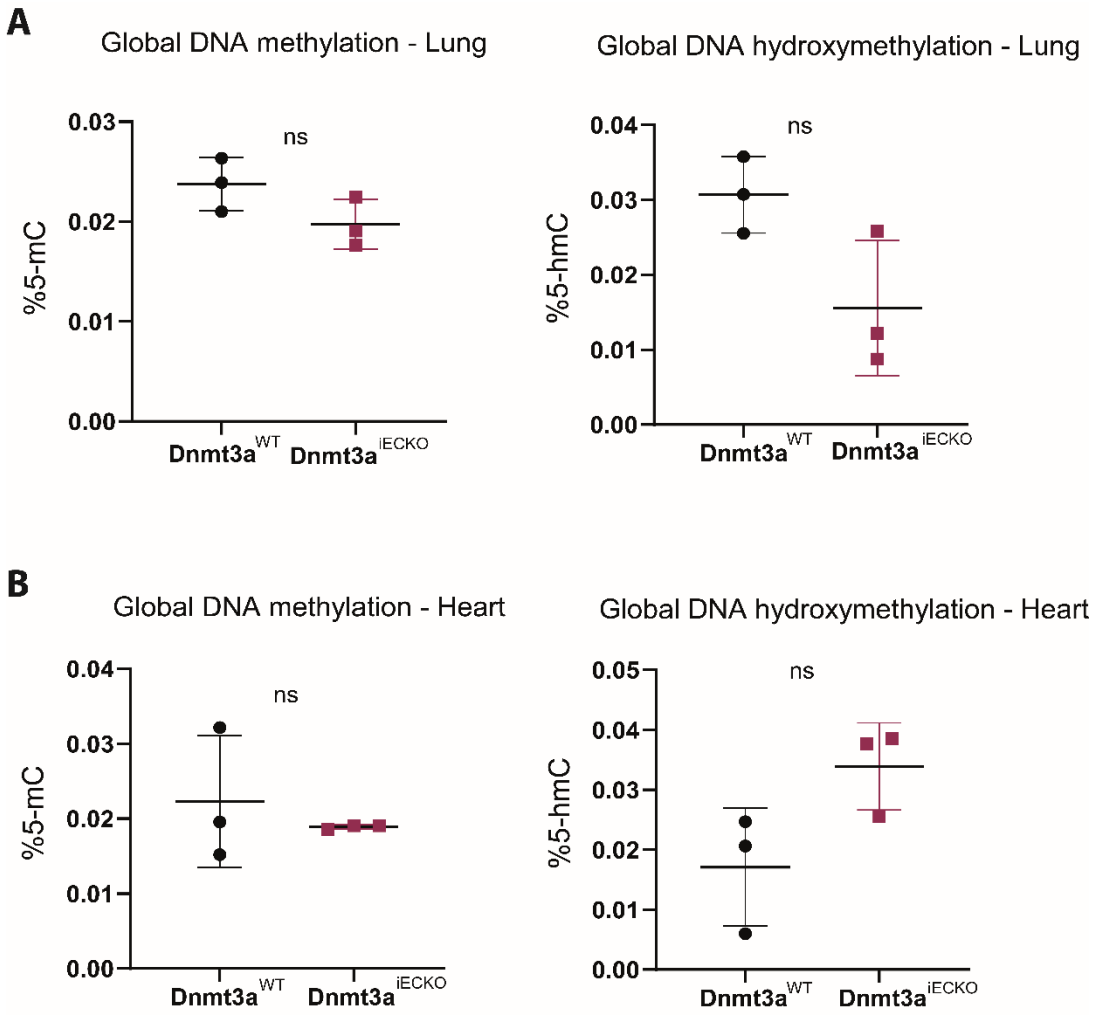

Figure 7: Effect of the loss of endothelial Dnmt3a in DNA methylation of Lung and Heart.
(A-B) Quantification of 5-mC (left) and 5-hmC (right) in DNA of isolated lung **(A)** and heart **(B)** ECs measured by ELISA. Data are shown as mean±sd (n=3; Mann-Whitney test).

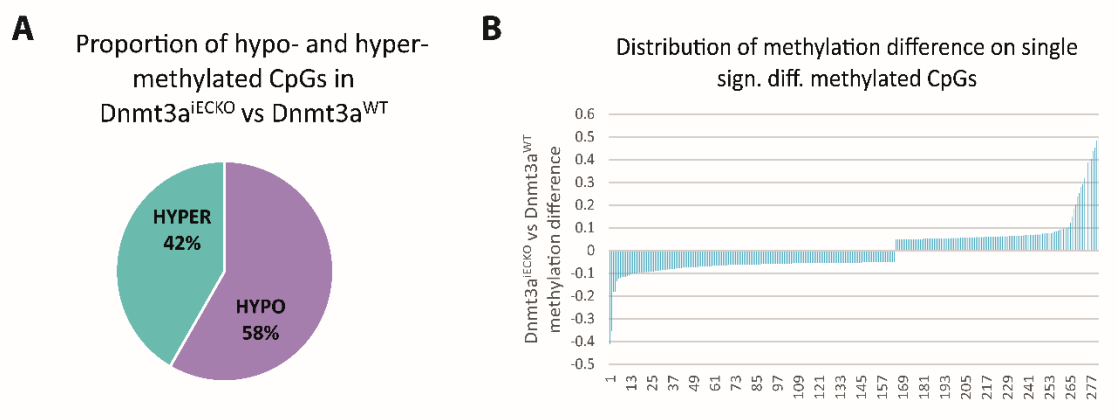

Figure 8: Effect of the loss of endothelial Dnmt3a in DNA methylation.

Methylation array analysis from lung EC from Dnmt3aiECKO and Dnmt3aWT mice. **(A)** Proportion of hypo- and hyper- methylated CpGs in Dnmt3aiECKO vs Dnmt3aWT mice. **(B)** Distribution of the methylation difference on single significantly differentially methylated CpGs in Dnmt3aiECKO vs Dnmt3aWT. (n=3).

As previous data from our group revealed that Dnmt3a modulates angiogenesis during development, I hypothesized that the expression of Dnmt3a will be induced during disease-associated angiogenesis as observed in developmental angiogenesis. To investigate this, Dnmt3a mRNA levels in isolated ECs from lung and heart from homeostatic, high fat diet-fed and tumor inoculated Dnmt3a^{WT} mice were measured via qPCR. A 3- to 2-fold induction of Dnmt3a expression after high fat diet treatment and tumor inoculation was observed in both heart and lung EC when compared to the basal Dnmt3a expression during homeostasis (Fig- 9A-B). These data demonstrate that endothelial re-activation due to inflammation induces Dnmt3a expression.

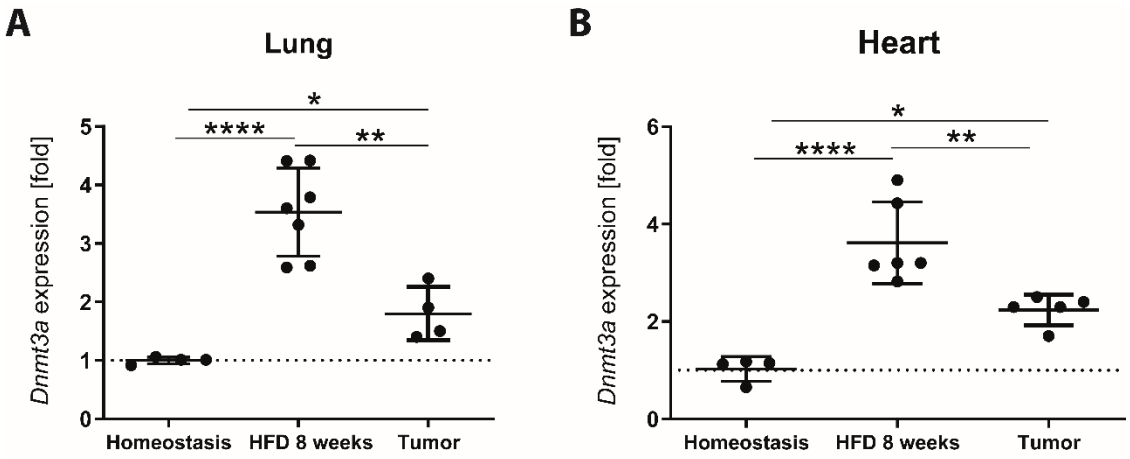

Figure 9: Dnmt3a expression is induced in wildtype EC after inflammatory stimulus.
Dnmt3a expression in sorted lung **(A)** and heart **(B)** EC from homeostatic (non-treated), high fat diet-fed and tumor inoculated Dnmt3a^{WT} mice. Gene expression is normalized to *βActin* expression and to homeostasis. Data are shown as mean±sd (n=3-7; One-Way ANOVA, multiple comparisons test).

3.2 Tumor angiogenesis is impaired upon loss of endothelial Dnmt3a in LLC model

To characterize the role of endothelial Dnmt3a during vascular re-activation, primary tumor development was used as a disease model. Tamoxifen was administered to Dnmt3a^{iECKO} mice according to the established protocol as described previously (section 3.1) and after 21 days of washout period, the mice were subcutaneously injected with Lung Lewis Carcinoma (LLC) cells (Fig. 10A). Mice were sacrificed 14 days post tumor-inoculation, and ECs from lung, heart and primary tumor were isolated. Cre/Lox recombination efficiency was determined, which revealed a reduction of 95-90% of Dnmt3a expression in lung, heart and tumor EC (Fig. 10B-D). The effect of the endothelial loss of Dnmt3a in tumor growth was assessed by monitoring tumor volume every second day for the duration of the experiment (Fig. 11A) and by measuring the tumor weight and volume at the endpoint (Fig. 11B). Tumor growth and weight showed no difference between Dnmt3a^{WT} and Dnmt3a^{iECKO} mice.

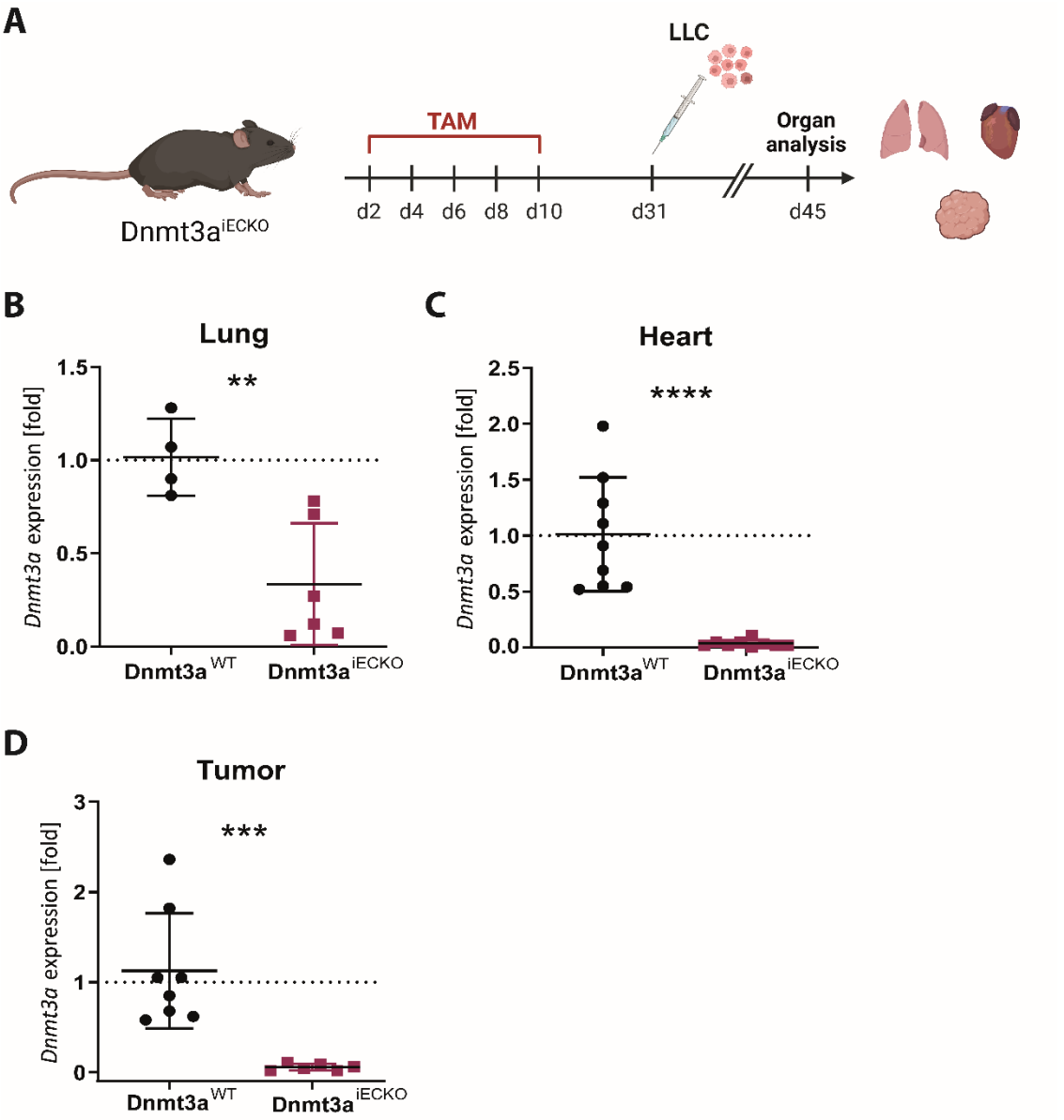

Figure 10: LLC tumor model in Dnmt3a^{iECKO} mice.

(A) Experimental model for tumor inoculation. Endothelial-specific Dnmt3a deletion was induced via tamoxifen administration and at d31 Lewis lung carcinoma (LLC) cells were injected. Mice were sacrificed at d45. **(B-D)** Dnmt3a expression in sorted lung **(B)**, heart **(C)** and tumor **(D)** EC from Dnmt3a^{iECKO} and Dnmt3a^{WT} mice. Gene expression is normalized to *βActin* expression and to WT. Data are shown as mean±sd (n=4-15; Mann-Whitney test).

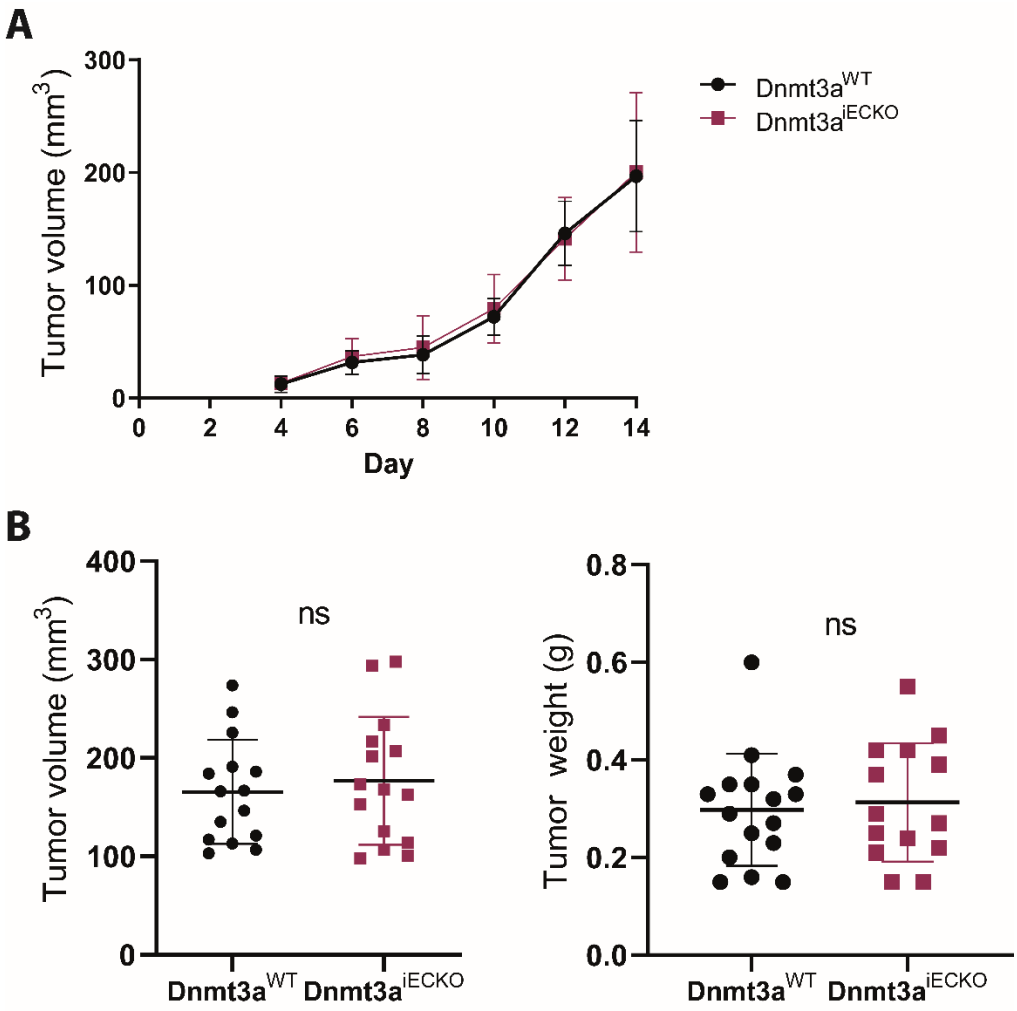

Figure 11: Dnmt3a loss in EC does not alter tumor growth.

(A) Tumor growth curve during the duration of the experiment. **(B)** Tumor volume (left) and weight (right) at the end point of the experiment. Data are shown as mean±sd (n=4-15; Mann-Whitney test).

Subsequently, a histological characterization of the primary tumor was performed. Blood vessel density and pericyte coverage of the primary tumors were assessed through immunofluorescent staining of CD31 (endothelial cell marker) and Desmin (pericyte marker). This analysis revealed a significant reduction of vascular area and microvascular density in Dnmt3a^{iECKO} mice when compared to Dnmt3a^{WT}, yet vessel coverage was not affected (Fig 12A-E). In addition, apoptosis, DNA damage, hypoxia, and proliferation were evaluated. This analysis yielded comparable levels of apoptosis, DNA damage and hypoxia in Dnmt3a^{WT} and Dnmt3a^{iECKO} mice (Fig 13B-D). However, endothelial proliferation was significantly reduced in Dnmt3a^{iECKO} mice (Fig. 13A, E) when compared to the controls. Taken together these data show that the loss of Dnmt3a in the endothelium alters angiogenesis in the primary tumor, without affecting overall tumor development on the LLC tumor model.

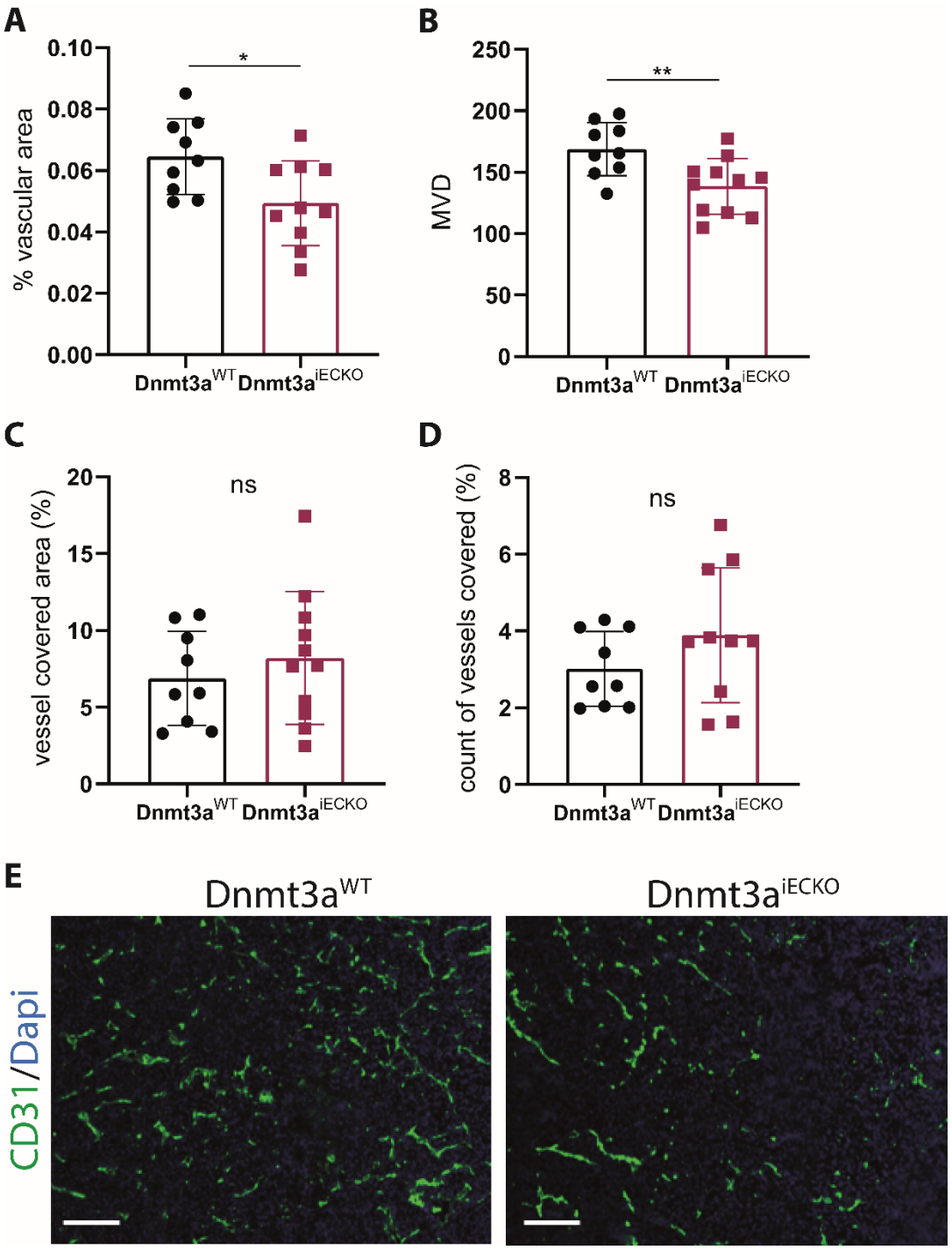

Figure 12: Endothelial Dnmt3a loss affects tumor vascularization.

Histological characterization of tumor from Dnmt3a^{iECKO} and Dnmt3a^{WT} mice. **(A-B)** Vascular area **(A)** and microvascular density **(B)** quantification. **(C-D)** Quantification of vessel covered area **(C)** and vessel covered count **(D)** by pericytes relative to CD31^{+} area. **(E)** Representative microscopy images of CD31^{+} (green) and dapi (blue) stained tumor sections. Scale bar indicates 100µm. Data are shown as mean±sd (n=4-10; Mann-Whitney test).

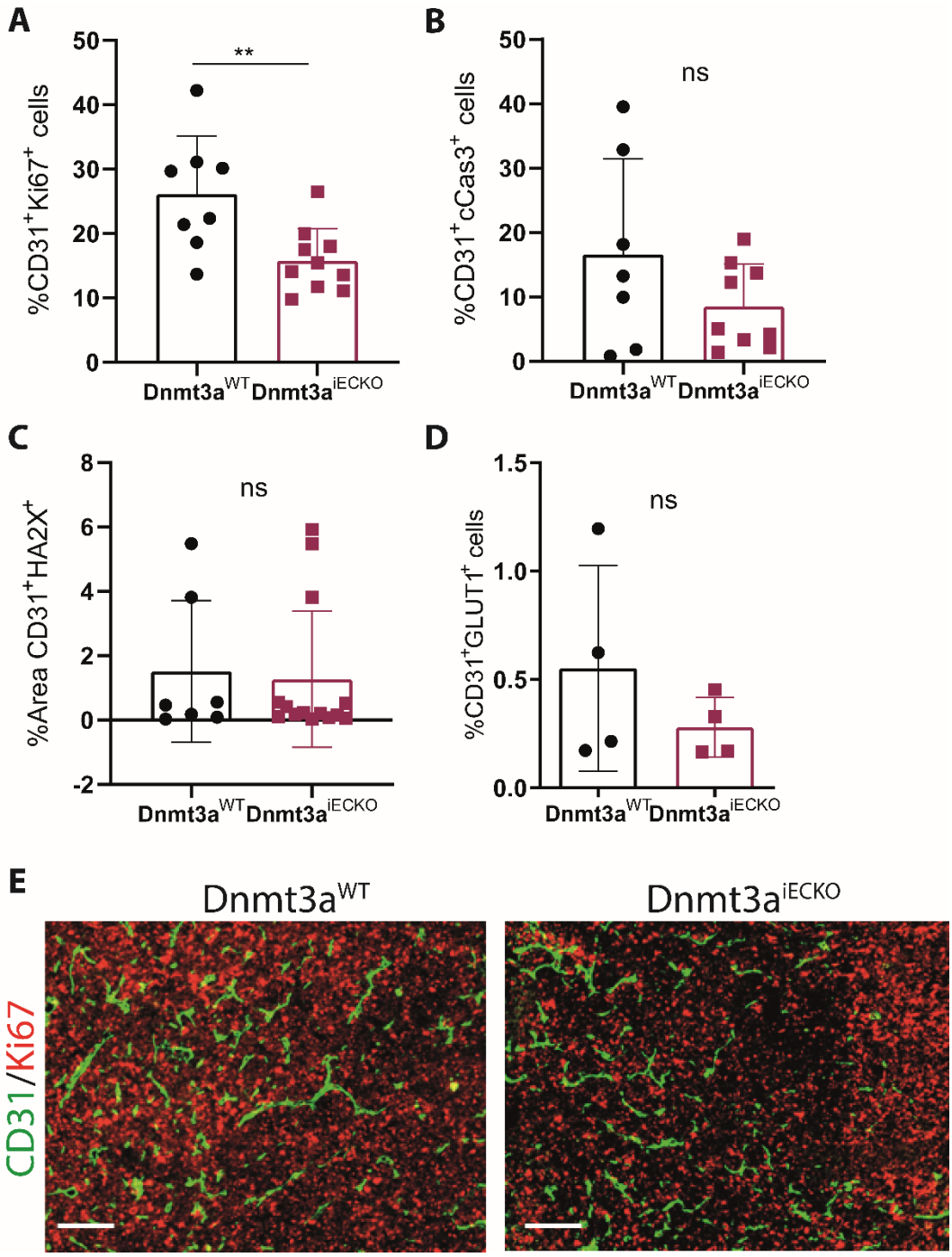

Figure 13: Endothelial Dnmt3a loss affects endothelial proliferation in the primary tumor.
Histological characterization of tumor from Dnmt3a^{iECKO} and Dnmt3a^{WT} mice. **(A)** Quantification of endothelial proliferation by the presence of Ki67, **(B)** endothelial apoptosis by the presence of cleaved caspase 3 (cCas3), **(C)** DNA damage in the endothelial cells by presence of γHA2X and **(D)** hypoxic endothelial cells by presence of glucose transporter 1 (GLU1). All stainings were normalized to the total tumor area. **(E)** Representative microscopy images of CD31$^+$ (green) and Ki67$^+$ (red) tumor sections. Scale bar indicates 100µm. Data are shown as mean±sd (n=4-10; Mann-Whitney test).

3.3 Cardiac growth and vascularization is impaired in obese Dnmt3a^{iECKO} mice

Obesity was used as a model to investigate the impact of chronic inflammation on Dnmt3a-mediated vascular re-activation. Following Dnmt3a deletion, mice were fed a high fat diet (HFD) for 8 weeks, after which they were sacrificed to isolate heart and lung EC (Fig. 14A). Deletion efficiency was determined by Dnmt3a gene expression analysis and a 95-90% deletion of Dnmt3a was observed in Dnmt3a^{iECKO} mice when compared with Dnmt3a^{WT} (Fig. 14B-C). Dnmt3a^{iECKO} and Dnmt3a^{WT} mice fed a HFD for 8 weeks gained weight (Fig. 15A). In addition, the mice exhibited higher levels of glucose and cholesterol in the serum (Fig. 15B-D), when compared to those who were fed a normal diet (homeostasis). These findings support the notion that HFD feeding is a viable model for obesity. However, comparable levels of serum parameters and weight gain were observed between Dnmt3a^{iECKO} and Dnmt3a^{WT} mice both in HFD-fed and normal diet groups. Since I previously observed that Dnmt3a expression was induced in HFD-fed mice, I next investigated if the global DNA methylation landscape was altered upon loss of endothelial Dnmt3a in the HFD-induced inflammation model. For this reason, quantification of global DNA methylation and hydroxymethylation from isolated Dnmt3a^{iECKO} and Dnmt3a^{WT} lung and heart EC was performed by ELISA (Fig. 16A-B). The deletion of Dnmt3a on EC did not have an effect on the percentage of 5-mC and 5-HmC DNA in heart and lung ECs when compared to Dnmt3a^{WT}, suggesting that there are no major methylation changes in EC due to Dnmt3a loss in the context of obesity.

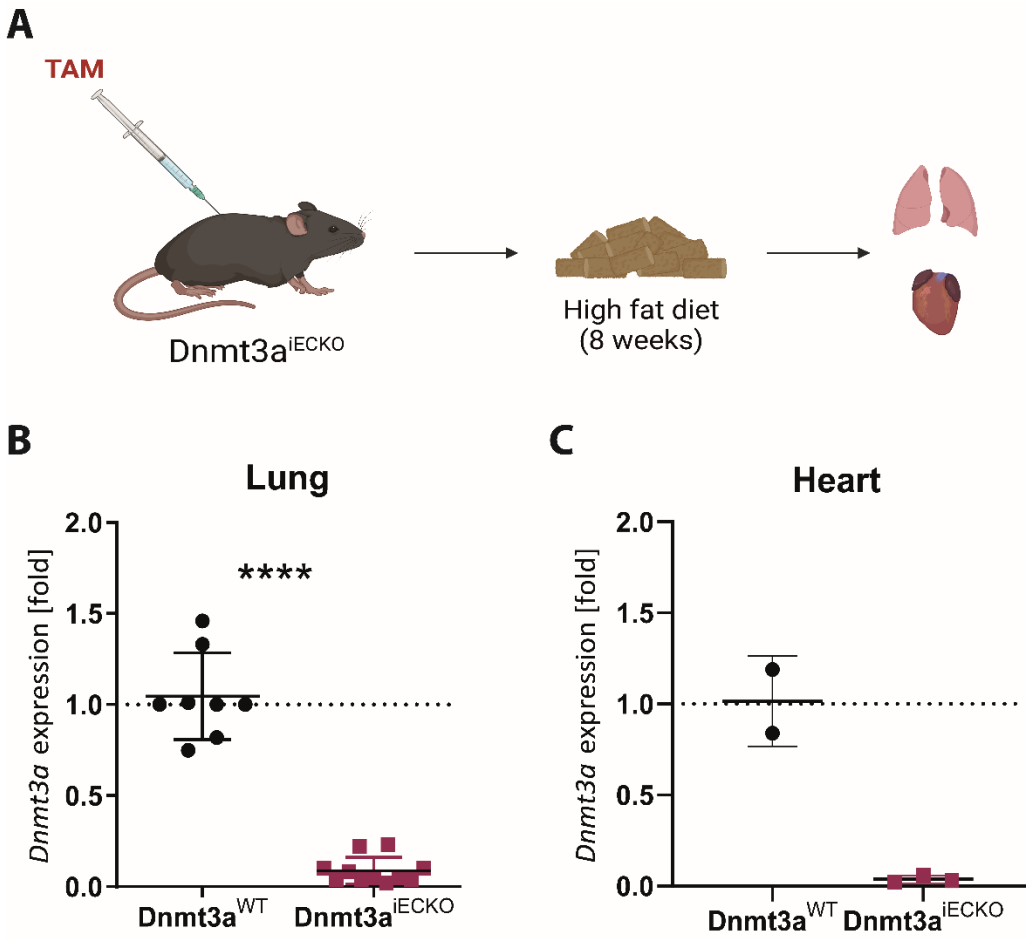

Figure 14: High fat diet-induced inflammation model in Dnmt3a^{iECKO} mice.

(A) Schematic representation of experimental model of high fat diet-induced inflammation. Endothelial-specific Dnmt3a deletion was induced via 5 doses of tamoxifen administration. Mice were fed with high fat diet (HFD) during 8 weeks and subsequently sacrificed. **(B-C)** Dnmt3a expression in sorted lung **(B)** and heart **(C)** EC from Dnmt3a^{iECKO} and Dnmt3a^{WT} mice. Gene expression is normalized to *βActin* expression and to WT. Data are shown as mean±sd (n=4-15; Mann-Whitney test).

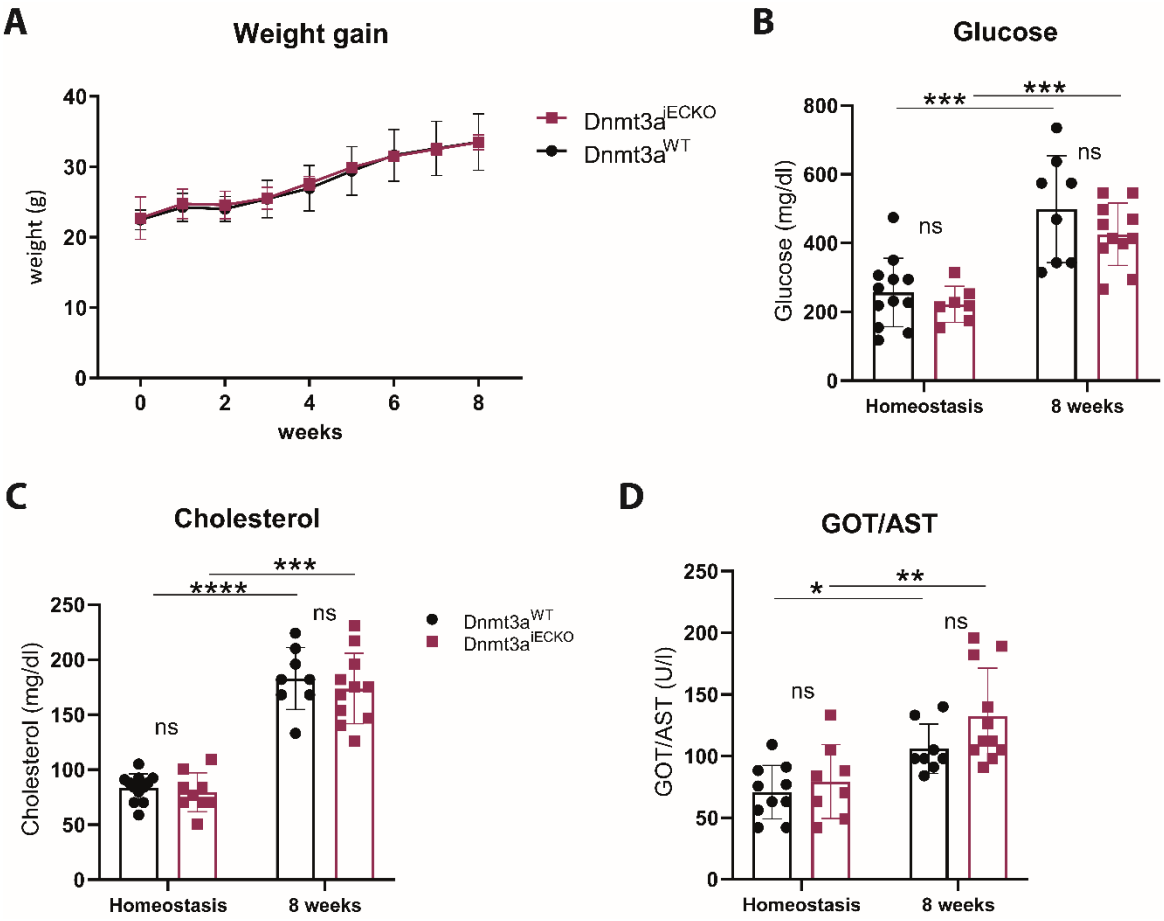

Figure 15: Loss of endothelial Dnmt3a does not alter weight gain and blood parameters after high fat diet treatment.

(A) Weight gain curve during the administration of the diet. **(B-D)** Glucose **(B)**, cholesterol **(C)** and GOT/AST **(D)** blood levels in homeostatic (non-treated) and HFD-fed mice. Data are shown as mean±sd (n=4-15; Two way ANOVA – Multiple comparisons).

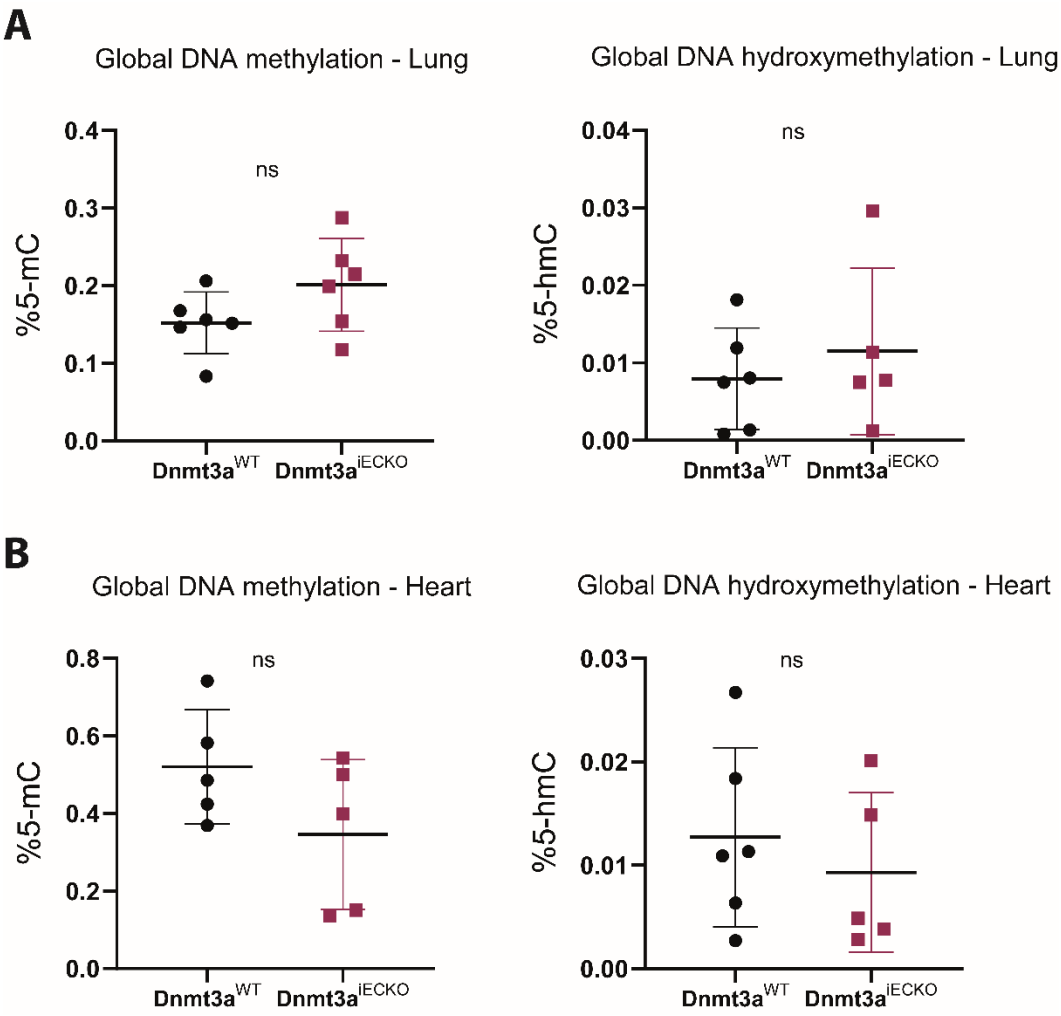

Figure 16: Effect of the loss of endothelial Dnmt3a in DNA methylation of Lung and Heart after High fat diet-induced inflammation.

(A-B) Quantification of 5-mC (left) and 5-hmC (right) in DNA of isolated lung **(A)** and heart **(B)** ECs measured by ELISA. Data are shown as mean±sd (n=5-6; Mann-Whitney test).

Obesity can lead to significant alterations in liver function, such as the development of steatosis, fibrosis, and liver damage[148]. In order to identify if the lack of endothelial Dnmt3a has an effect on the liver morphological and functional changes induced by obesity, a characterization of the liver from HFD-fed Dnmt3a^{iECKO} mice was performed. Relative liver weight (Fig. 17A) was not altered due to the endothelial deletion of Dnmt3a after HFD. Additionally, serum parameters for liver damage were analyzed, and comparable amounts of high-density lipoprotein, low-density lipoprotein, Aspartate aminotransferase and Alanine aminotransferase (Fig. 17B-F) were observed in Dnmt3a^{WT} and Dnmt3a^{iECKO} mice. Finally, liver sections of HFD-treated mice were stained with Sirius red, Masson's trichrome, and Hematoxylin & Eosin staining (data not shown) to assess liver fibrosis, necrosis, and lipid accumulation. This analysis yielded comparable levels of liver fibrosis, necrosis and lipid accumulation between Dnmt3a^{WT} and Dnmt3a^{iECKO} mice after HFD treatment. Therefore,

this data indicates that the loss of Dnmt3a in the ECs did not alter obesity-induced functional and morphological changes of the liver.

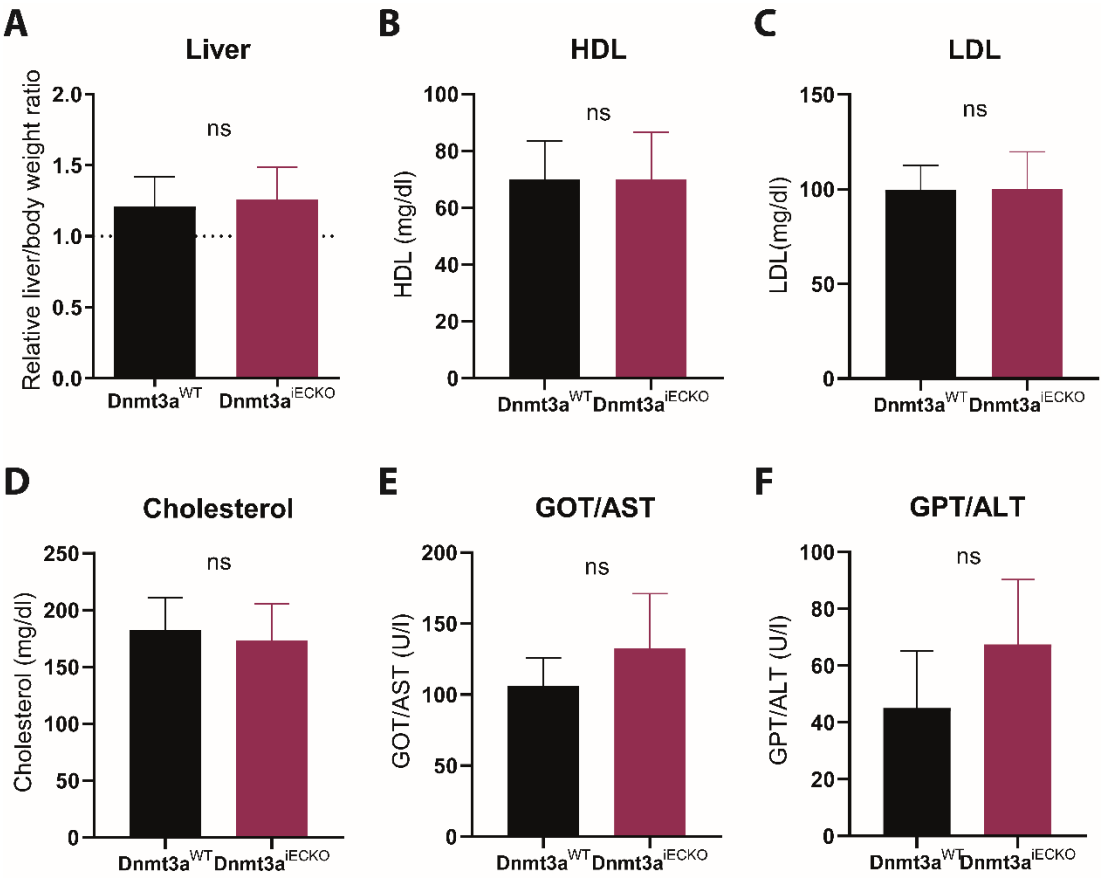

Figure 17: Loss of endothelial Dnmt3a does not affect liver morphology and function after HFD. **(A)** Liver weight to body weight ratio of Dnmt3a^{iECKO} and Dnmt3a^{WT} mice. **(B)** High density lipoprotein (HDL), **(C)** low density lipoprotein (LDL), **(D)** cholesterol and **(E)** aspartate aminotransferase (GOT/AST) (left) and alanine aminotransferase (GPT/ALT) (right) blood levels in HFD-fed Dnmt3a^{iECKO} and Dnmt3a^{WT} mice. Data are shown as mean±sd (n=8-12; Mann-Whitney test).

As obesity is a risk factor for cardiovascular disease and can lead to changes in the structure and function of the heart[70], the next aim was to investigate whether the interference with Dnmt3a-dependent DNA methylation in EC will affect obesity-induced morphological changes in the heart. First, I analyzed the heart weight of homeostatic and HFD-fed Dnmt3a^{WT} mice (Fig. 18). In line to the available literature, Dnmt3a^{WT} mice developed cardiac hypertrophy due to obesity[70]. However, obese Dnmt3a^{iECKO} mice had significantly reduced heart weight when compared to Dnmt3a^{WT} mice (Fig. 19A), indicating that endothelial deletion of Dnmt3a impairs obesity-induced heart growth. To gain better understanding of the heart morphology of HFD-fed Dnmt3a^{iECKO} mice, cardiomyocyte area, vascular density and endothelial proliferation were analyzed employing wheat germ

agglutinin, CD31 and Ki67 staining, respectively. A reduced cardiomyocyte area in Dnmt3a^{iECKO} mice was detected (Fig. 19B), correlating with the observed weight difference. Vascular density was significantly reduced in Dnmt3a^{iECKO} mice, yet there was no difference in endothelial proliferation (Fig. 19C-D). Taken together, this analysis showed that endothelial Dnmt3a is required for obesity-induced pathological heart growth.

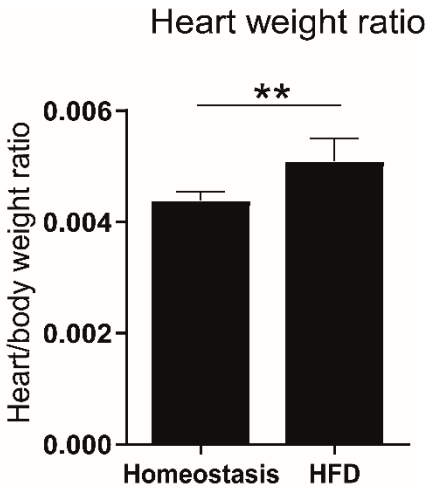

Figure 18: Cardiac hypertrophy is developed in wildtype mice after high fat diet treatment.
Heart weight to body weight ratio from homeostatic (non-treated) and high fat diet-fed Dnmt3a^{WT} mice. Data are shown as mean±sd (n=8; Mann-Whitney test).

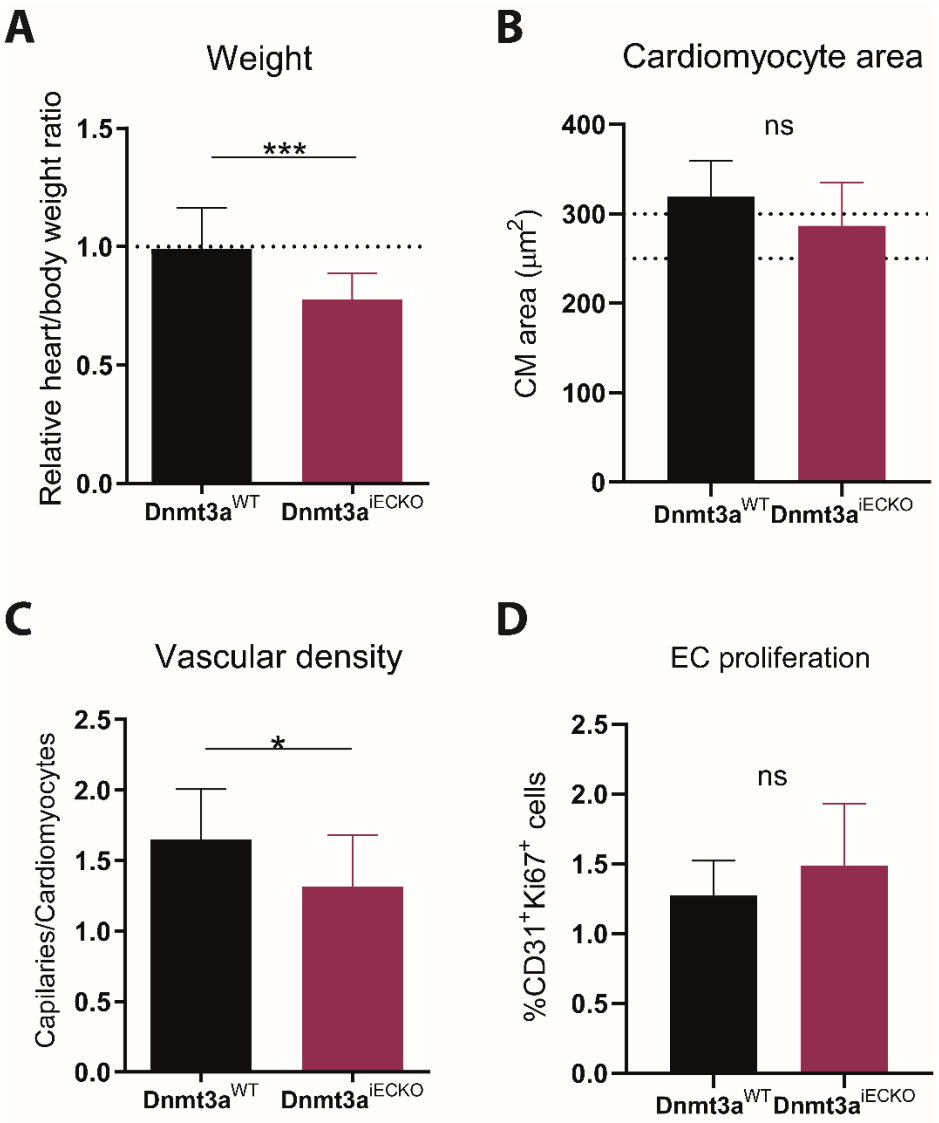

Figure 19: Morphological characterization of the heart from Dnmt3a^{iECKO} and Dnmt3a^{WT} mouse after high fat diet-induced inflammation.

(A) Heart weight to body weight ratio, relative to the Dnmt3a^{WT} mice. **(B)** Cardiomyocyte (CM) area quantification by staining with wheat germ agglutinin (WGA). The dotted lines represent the normal range of CM area. Quantification of **(C)** Vascular density and **(D)** endothelial proliferation by presence of Ki67. Data are shown as mean±sd (n=6-8; Mann-Whitney test).

3.4 Endothelial Dnmt3a deletion induces cardiac dysfunction due to obesity

To further characterize the effect of the endothelial deletion of Dnmt3a in obesity-induced cardiac remodeling, Sirius red, Masson's trichrome, TUNEL, collagen I and collagen III staining were performed on HFD-fed Dnmt3a^{iECKO} and control heart tissue. Dnmt3a^{iECKO} mice displayed increased incidence of cardiac fibrosis (Fig. 20A-C) and apoptosis (Fig. 20D) after being fed with HFD compared to control animals. Considering that immune cell infiltration is among the contributing factors to

fibrosis[49], a CD45 staining and later quantification was conducted on heart sections to evaluate whether this contributed to the increased cardiac fibrosis observed in Dnmt3a^{iECKO} mice. Nevertheless, a comparable immune cell infiltration in hearts from Dnmt3a^{WT} and Dnmt3a^{iECKO} mice was observed (Fig. 20E). This suggests that the susceptibility to developing cardiac fibrosis observed in Dnmt3a^{iECKO} mice is a result of the increased cell death rather than immune cell infiltration.

In order to investigate the functional impact of the increased fibrosis in Dnmt3a^{iECKO} mice due to HFD-induced inflammation, an echocardiography was performed in collaboration with Prof. Dr. Jörg Heineke and Prof. Dr. Gergana Dobreva. Echocardiography is an advanced imaging technique that allows for detailed visualization and assessment of cardiac structures providing detailed information about myocardial function, valve abnormalities, wall thickness and vascular abnormalities. Wall thickness in Dnmt3a^{iECKO} mice was slightly reduced (Fig. 21A-B), correlating with the reduction in weight and cardiomyocyte area previously identified. Diastolic function analysis showed that Dnmt3a^{iECKO} mice presented a significant decrease in the global longitudinal strain percentage in addition to a significant decrease in the mitral deacceleration time when compared to Dnmt3a^{WT} (Fig. 21C-D), indicating an impaired relaxing capacity and ventricular blood filling and consequently compromising the heart capacity to efficiently receive blood. Systolic function parameters were analyzed and there was no difference between Dnmt3a^{WT} and Dnmt3a^{iECKO} mice (Fig. 22A-C). These data indicate diastolic dysfunction due to HFD-induced inflammation when endothelial Dnmt3a is lost.

In summary, the interference with endothelial Dnmt3a during obesity compromises cardiac function and increase the susceptibility of fibrosis. The impairment of cardiac relaxation as a consequence of cardiac fibrosis leads to diastolic dysfunction.

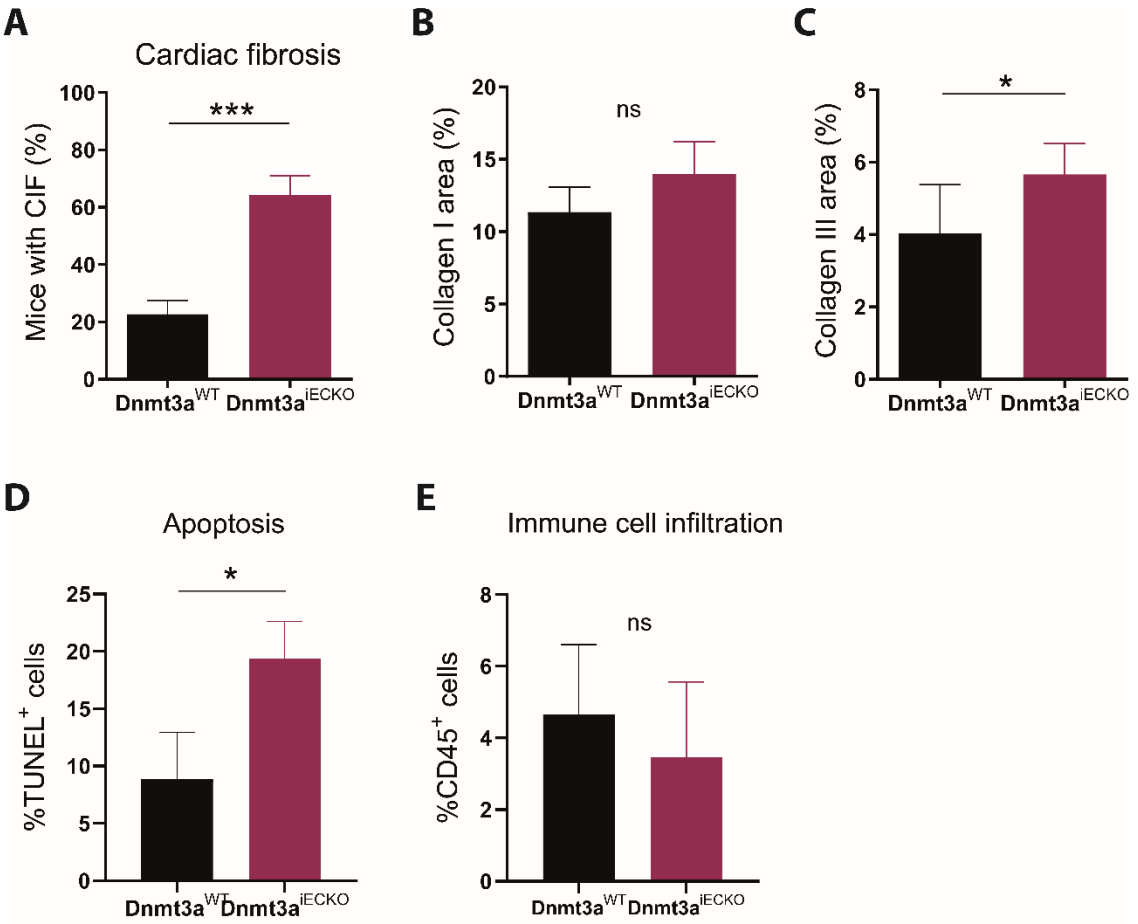

Figure 20: Cardiac fibrosis characterization from obese Dnmt3a^{iECKO} and Dnmt3a^{WT} mouse.
Quantification of **(A)** cardiac interstitial fibrosis (CIF) by staining with Sirius red and Masson's Trichrome staining, **(B)** collagen I and **(C)** collagen III area, **(D)** apoptotic cells by TUNEL staining and **(E)** Immune cell infiltration by presence of CD45$^+$ cells. Data are shown as mean±sd (n=6-8; Mann-Whitney test).

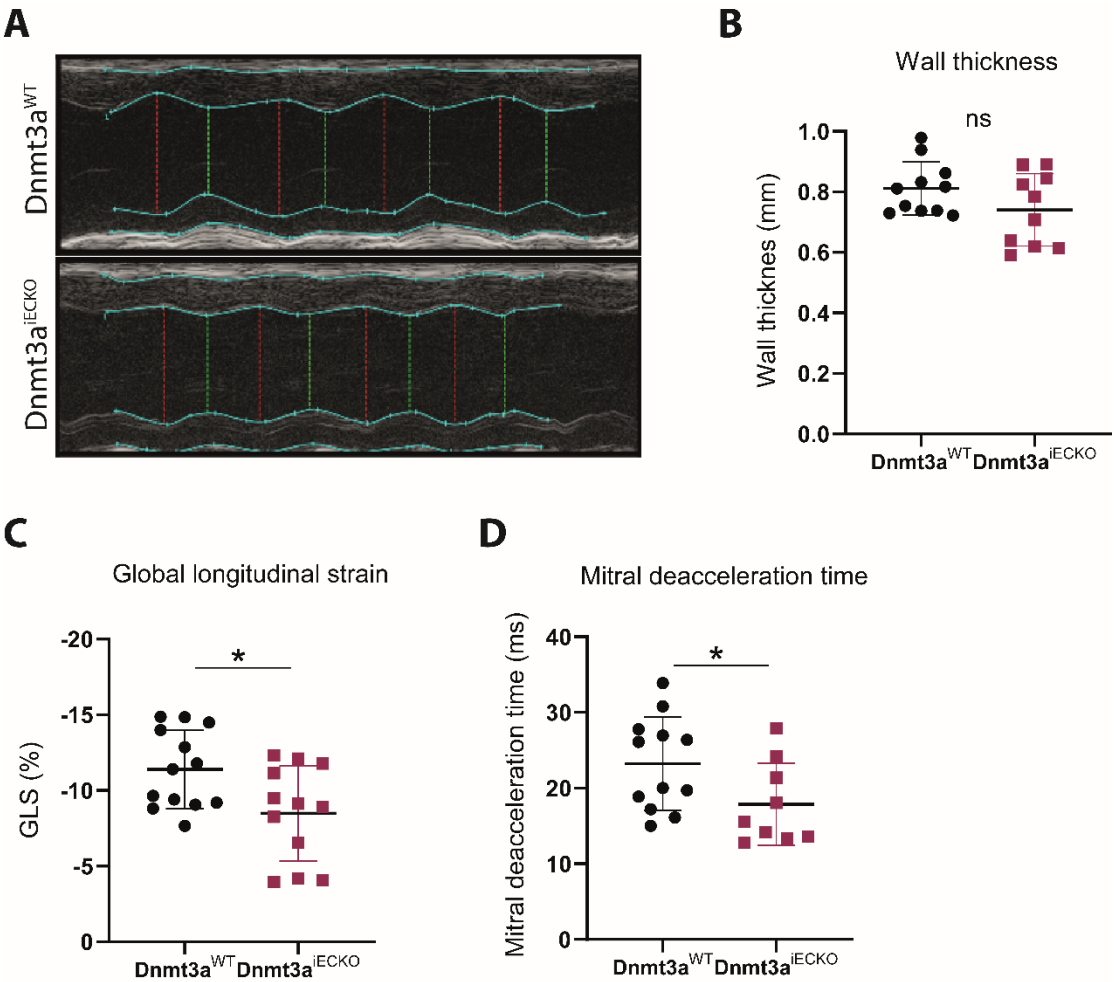

Figure 21: Functional characterization of the diastolic heart from Dnmt3a^{iECKO} and Dnmt3a^{WT} mouse after high fat diet-induced inflammation.

Echocardiography analysis from Dnmt3a^{iECKO} and Dnmt3a^{WT} mice after 8 weeks of HFD. **(A)** Representative images of the short-axis view M-mode, including the narrowest (green lines) and the widest (red lines) point per cycle. **(B)** Quantification of the left ventricular posterior wall thickness in diastole. **(C)** Quantification of global longitudinal strain (GLS). **(D)** Quantification of mitral deacceleration time. Data are shown as mean±sd (n=10-12; Mann-Whitney test).

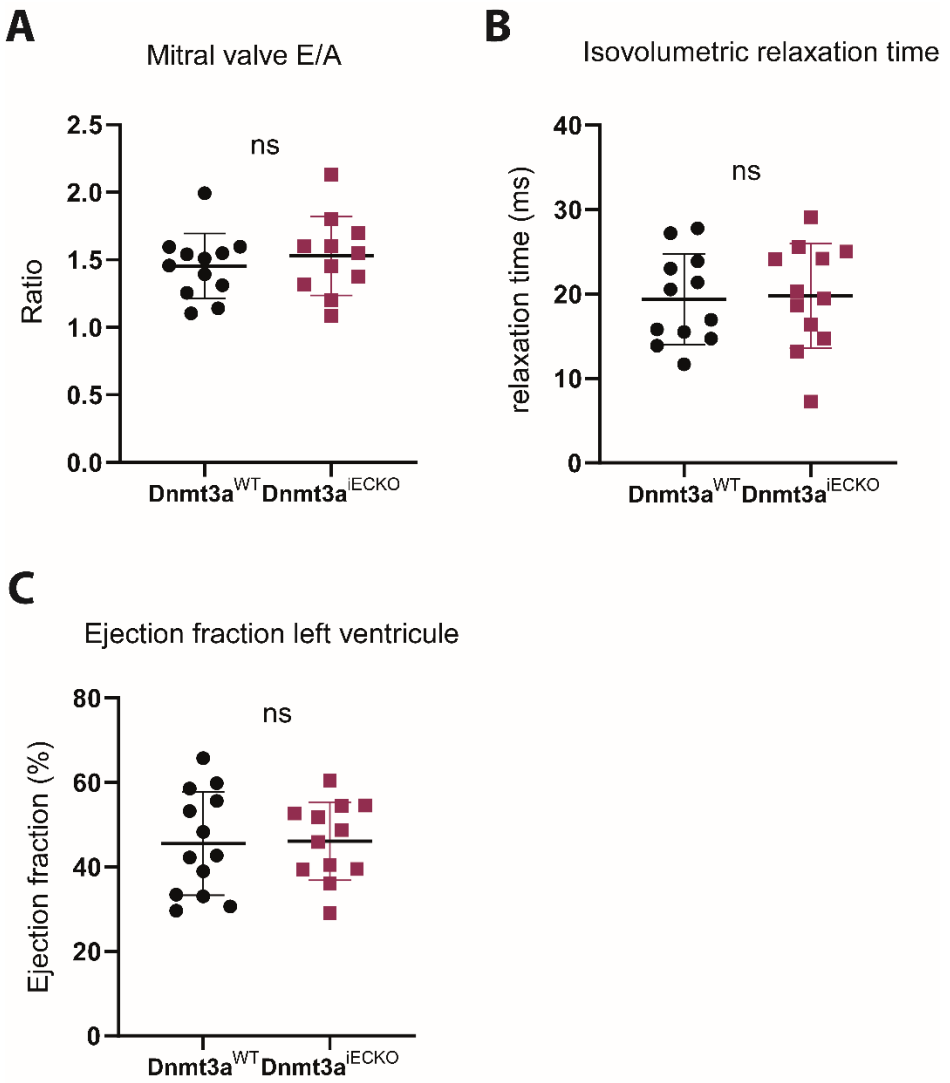

Figure 22: Functional characterization of the systolic heart from Dnmt3a^{iECKO} and Dnmt3a^{WT} mouse after high fat diet-induced inflammation.

Echocardiography analysis from Dnmt3a^{iECKO} and Dnmt3a^{WT} mice after 8 weeks of HFD. **(A)** Mitral valve E/A ratio. **(F)** Isovolumetric relaxation time and **(G)** ejection fraction in the left ventricle quantification. Data are shown as mean±sd (n=10-12; Mann-Whitney test).

3.5 Dnmt3a^{iECKO} mice present a morphologically and functionally healthy quiescent endothelium

The next goal was to assess if the interference with Dnmt3a-dependent DNA methylation impairs vascular quiescence during health. For this purpose, Dnmt3a deletion was induced via tamoxifen administration according to the previous protocol described in section 3.1 (Fig 5A). After 21 days from the last injection of TAM, mice were sacrificed and phenotypical analysis of lung, liver and heart were performed. Hematoxylin & Eosin staining of lung, liver and heart of Dnmt3a^{iECKO} mice

and further analysis by a pathologist did not show a difference in organ morphology when compared to Dnmt3a^{WT} mice (data not shown). CD31 staining and relative organ weight analysis of lung and liver yielded comparable vascularization and organ weight between Dnmt3a^{WT} and Dnmt3a^{iECKO} mice (data not shown). As cardiac morphology and function were affected by the endothelial deletion of Dnmt3a during obesity, an in-depth characterization of the homeostatic Dnmt3a^{iECKO} heart was performed. Relative heart weight analysis evidenced a significant increase in Dnmt3a^{iECKO} when compared to Dnmt3a^{WT} hearts (Fig. 23A). Staining of the endothelium revealed that there was no difference between Dnmt3a^{WT} and Dnmt3a^{iECKO} mice in cardiac vascularization (Fig. 23B). However, there was a detectable increase in endothelial proliferation in the hearts of Dnmt3a^{iECKO} mice (Fig. 23C). Further histological analysis yielded undetectable levels of fibrosis when Sirius Red and Masson's trichrome staining were analyzed (data not shown), in addition to comparable levels of collagen I and collagen III, immune infiltration and apoptosis in hearts of Dnmt3a^{WT} and Dnmt3a^{iECKO} mice (Fig. 23D-G).

Cardiac function of the homeostatic Dnmt3a^{iECKO} mice was studied via an echocardiography in collaboration with Prof. Dr. Jörg Heineke and Prof. Dr. Gergana Dobreva. No difference between Dnmt3a^{WT} and Dnmt3a^{iECKO} mice was observed when analyzing wall thickness (Fig. 24A-B), global longitudinal strain percentage (Fig. 24C) and mitral deacceleration (Fig. 24D) as markers for diastolic function, as well as systolic function parameters (Fig. 25A-C). Taken together, these data show that endothelial deletion of Dnmt3a during vascular quiescence did not originate major morphological changes in lung and liver. However, an enlarged heart was observed though there was no impact on cardiac function.

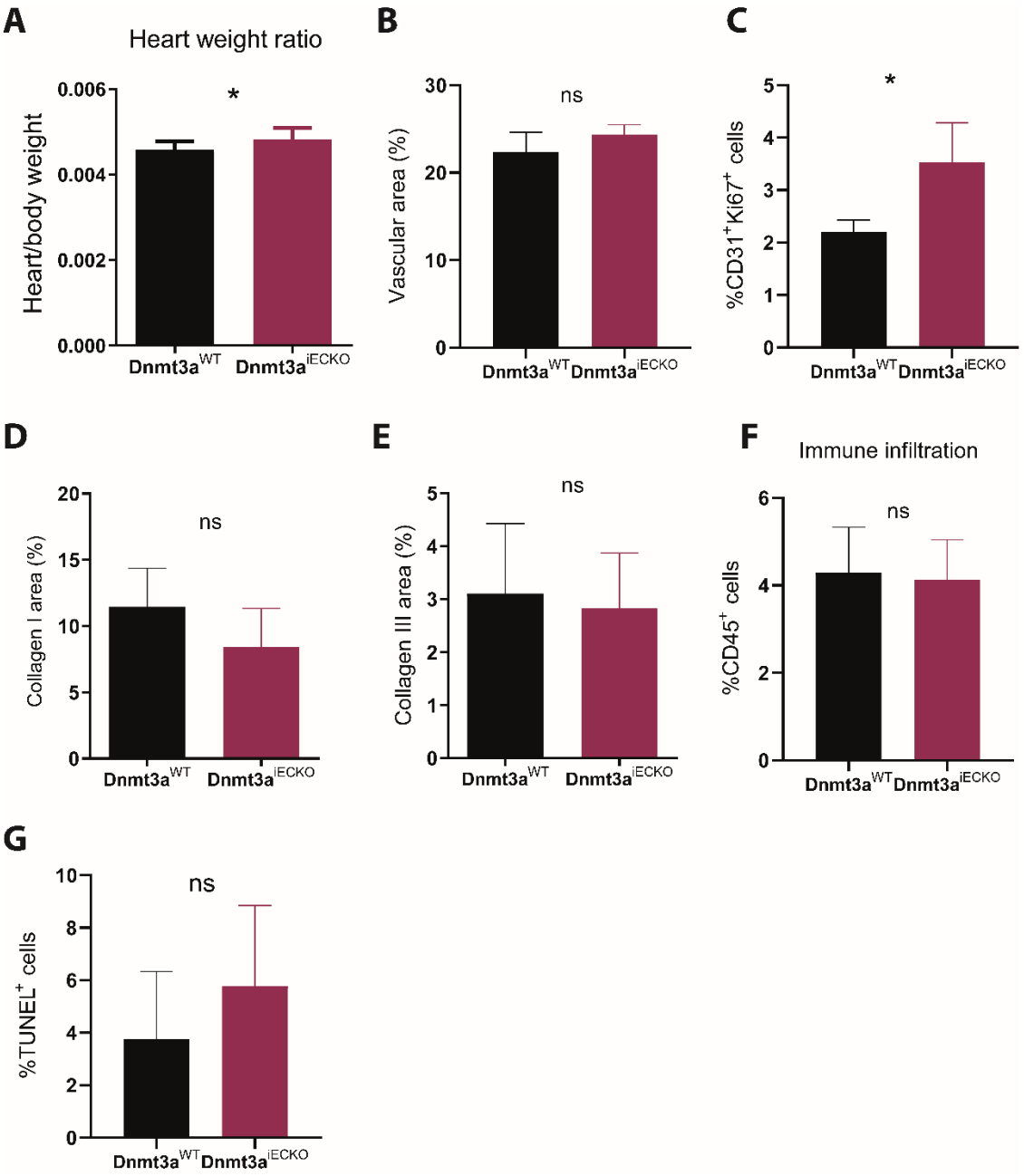

Figure 23: Morphological characterization of the heart from Dnmt3a^{iECKO} and Dnmt3a^{WT} mouse. **(A)** Heart weight to body weight ratio of Dnmt3a^{iECKO} and Dnmt3a^{WT} mice. **(B)** Vascular area, **(C)** endothelial proliferation, **(D)** collagen I and **(E)** collagen III area, **(F)** Immune infiltration and **(G)** TUNEL staining quantification. Data are shown as mean±sd (n=6-8; Mann-Whitney test).

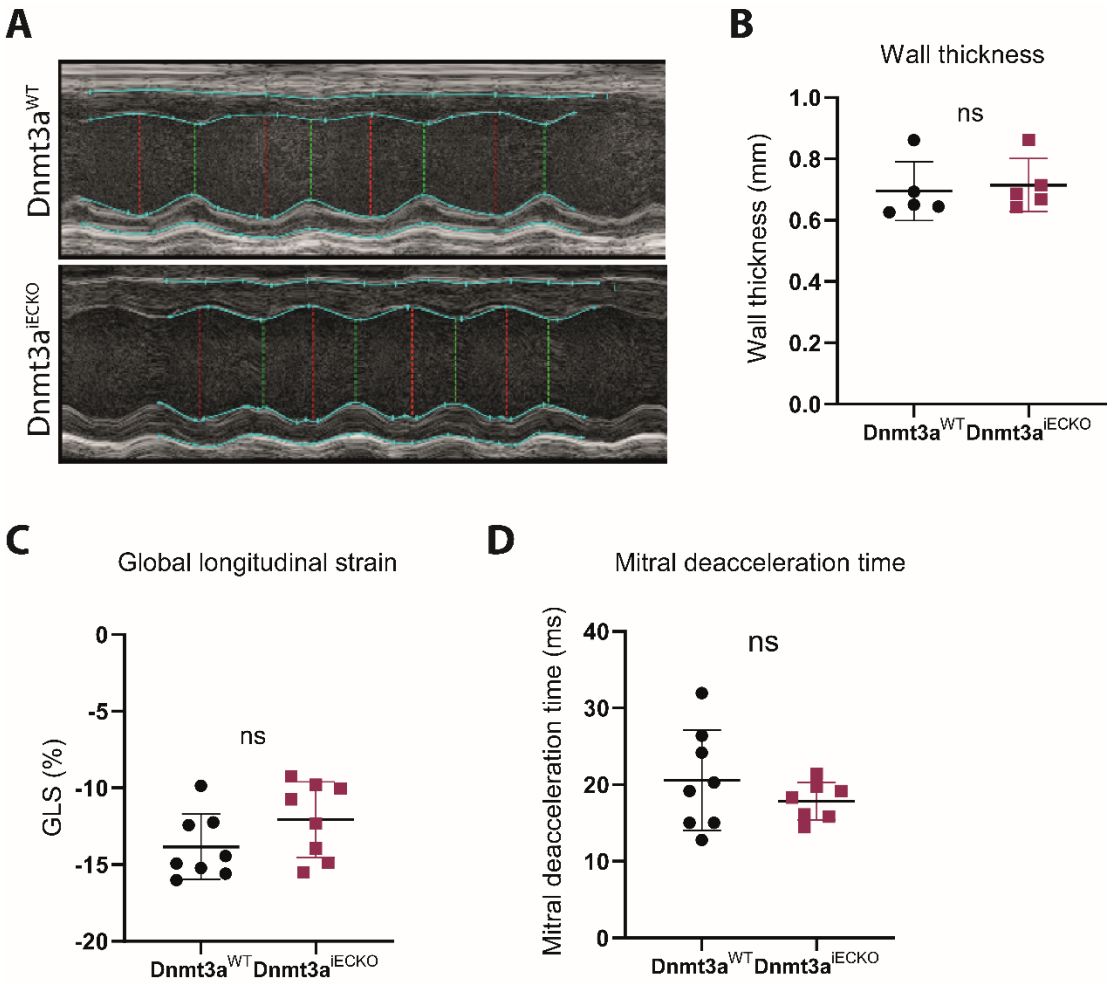

Figure 24: Functional characterization of the diastolic heart from Dnmt3a^{iECKO} and Dnmt3a^{WT} mouse.

Echocardiography analysis from Dnmt3a^{iECKO} and Dnmt3a^{WT} mice. **(A)** Representative images of the short-axis view M-mode, including the narrowest (green lines) and the widest (red lines) point per cycle. **(B)** Quantification of the left ventricular posterior wall thickness in diastole. **(C)** Quantification of global longitudinal strain (GLS). **(D)** Quantification of mitral deacceleration time. Data are shown as mean±sd (n=5-8; Mann-Whitney test).

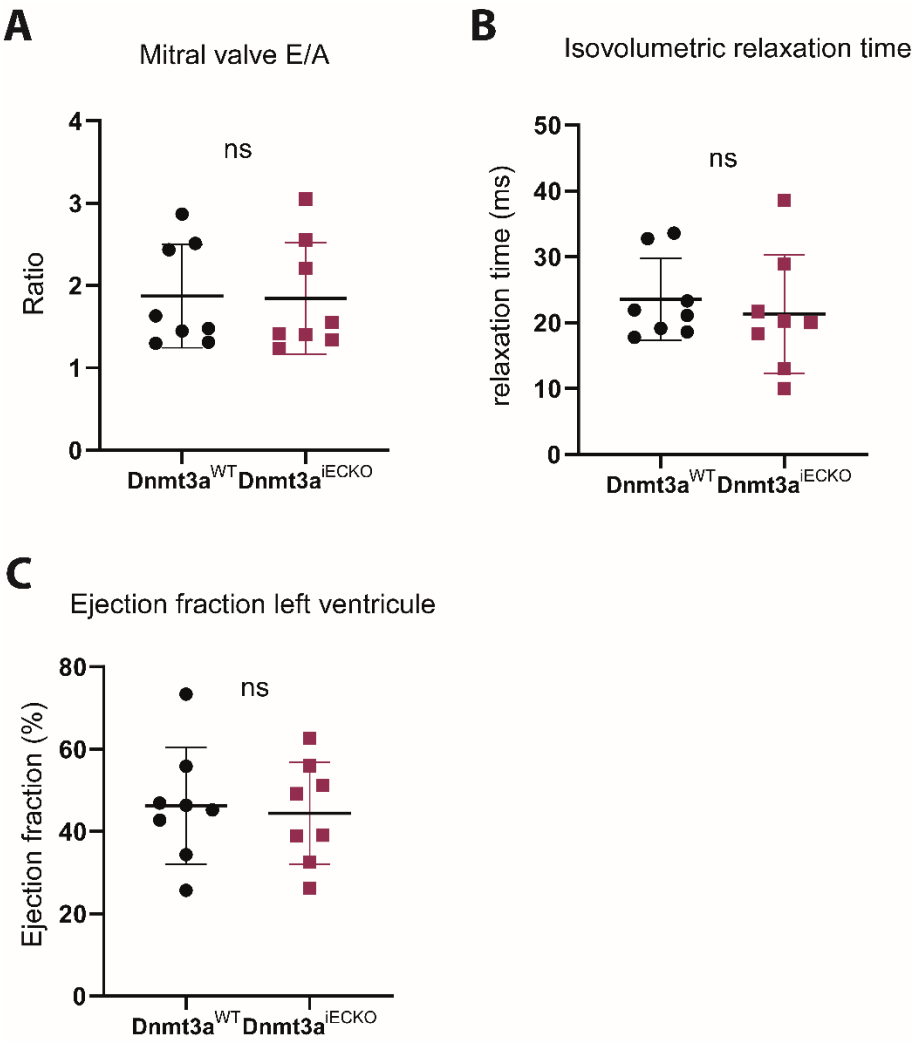

Figure 25: Functional characterization of the systolic heart from Dnmt3a^{iECKO} and Dnmt3a^{WT} mouse.

Echocardiography analysis from Dnmt3a^{iECKO} and Dnmt3a^{WT} mice. **(A)** Mitral valve E/A ratio. **(B)** Quantification of isovolumetric relaxation time. **(C)** Quantification of ejection fraction in the left ventricle. Data are shown as mean±sd (n=5-8; Mann-Whitney test).

3.6 Endothelial loss of Dnmt3a affects gene expression in the quiescent lung and heart endothelium

Since endothelial proliferation was induced in the quiescent heart after the loss of Dnmt3a in EC, a transcriptomic analysis of isolated heart EC from Dnmt3a^{iECKO} and Dnmt3a^{WT} mice was performed aimed at identifying the molecular mechanism of Dnmt3a interference in endothelial proliferation. Dnmt3a deletion was induced and total RNA was isolated from sorted heart EC 21 days after the last injection of TAM. Following the evaluation of the deletion efficiency of Dnmt3a by qPCR, the

RNA was used for bulk RNA-sequencing analysis to unravel changes in global gene expression. Differential gene expression analysis with a p-value cut-off at 0.05 revealed 126 up-regulated and 10 down-regulated genes when comparing Dnmt3a^{iECKO} and Dnmt3a^{WT} (Fig. 26A). To better understand the biological relevance of transcriptional changes in heart EC, gene set enrichment analysis (GSEA) was performed. Significantly altered genes belonging to hallmark gene sets related to G2M checkpoint, mitotic spindle, p53 pathway and mTORC1 signaling were observed (Fig. 26B). Over-representation analysis (ORA) of gene ontology of biological processes showed significant regulation of genes related to organelle fission, nuclear division, chromosome segregation and mitotic nuclear division, such as *Ccnb1*, *Ccnb2*, *Mki67*, *Ccnf* and *Haspin* (Fig. 26C). Altogether these data suggest that cardiac endothelial Dnmt3a under physiological conditions modulates the expression of genes related to cell division.

In addition, the effect on the lung endothelial transcriptome after the loss of endothelial Dnmt3a during vascular quiescence was assessed. For this purpose, lung ECs were isolated from Dnmt3a^{iECKO} and Dnmt3a^{WT} mice and bulk RNA-sequencing analysis was performed. In lung EC, differential gene expression analysis according to the described cut-off revealed 203 up-regulated and 115 down-regulated genes when comparing Dnmt3a^{iECKO} and Dnmt3a^{WT} (Fig. 27A). Significantly altered genes belonging to hallmark gene sets related to angiogenesis, myogenesis, coagulation, apical junction and epithelial-mesenchymal transition were observed when performing GSEA (Fig. 27B). In order to determine if the deletion of Dnmt3a had an effect on the lung capillary cell composition, an overlap analysis with markers previously described by Gillich et al. for different lung alveolar capillary cell populations was executed, comparing aerocytes and general capillaries markers with the differentially regulated genes in lung EC. Aerocytes or aCap are large and complex cells, unique to the lung that are specialized for gas exchange and have minimal proliferation capacity. General capillaries or gCap are smaller and less complex cells that resemble capillaries found in other organs, and are responsible for maintaining and repairing the alveolar endothelium due to their highly proliferative capacity[149]. There was no gene overlap between gCap markers and differentially regulated genes. However, 49% of the differentially up-regulated genes of Dnmt3a^{iECKO} overlap with aCap markers (Fig. 27C). This analysis was validated via qPCR by measuring the expression of a subset of the up-regulated aCap marker genes in independently sorted lung EC samples from Dnmt3a^{iECKO} and Dnmt3a^{WT} mice (Fig. 27D).

In summary, the data show that the lack of endothelial Dnmt3a in the healthy quiescent endothelium impacts the heart and lung transcriptome, despite not arising major organ morphological changes or functional impairments.

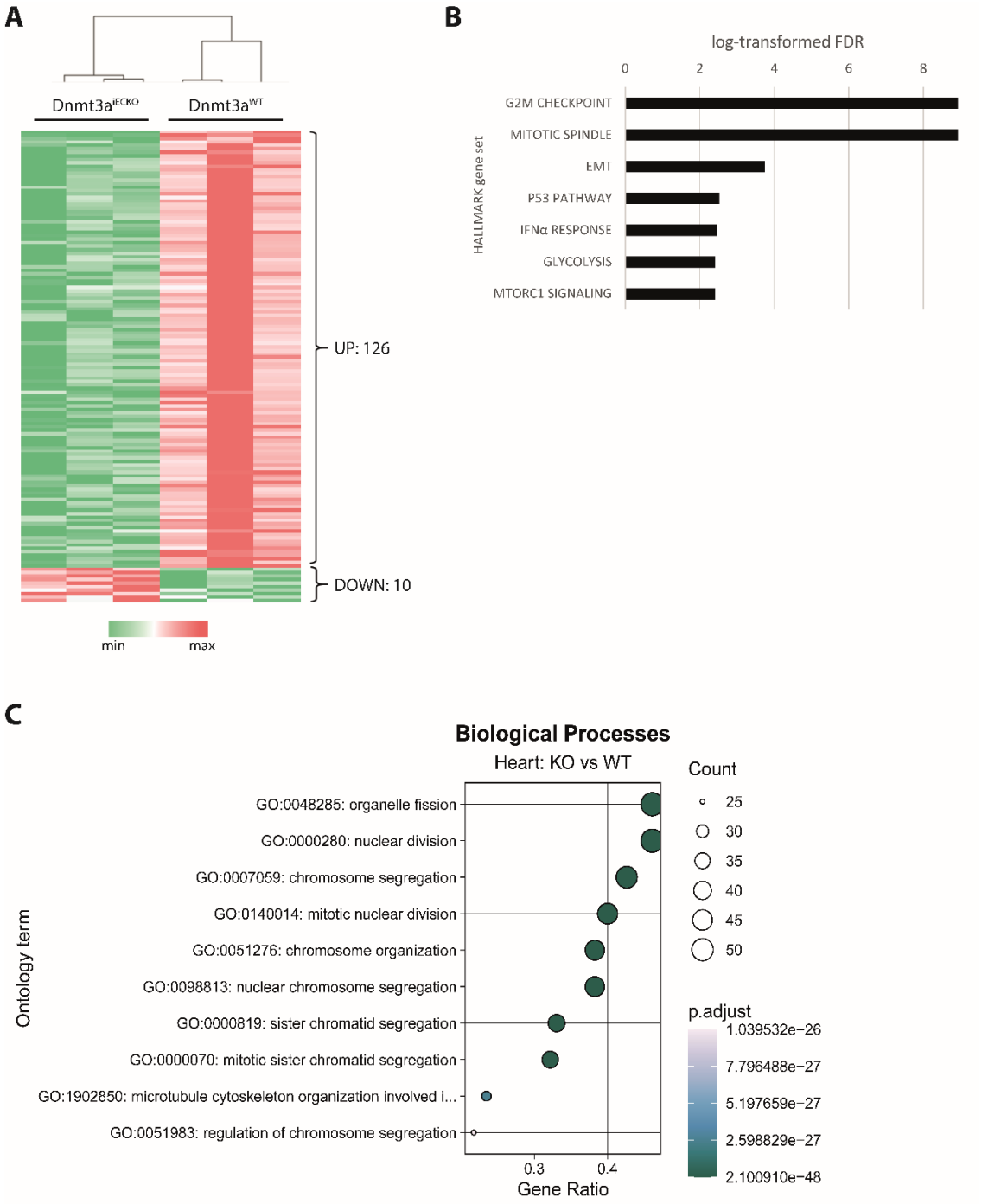

Figure 26: RNAseq analysis of the homeostatic heart endothelium from Dnmt3a^{iECKO} mouse.
(A) Heat map of differentially regulated genes between Dnmt3a^{iECKO} and Dnmt3a^{WT} mice. **(B)** GSEA hallmark analysis of the differentially regulated genes from the homeostatic heart endothelium between Dnmt3a^{iECKO} and Dnmt3a^{WT} mice. **(C)** Dot plot of the over representation analysis (ORA) of gene ontology of biological processes between Dnmt3a^{iECKO} and Dnmt3a^{WT} mice.

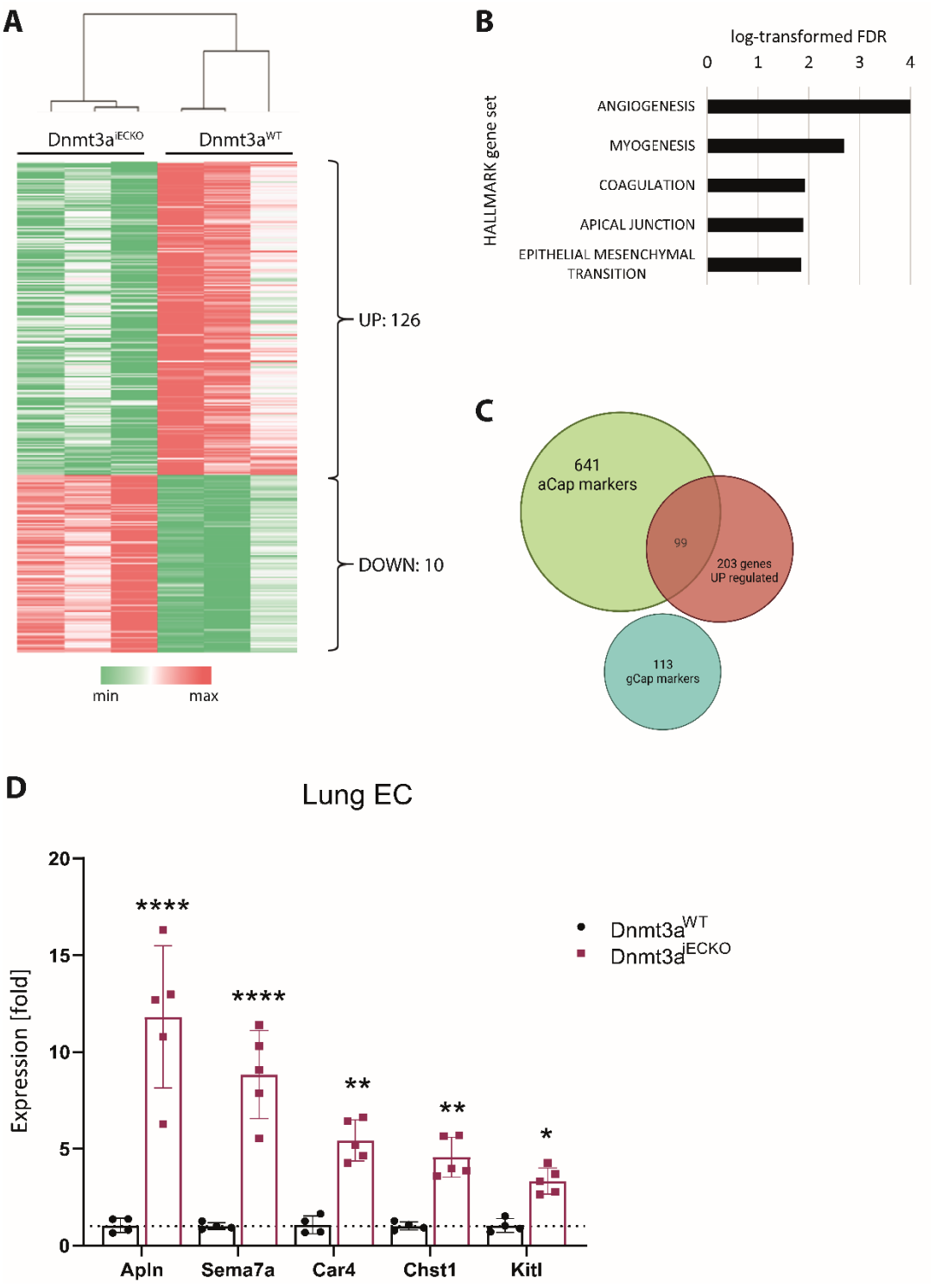

Figure 27: RNAseq analysis of the homeostatic lung endothelium from Dnmt3a^{iECKO} mouse.

(A) Heat map of differentially regulated genes between Dnmt3a^{iECKO} and Dnmt3a^{WT} mice. **(B)** GSEA hallmark analysis of the differentially regulated genes from the homeostatic lung endothelium between Dnmt3a^{iECKO} and Dnmt3a^{WT} mice. **(C)** Venn diagram of the overlap analysis between the defined aCap markers, gCap markers and differentially UP regulated genes of lung EC from Dnmt3a^{iECKO} mice. **(D)** Expression of a subset of aCap markers in independent samples of sorted homeostatic lung EC from Dnmt3a^{iECKO} and Dnmt3a^{WT} mice. Gene expression is normalized to *βActin* expression and to WT. Data are shown as mean±sd. (n=4-5; Two way ANOVA – Multiple comparisons).

4. Discussion

Vascular remodeling represents an adaptive mechanism to physiological alterations. However, when this mechanism is dysregulated, it results in pathological vascular re-activation – a key determinant of life-threatening diseases[16]. Pathological vascular re-activation is involved in tumor progression, CVDs and chronic inflammatory conditions, and it leads to impaired vascular function, formation of an aberrant vascular network and disease progression[16,26]. Numerous studies have focused on targeting different key molecules that regulate pathological vascular re-activation, with the purpose of developing anti-angiogenic therapies to tackle various diseases[150,151]. However, the results of these therapies in the clinic are deficient. Therefore, further research is necessary in order to generate novel, and improve current, strategies capable of effectively modulating this process to prevent, diagnose and treat endothelial dysfunction-driven pathologies. As epigenetic modifications are reversible, there is a growing interest to identify agents targeting epigenetic regulation to reprogram cells. Different epigenetic therapies to tackle cancer cells and other diseases have gone through clinical trials, and they primarily involve the regulation of DNA methylation and histone acetylation[152]. Since previous studies from our group identified the DNA methyltransferase DNMT3A as a potential epigenetic regulator in ECs, the present study employs a mouse model lacking Dnmt3a specifically in ECs to investigate if the interference with Dnmt3a-dependent DNA methylation affects vascular re-activation during cancer progression and obesity. The present study demonstrates that i) interfering with Dnmt3a during tumor-associated vascular re-activation impairs angiogenesis yet tumor development remains unchanged in the LLC tumor model, ii) endothelial loss of Dnmt3a alters obesity-induced cardiac hypertrophy, iii) Dnmt3a deletion in the endothelium facilitates obesity-induced diastolic dysfunction and cardiac fibrosis, and iv) disrupting endothelial Dnmt3a in healthy quiescent vasculature affects cardiac morphology, while inducing minimal effects on organ cross-morphology.

4.1 Dnmt3a deletion in EC decreases tumor vascularization

Tumor angiogenesis is a fundamental process for tumor growth, development and metastasis[29]. While the association between tumor angiogenesis and tumor development is widely acknowledged, it is important to note that there is not always a direct correlation between them. Indeed, there is evidence of cases in which tumor progression occurs without a significant simultaneous increase in angiogenesis[153,154]. It has been reported that tumors show the ability to switch from an angiogenic to a non-angiogenic phenotype, being one of the possible mechanisms for intrinsic or acquired drug resistance[29,154,155]. For example, in a model of hepatocellular carcinoma xenografts, upon treatment with the anti-angiogenic drug sorafenib, tumor cells switched from an

angiogenic to a non-angiogenic phenotype and exploited the pre-existent healthy liver vasculature to overcome the inhibition of angiogenesis[155]. Moreover, there is evidence that tumors comprise a mixture of non-angiogenic and angiogenic regions, or are completely non-angiogenic[154]. It has been described for breast cancer, melanoma, glioblastoma, ovarian and hepatocellular carcinoma that tumor cells can undergo a process called vascular mimicry. This process consist of tumor cell assembling into tubular structures, mimicking ECs, and attaching to existing blood vessels to form vascular-like channels[156-158].

In the present study, the deletion of endothelial Dnmt3a in an LLC tumor model did not affect tumor growth and development, even when reduced tumor vascularization and tumor endothelial proliferation was observed. This phenomenon may be attributed to the activation of alternative cellular mechanisms by tumor cells, facilitating the nutrient acquisition required for their proliferation and development. This is supported by the literature that describes vascular mimicry as a mechanism that promotes tumor growth, invasion and metastasis, and correlates with poor prognosis in various aggressive malignancies[156,158,159]. Moreover, previous studies have reported that subcutaneous injection of LLC cells results in highly vascularized tumors[31,160]. This phenomenon can lead to a surplus of blood vessels, transcending the actual requirements for tumor growth. Consequently, the tumor may continue to develop despite the reduction in vascularization. Is important to consider that in the course of this study, the tumors only grew to approximately 200mm^3 by the end of the experiment. This size may be considered small, which could potentially explain the reason why the impaired tumor vascularization was not a limiting factor in tumor development and growth at this stage. In concordance, comparable levels of apoptosis and hypoxia were observed in the primary tumor of Dnmt3a^{iECKO} and Dnmt3a^{WT} mice in the present study. Different investigations exploring the transcriptome of angiogenic and non-angiogenic tumors have demonstrated similar transcription and expression profiles of genes linked to hypoxia in these two tumor cell types. Demonstrating that the sensing of hypoxia and the expression of angiogenic factors by cancer cells do not always lead to new vessel formation[161-163]. The effect on vascularization observed in the primary tumor of Dnmt3a^{iECKO} mice suggests that the lack of Dnmt3a in the endothelium can partially impair endothelial re-activation as a consequence of the secreted growth factors and hypoxia in the primary tumor.

Given the intricate interplay between tumor development and angiogenesis, which can vary depending on the tumor type, stage and microenvironment, further experiments, including different tumor models, have to be performed in order to assess whether the comparable overall tumor development observed in Dnmt3a^{iECKO} mice arises from the activation of compensatory mechanisms, such as vascular mimicry or co-opting. Subsequent experimental assessment at a later

time point, aimed at increasing tumor size, may be performed to investigate potential disruptions in tumor development during advanced stages. Furthermore, the presence of tumor cell-lined vascular channels can be determined within the tumors derived from Dnmt3a^{iECKO} mice.

4.2 Obesity-induced cardiac hypertrophy is alleviated after endothelial deletion of Dnmt3a

Obesity can lead to various morphological changes in the heart. These changes occur as a response to the increased workload and metabolic alterations associated with the excess of nutrients. These include cardiomyocyte remodeling, cardiac hypertrophy, myocardial fibrosis, impaired flow of coronary microcirculation and myocardial lipid accumulation[49,70,164]. Obesity-associated cardiac remodeling can increase the risk of CVDs, such as hypertension, coronary artery disease and heart failure[164]. Cardiac hypertrophy corresponds to an increase in heart size and mass, and is a compensatory response to the increased workload on the heart such as elevated blood pressure, increased circulating volume and insulin resistance[134]. Multiple signaling pathways have been identified to participate in the regulation of cardiac hypertrophy induced by obesity. These include Rho-associated protein kinase pathway[165,166], inflammatory response[134], oxidative stress and autophagy[167]. In the present study, the endothelial deletion of Dnmt3a prevented obesity-induced cardiac hypertrophy after 8 weeks of HFD. Unlike Dnmt3a^{WT} mice, which exhibited an increased cardiac size in response to the diet, the Dnmt3a^{iECKO} mice did show a decreased heart size after the diet when comparing to the controls. These findings suggest that Dnmt3a may have a detrimental role in the development of pathological cardiac hypertrophy induced by obesity. Epigenetic regulation of cardiac remodeling has gained significant attention in recent years, with studies highlighting the role of epigenetic mechanisms in cardiac remodeling and their association with heart failure[168-170]. However, Dnmt3a^{iECKO} mice presented equivalent amounts of global DNA 5-mC and 5-HmC in cardiac ECs when compared to Dnmt3a^{WT} after obesity-induced inflammation in the current study. This may be attributed to a non-canonical function of DNMT3A[171]. It has been demonstrated that DNMT3A can interact with protein complexes, such as the polycomb repressive complexes 2 (PRC2), and through this interaction can contribute to the silencing of target genes[172-174]. Nevertheless, further research is necessary in order to decipher the non-canonical functions of DNMT3A, as well as their biological implications. Moreover, the methods used in this study to analyze the global DNA methylation differences between Dnmt3a^{iECKO} and Dnmt3a^{WT} mice do not provide a detailed and sensitive analysis of the methylation status of specific genes or regulatory regions. Alternative DNA methylation analyses, such as Whole Genome Bisulfide Sequencing, have to be performed in order to assess whether specific regions are differentially methylated upon the

deletion of Dnmt3a in obese mice. This analysis could give more insight into the molecular mechanism of Dnmt3a function in the heart.

In the present investigation, the lack of endothelial Dnmt3a led to reduced vascular density in the heart upon obesity-induced inflammation. Reduced cardiac vascularization has several biological implications that can affect cardiac function and contribute to the progression of CVDs[44,175]. These biological implications include impaired oxygen and nutrient delivery to cardiac cells, leading to hypoxia and the sequentially increase of inflammation, and fibrosis[175]. As previously noted in this study, the deletion of Dnmt3a in the endothelium resulted in impaired pathological endothelial re-activation in primary tumor. This suggests that the absence of endothelial Dnmt3a may present a challenge in the formation of new blood vessels in the heart as a response to the damage caused by obesity-induced inflammation.

4.3 Endothelial Dnmt3a modulates obesity-induced cardiac dysfunction

The abnormal lipid metabolism and accumulation of FFA in the bloodstream due to obesity produces inflammatory signals, increased oxidative stress and metabolic abnormalities, and these contribute to increased apoptosis in the heart, leading to cardiac damage and dysfunction[65,77,176]. Apoptosis contributes to the loss of CM and the disruption of the delicate balance between cell death and cell renewal. As CM possess limited regenerative capacity, excessive apoptosis can lead to fibrosis, impaired contractile function, and the development of cardiac dysfunction[177]. Myocardial fibrosis is characterized by the excessive collagen accumulation and formation of non-contractile scar tissue, reducing cardiac compliance and stiffening of the myocardium[49]. Is important to consider that obese Dnmt3a^{iECKO} mice presented an increased incidence of fibrosis but rather uniform extent of fibrosis. Suggesting that the loss of endothelial Dnmt3a may render mice to be more susceptible to developing fibrosis. The significant increase in cardiac apoptosis and incidence of fibrosis of Dnmt3a^{iECKO} obese mice seen in this study suggests that the adaptive response to the obesity-induced cardiac damage is impaired by the loss of Dnmt3a in the endothelium.

Additionally, the current study revealed impaired diastolic function in obese Dnmt3a^{iECKO} mice. This dysfunction is likely caused by the increased apoptosis and fibrosis resulting in cardiac stiffness and impaired relaxation. There is growing evidence that DNA methylation is associated with cardiac dysfunction and CVDs[178]. It was previously shown that global DNA methylation level is tightly associated with different CVDs, such as atherosclerosis and coronary artery disease[178], and that DNA methylation can be associated with cardiac hypertrophy and reduction of cardiac contractility[97,179]. Zhang et al. revealed that even though no global changes in DNA methylation were detected in the

heart of mice after chronic restrain stress (CRS), the methylation of specific genes associated with cardiomyopathy and signaling pathways of CM was altered. This suggests that CRS-induced cardiac remodeling and arrhythmia are produced through altered methylation of specific cardiac genes[180]. Despite this, there is still little evidence of the relationship between epigenetic modifications in the heart and cardiac dysfunctions. According to this notion, further experiments have to be performed in order to assess whether the cardiac dysfunction and fibrosis observed in Dnmt3a^{iECKO} obese mice is due to the loss of methylation of specific cardiac genes, or if corresponds to a secondary effect of the partial inhibition of the pathological re-activation of the cardiac endothelium.

4.4 The absence of Dnmt3a in the healthy quiescent endothelium has minimal effects

During development, the DNA methylation levels increase rapidly and then stabilize during adulthood. In healthy conditions, the methylation landscape remains stable over time and as individuals enter advanced age, there is a decrease in DNA methylation levels[181-185]. Natural loss of DNA methylation during life, particularly during aging, can have implications for gene regulation and disease susceptibility[181]. However, the extent of the impact and its effect on health may vary depending on various factors such as tissue-specific differences, genetics, and environmental factors[186]. During adulthood, the maintenance of stable methylation patterns is crucial for normal cellular function, gene expression and tissue homeostasis[186]. In the present study, the deletion of endothelial Dnmt3a in healthy adults did not affect the methylation landscape of lung and heart endothelial cells during physiological conditions. This observation is supported by the literature since the maintenance of a stable methylation landscape is essential for the normal functioning of healthy cells, and methylation patterns typically undergo modifications during cellular re-activation suggesting that DNMT3A function is not essential during homeostasis. In addition, while the heart of Dnmt3a^{iECKO} mice presented an increased size under physiological conditions, no significant changes were found in other morphological and functional aspects analyzed such as fibrosis, apoptosis, immune infiltration, and diastolic and systolic function. Suggesting that the impact of the deletion of Dnmt3a in the hearts of obese mice resulted from the pathological re-activation of ECs and that the healthy quiescent endothelium is not morphologically neither functionally affected by the endothelial deletion of Dnmt3a. These data along with the DNA methylation results, indicates that Dnmt3a deletion in the healthy quiescent endothelium does not impair vascular function.

Gene expression changes in lung and heart ECs from healthy Dnmt3a^{iECKO} mice were observed in this study, even when no changes in DNA methylation were detected. This may be attributed to the fact that gene expression is a complex process regulated by various elements, including chromatin

structure, transcription factors, and histone modifications[187]. While DNA methylation is a well-known epigenetic mechanism involved in gene regulation, it is not the only determinant. It has been demonstrated that other epigenetic modifications and regulatory elements can influence gene expression independently of DNA methylation[187]. For example, histone modifications can alter chromatin structure and the accessibility of the transcriptional machinery, and transcription factors can bind to specific DNA sequences in gene promoters and enhancer regions influencing gene expression[92,187,188]. These mechanisms can act independently of the DNA methylation status and regulate gene expression in a dynamic and context-specific manner. Upon the deletion of Dnmt3a under physiological conditions, a shift in the identity of lung EC was observed as a result of the overexpression of aCap markers. This phenomenon is potentially due to the role of gCap cells of repairing and maintaining the lung vasculature following injury[149]. Prior results from this study showed that the deletion of Dnmt3a impacts the proliferation and vascularization capacity of ECs during pathological conditions, suggesting that a non-proliferative phenotype is promoted during physiological conditions leading to a shift in the population of the lung vasculature towards an aCap identity. However, the overall effects of the interference with Dnmt3a-dependent DNA methylation in the transcriptome of healthy lung and heart EC observed in the present study are minimal.

Overall, the present study has revealed that the activity of endothelial Dnmt3a plays an important role in angiogenesis and vascularization during pathological vascular re-activation, identifying it as an interesting target to study for drug intervention. Nonetheless, it is important to note that the deletion of Dnmt3a in pathological settings can lead to organ-specific side effects, requiring further investigation.

5. Materials

5.1 Chemicals

Table 1 Chemicals

Company
AppliChem (www.appliedchem.com)
Carl Roth (www.carl-roth.de)
Gerbu (www.gerbu.de)
Merck (www.merk.de)
Roche (www.roche-apllied-science.com)
Sigma-Aldrich (www.sigmaaldrich.com)
Thermo Fisher Scentific (www.thermofisher.com)

5.2 Cell digestion reagents

Table 2 Cell digestion reagents

Reagent	Company
DMEM/F12	Thermo Fischer Scientific
Fetal calf serum (FCS), heat inactivated	PAA Laboratories
Collagenase I	Merck
Dispase	Merck
Liberase	Roche
DNAseI	Roche

5.3 Primers and Oligonucleotides

5.3.1 Genotyping primers

Table 3 Genotyping primers

Genotype	Primer name	Sequence
$Dnmt3a^{flox/flox}$	Dnmt3a for	CTGGTGATTGGAGGCAGTCCATGCA
	Dnmt3a rev	TAGCTGAGGCTGTCTGCATCGGACA
$Cdh5\text{-}Cre^{ERT2}$	Cre for	CAGGGTGTTATAAGCAATCCC
	Cre rev	CCTGGAAAATGCTTCTGTCCG
	Actin for	CAATGGTAGGCTCACTCTGGGAGATGATA
	Actin rev	AACACACACTGGCAGGACTGGCTAGG

5.3.2 TaqMan™ probes for RT-qPCR

All TaqMan™ probes were purchased from Thermo Fisher Scientific

Table 4 TaqMan™ probes for RT-qPCR

Target gene (ms)	Ordering number
Actb	Mm00607939_S1
Dnmt3a	Mm00432881_m1
Apln	Mm00443562_m1
Sema7a	Mm00441361_m1
Car4	Mm00483021_m1
Chst1	Mm01334076_m1
Kitl	Mm00442972_m1

5.4 PCR/RT-qPCR reagents

Table 5 PCR/RT-qPCR reagents and buffers

Reagent	Company
Direct PCR lysis Reagent	PeqLab
DNase/RNase free H2O	Gibco
RedTaq® ReadyMix™ PCR Reaction Mix	Sigma Aldrich
Taq DNA polymerase (5U/µl)	Qiagen
TaqMan™ Fast Advanced Master Mix	Thermo Fisher Scientific

5.5 Company kits

Table 6 Company kits

Reagent	Company
Arcturus PicoPure RNA Isolation Kit	Thermo Fisher Scientific
GenElute™ Total RNA purification Kit	Merck
Global DNA methylation ELISA kit	Abcam
Global DNA hydroxymethylation ELISA kit	Abcam
Quantitect Reverse Transcription Kit for cDNA Synthesis	Qiagen
QIAamp DNA Micro Kit	Qiagen
Trichrome Stain (Masson) Kit	Sigma Aldrich

5.6 Immunohistochemistry

5.6.1 Primary antibodies

Table 7 Primary antibodies

Antigen	Reactivity	Species	Conjugate	Dilution	Source (cat.no)
CD45	mouse	rat	FITC	1:400	BD Biosciences (553080)
Ter119	mouse	rat	FITC	1:200	BD Biosciences (557915)
Lyve-1	mouse	rat	AF-488	1:250	eBioscience (53-0443)
Podoplanin	mouse	hamster	AF-488	1:100	eBioscience (53-5381-82)
CD31	mouse	rat	APC	1:100	BD Pharmingen (551262)
CD34	mouse	rat	PacificBlue	1:50	eBioscience (48-0341)
CD31	mouse	rat	-	1:100	BD Bioscience (557355)
Desmin	mouse	rabbit	-	1:100	Abcam (ab15200-1)
Ki67	mouse	rabbit	-	1:100	BETHYL Laboratories (IHC-00375)
cCas3	mouse	rabbit	-	1:100	Cell Signaling (9661)
pH2AX	mouse	rabbit	-	1:300	Cell Signaling (9718)
GLUT1	mouse	rabbit	-	1:200	Abcam (ab115730)
WGA	-	-	Texas red	1:100	Invitrogen (W21405)
Isolectin B4	-	-	AF-488	1:100	Invitrogen (I21411)
Collagen I	mouse	rabbit	-	1:100	Biotrend (BT21-5014-10)
Collagen III	mouse	rabbit	-	1:100	Abcam (ab7778)
CD45	mouse	rat	-	1:100	Invitrogen (RM2604)

5.6.2 Secondary antibodies

Table 8 Secondary antibodies

Reactivity	Species	Conjugate	Dilution	Source (cat.no)
Rat IgG	Goat	AF-488	1:200	Life technologies (A21049)
Rabbit IgG	Goat	AF-546	1:500	Life technologies (A31556)

5.6.3 Staining reagents

Table 9 Staining reagents

Staining	Company
CD31 MicroBeads, mouse	Thermo Fisher Scientific
Direct Red 80 (Sirius Red solution)	Sigma Aldrich
Eosin	Sigma Aldrich
Fluorescence mounting medium	DAKO
Hemalaun	Sigma Aldrich
Histomount	Invitrogen
Hoechst Dye 33258, 1mg/ml	Merck
Normal goat serum ready-to-use (10%)	Zymed
Propidium Iodide Staining Solution	Invitrogen
Proteinase K	Gerbu
Roti-Histofix 4% (pH 7)	Carl Roth
Sucrose	Merck
Tissue-Tek O.C.T.™ Compound	Scigen
Triton X-100	Thermo Fisher Scientific
Paraffin / TE-Buffer / Tween / EtOH / Xyleno / Methanol / Acetic Acid	

5.7 Reagents for animal experimentation

Table 10 Reagents for animal experimentation

Reagent	Company
Bepanthen® eye cream	Roche
Ketavet	Pfizer
NaCl solution	Braun
Rompun	Bayer
Sevofluran	Baxter
Shaving cream	veet
Tamoxifen	Merck
Ultrasound gel	Parker Laboratories
Western diet 1.25% cholesterol (EF-TD88137)	Ssniff Spezialdiäten

5.8 Solutions and Buffers

Table 11 Solutions and buffers

Buffer		Composition
Ammonium chloride potassium buffer (ACK)	150 mM 10 M 100 mM	NH4Cl KHCO3 Na2EDTA adjust pH 7.2-7.4
Phosphate buffered saline (PBS)	1.34 M 27 mM 200 mM 4.7 mM	NaCl KCl Na2HPO4 KH2HPO4 adjust pH 7.4
Tris-Buffered Saline Tween-20 (TBS-T)	10 mM 100 mM 0.1%	Tris/HCl, pH 7.5 NaCl Tween-20
FACS Buffer	3% (v/v)	Fetal calf serum in PBS
TE-Buffer	10 mM 1 mM	Tris Na2EDTA adjust pH 8.0

5.9 Consumables

Table 12 Consumables

Consumables	Company
96 well plates	Steinbrenner Laborsystem
384 well plates	4titute
Cannula (18G, 19G, 27G, 30G)	BD
Cell culture dishes (10cm, 15cm)	TPP
Cell strainer (100 µm)	BD Biosciences
Countess™ cell counting chamber slides	Thermo Fisher Scientific
Cryotubes	Carl-Roth
FACS tubes	BD Biosciences
Filter containing pipette tips	Biozym
Freezing box	Thermo Scientific
Insulin syringe	BD
MS Columns MACS®	Thermo Fisher Scientific
Microscope cover glasses	VWR international
Microscope glass slides	Menzel-Gläser
Peel-A-Way™ Embedding Molds	Merck

Pipette tips	Nerbe
qPCR plates (96-well)	Biozyme
qPCR plates (384-well)	Roche
Reaction tubes (0.5ml, 1.5ml, 2ml)	Eppendorf
Reaction tubes (15ml, 50 ml)	Greiner
Sealing foil	Applied Biosystems
Sterile pipettes	Corning
Syringes	Dispomed
Tissue cultures 6-well plates	Greiner

5.10 Equipment

Table 13 Equipment

Equipment	Company
Aria cell sorting platform	BD Bioscences
Axio ScanZ7.1 slide scanner	Zeiss
Cell culture hood	Thermo Fisher Scientific
Cell culture incubator	Thermo Fisher Scientific
Centrifuge	Thermo Fisher Scientific
Countess™ automated cell counter	Thermo Fisher Scientific
Digital Electronic Caliper	Fine Science Tools
Freezing box	Thermo Fisher Scientific
Heating block	Eppendorf
HM3551 microtome	Thermo Fisher Scientific
Light cycler 480	Roche
iMark™ Microplate Reader	BioRad
Magnetic stand	Thermo Fisher Scientific
Microtome Hyrax C50	Zeiss
MACS Magnetic separators	Miltenyi
Multistep pipette	Eppendorf
Mr. Frosty Freezing Container	Thermo Fisher Scientific
NanophotometerR N60	INTAS
Novaseq 6000	Illumina
Olympus IX 71	Olympus
Pipettes	ErgoOne
QIAxcel Advanced System Qiagen	Qiagen

QuadroMACS Separator	Miltenyi Biotech
Scale	Ohaus
Special accuracy weighing scale	Mettler Toledo
StepOnePlus Real-Time PCR System	Thermo Fisher Scientific
Shaver	Moser
Surgery and dissection tools	Fine Science Tools
Table centrifuge (5417R)	Eppendorf
Thermocycler	Applied Biosystems
Vevo 3100	Visualsonics
Vortex	Neolab
Water bath	Julabo

5.11 Cell culture reagents

Table 14 Cell culture reagents

Reagent	Company
Dimethylsulfoxide (DMSO)	AppliChem
Dulbecco's Modified Eagle medium – Glutamax	Thermo Fisher Scientific
Dulbecco´s phosphate buffered saline (PBS)	PAA
Fetal Calf Serum (FCS, heat inactivated)	PAA
Penicillin/streptomycin (100x 104U/10mg/ml)	PAA
Trypan blue	Gibco
Trypsin-EDTA (10x)	Sigma Aldrich

5.12 Software

Table 15 software

Software	Company
Fiji	ImageJ
FlowJo	Miltenyi Biotec
FACSDiva™	BD Biosciences
Biorender	www.biorender.com
Light Cycler 480 software	Roche
Microsoft office	Microsoft
Prism	Graph Pad
Gene Set Enrichment Analysis	Broad Institute

Ingenuity Pathway Analysis	Qiagen
ZEN blue	Zeiss

6. Methods

6.1 Mouse experimentation

6.1.1 Animal welfare

Mice in C57BL/6 background with inducible deletion of *Dnmt3a* gene were obtain from RIKEN BioResource Center (No. RBRC03731). To generate Dnmt3a$^{flox/flox}$ mice, a Cre/loxP system to induce conditional deletion of the exon 19 that encodes the conserved PC motif of the catalytic domain of Dnmt3a was used[146]. Dnmt3a$^{flox/flox}$ mice were crossed with *Tg(Cdh5-cre/ERT2)1Rha* (Cdh5CreERT2) mice to specifically delete endothelial *Dnmt3a* gene (Table 16). Induction of Cre recombination was carried out by administration of tamoxifen according the protocol indicated on each experiment. Animals were housed in sterile cages maintained in temperature controlled rooms and had access *ab libitum* autoclaved food and water. All animals were monitored daily for signs of illness. Mice were euthanized via rapid cervical dislocation of spinal cord unless stated otherwise. Part of the tail was taken for re-genotyping. All animal experiments were carried out according to the guidelines of the local Animal Use and Care Committees and were approved by the local regulatory committee Bezirksregierung Karlsruhe, Germany (G283/18 and G76/19).

Table 16 In-house mouse lines

GOI	Short name	Full name	Induction	Purpose
Dnmt3a	Dnmt3a^{iECKO}	B6;129S4-Dnmt3atm3.1Enl Tg(Cdh5-cre/ERT2)1Rha / Aug	5x2mg tamoxifen	Endothelial cell-specific *Dnmt3a* deletion

6.1.2 Cre recombination induction

To induce *Dnmt3a* deletion in the Dnmt3a^{iECKO} mouse line, both control and mutant animals were intraperitoneally treated with five doses of 2mg tamoxifen (Merck) dissolved in ethanol/peanut oil.

6.1.3 Tumor implantation

1x10^6 LLC cells were inoculated subcutaneously in 6-8 weeks old female Dnmt3a^{iECKO} mice. Two weeks post tumor implantation, mice were sacrificed and primary tumors samples were collected for further processing. All mice were regularly monitored for humane endpoint criteria. Tumor volumes were measured with a digital caliper and tumor volumes were calculated using the following formula (volume = ½ length x width x height).

6.1.3.1 LLC cell culture

LLC were obtained from ATCC. The cells were cultured in DMEM high glucose (Gibco) supplemented with 10% FCS, 1% penicillin/streptomycin (Sigma) and 1% non-essential amino acid (Gibco). For passaging, 80-90% confluent cells were washed with PBS and were detached by Trypsin-EDTA incubation at 37°C for 2 min. Next, culture medium was added to neutralize Trypsin-EDTA and the cells were centrifuged for 5 min at 200 g. The supernatant was discarded, the pellet was resuspended in culture medium and the desired cell dilutions (1: 10) were prepared.

6.1.4 High fat diet-induced inflammation

6-8 weeks old male Dnmt3a^{iECKO} mice were fed with a high fat diet (Western diet 1.25% cholesterol, Ssniff Spezialdiäten, diet EF-TD88137) for 8 weeks. During this time, the body weight of the animals was checked twice a week by weighing. The mice were deprived of food for 5 hours prior sacrifice and blood and tissue samples were collected for further processing. All mice were regularly monitored for humane endpoint criteria. Only male animals were used for this experiment in order to exclude influences of the female cycle, and a more quickly development of a phenotype due to a high-fat diet.

6.1.5 Echocardiography

Dnmt3a^{iECKO} male mice fed with HFD during 8 weeks were anesthetized in a whole-body chamber with 3-4% sevoflurane and an airflow of 1 L/minute. The ventral thorax was shaved and lined with ultrasound gel and anesthesia was maintained using a mask (sevoflurane 1.5%, airflow 1 L/min). The left ventricular function, heart size and heart mass were then determined via non-invasive echocardiography using a 40-70 MHz transducer (Vevo 3100, Visualsonics).

6.2 Molecular biology methods

6.2.1 Genotyping PCR

Genotyping from mouse tissue was performed by PCR of genomic DNA. Tail tips were incubated in 100µL Direct PCR Reagent + 10µg Proteinase K at 55^{o}C overnight followed by 20 min at 95^{o}C for enzyme inactivation. Tail tip lysates were used directly or were stored at -20^{o}C until genotyped.
Genotyping was performed using the Taq polymerase kit (Qiagen). The PCR reaction was run with an Applied Biosystems thermocycler and analyzed with the QIAxcel Advanced system according to the manufacturer's instructions.

Table 17 Dnmt3a$^{flox/flox}$ genotyping PCR mix and program

Dnmt3a$^{flox/flox}$ genotyping PCR mix		**Genotyping PCR Program**		
	1x	Step	Temperature	Time
dd H2O	11.6 µL	1	94°C	3’
5x Q-Solution	4 µL	2	94°C	30”
10X Buffer	2 µL	3	60°C	30”
MgCl2	0.8 µL	4	72°C	1’
dNTP	0.5 µL	5	72°C	5’
Dnmt3a flox for (10µM)	0.25 µL	6	4°C	hold
Dnmt3a flox rev (10µM)	0.25 µL			
Taq	0.1 µL			
DNA	1 µL			

x35

Table 18 Cdh5-CreERT2 genotyping PCR mix and program

***Cdh5-CreERT2* genotyping PCR mix**		**Genotyping PCR Program**		
	1x	Step	Temperature	Time
dd H2O	15.1 µL	1	94°C	2’
10x Buffer	2 µL	2	94°C	30”
MgCl2	0.8 µL	3	58°C	45”
dNTP’s	0.4 µL	4	72°C	2’
MB182R Actin (10µM)	0.4 µL	5	72°C	2’
MB182R Actin (10µM)	0.4 µL	6	4°C	hold
MB183R Cre (10µM)	0.4 µL			
MB183F Cre (10µM)	0.4 µL			
Taq	0.1 µL			
DNA	1 µL			

x35

6.2.2 RNA Isolation

RNA isolation on sorted ECs was performed with the Arcturus™ PicoPure™ RNA isolation Kit (Thermo Fisher Scientific, KIT0204). Sorted cells were centrifuged at 500 g and 4°C for 8 min to form a pellet which was then lysed by 100 µL Arcturus PicoPure extraction buffer. The protocol was performed according to manufacturer’s instructions. RNA was eluted in 12µL RNase free H2O and concentration was measured via NanoPhotometer® N60. The RNA was stored at -80°C.

6.2.3 cDNA synthesis

cDNA generation was carried out using the Quantitect® Reverse Transcription Kit (Qiagen) according to manufacturer's instructions. Template RNA was thawed on ice and 1 µg RNA was incubated with 2 µL x DNA Wipeout buffer for 2min at 42°C and the total volume was adjusted to 14 µL adding RNase-free H2O. The mixture was further incubated with 1 µL reverse transcriptase, 4 µL 5xRT-buffer and 1 µL RT Primer mix at 42°C for 30min for reverse transcription and 95°C for 3min for inactivation of the enzyme. The cDNA was diluted 1:10 in H2O for qPCR reaction. cDNA was kept in -20°C for short term storage.

6.2.4 Quantitative Real Time-PCR (RT-qPCR)

Relative gene expression was quantified by RT-qPCR based on synthesized cDNA. RT-qPCR was performed by using the synthesized cDNA with TaqMan Fast Advanced Mastermix (Life Technologies) and TaqMan probes (Applied Biosciences) on a StepOnePlus Real-Time PCR System (Thermo Fisher Scientific). Each reaction was performed in triplicates.

Table 19 TaqMan™ RT-qPCR reaction mix

TaqMan™ RT-qPCR reaction mix	
cDNA (1:10 dilution)	3 µL
Taqman™ Fast Advanced Master Mix	5 µL
TaqMan™ probe	0.5 µL
ddH_2O	1.5 µL

Table 20 TaqMan™ RT-qPCR program

TaqMan™ RT-qPCR program		
Step	Temperature (°C)	Time (sec)
Pre-denaturation	95	30
Denaturation	95	2
Amplification	60	20

For analysis, the ΔΔCt method was applied as described in literature[189]. This is done by normalizing CT values of the genes of interest to the CT values of the housekeeping gene for each sample (ΔCT).

$$\Delta CT = CT_{\text{gene of interest}} - CT_{\text{housekeeping gene}}$$

The normalized CT valued were then further normalized to CT values of control samples (ΔΔCT).

$$\Delta\Delta CT = \Delta CT_{\text{sample of interest}} - \Delta CT_{\text{control sample}}$$

Respective fold changes were calculated from the ΔΔCT values.

$$\text{Fold change} = 2^{-\Delta\Delta CT}$$

6.2.5 DNA extraction

DNA isolation on FACS-sorted endothelial cells was performed with the QIAamp DNA Micro Kit (QIAGEN, 56304). Sorted cells were centrifuged at 500 x g at 4°C for 8 min to form a pellet which was then lysed by 300 µL of Buffer ATL and equilibrate to RT. The mixture was further incubated with 200 µL of provided Proteinase K and mixed by pulse-vortexing for 15 sec. The protocol was performed according to manufacturer's instructions. DNA was eluted in 25µL ddH2O and concentration was measured via NanoPhotometer® N60. The DNA was stored at -20°C.

6.2.6 Methylation array

Lung ECs from Dnmt3a^{iECKO} mice were FACS-sorted and total DNA was isolated using QIAamp DNA Micro Kit (QIAGEN, 56304) according to the manufacturer's protocol. Genome-wide screening of DNA methylation patterns was performed using the Infinium™ Mouse Methylation 285k BeadChip (Illumina, San Diego, US) with 400 ng of base material. The quality of genomic DNA samples was checked and samples with an average fragment size > 3kb were selected for methylation analysis. The laboratory work and data processing was done in the Microarray Core Facility at the German Cancer Research Center, Heidelberg, Germany (DKFZ).

6.2.7 Bulk RNA sequencing and data analysis

Lung and heart ECs from Dnmt3a^{iECKO} mice were FACS-sorted and total RNA was isolated using Arcturus PicoPure RNA isolation kit (Thermo Fisher Scientific) according to the manufacturer's protocol. The sequencing libraries were prepared using SMARTer Ultra Low RNA v4 Kit (Clontech) with 10 ng of base material and sequenced on Novaseq 6000 S1 (100-bp paired-end). The RNA sequencing data was processed and aligned using the DKFZ OTP RNAseq workflow (Reisinger et al., 2017). Raw RNA-seq data was initially aligned to the mouse reference genome (mm10) and differential gene counts as normalized to the gene length and overall coverage was calculated per

sample. Following quality control, genes with Reads Per Kilobase of transcript, per Million mapped reads (RPKM) ≥ 1 in at least one of the samples were considered for further analysis. Differential gene expression analysis was performed using DESeq2 and the downstream gene set enrichment analysis was conducted employing clusterProlifer 4.0 (Love et al., 2014; Wu et al., 2021).

6.3 Tissue staining

6.3.1 Preparation of cryoblocks and cryosections

Excised tissues and tumors were embedded in TissueTek O.C.T. compound (Sakura) on dry ice. Subsequently, samples were stored at -80°C. The cryomicrotome Hyrax C50 (Zeiss) was used to cut 5-7 µm cryosections. Sections were dried for 10 min at RT and subsequently stored at -80°C.

6.3.2 Preparation of paraffin blocks and paraffin sections

Excised tissues and tumors were fixed in zinc-fixative over night at 4 °C. Next day, samples were washed with VE-water and further processed with the spin tissue processor STP120. Automated steps included incubations in a graded ethanol series (70-85-96 %), isopropanol, xylol and paraffin. Thereafter, samples were manually embedded in paraffin blocks. 7µm sections were cut using the rotary microtome HM355S.

6.3.3 Immunofluorescence

Cryosections were fixed in ice-cold methanol (-20°C) for 10 min. Paraffin sections were dewaxed and rehydrated by consecutive incubations in a graded ethanol series, washed two times in VE-water and incubated in 20ng/µL of Proteinase K (Gerbu) in TE-buffer pH 8.0 for 5 min at 37°C. Afterwards, sections were washed and blocked in 10% ready-to-use normal goat serum (Life Technologies) for 1h. The primary antibody was incubated overnight at 4°C. After primary antibody incubations, the sections were washed three times in TBS-T for 5 min each and incubated with the secondary antibodies for 1h at RT. Next, sections were washed three times with TBS-T for 5 min. Afterwards, Hoechst staining (1:5000, Merck) was performed and sections were mounted with DAKO mounting medium (Agilent).

6.3.4 Histochemistry

6.3.4.1 Hematoxylin and eosin staining

Paraffin sections were dewaxed and rehydrated by consecutive incubations in a graded ethanol series. Afterwards, slides were washed two times in VE-water and incubated in freshly filtered hemalaun for 4 min, washed with running tap water for 10 min, washed in VE-water and stained with 1% ethanoic eosin for 2 min. Following three times of washing with VE-water, sections were dehydrated by dipping them into graded ethanol series (70%-80%-99%), isopropanol and xylol. Slides were mounted with Histomount and whole area bright field images were acquired with the Zeiss Axio ScanZ.1.

6.3.4.2 Masson's trichrome

Paraffin sections were dewaxed and rehydrated by consecutive incubations in graded ethanol series. Afterwards, slides were stained using Masson Trichrome Stain Kit (Sigma-Aldrich, HT15) according to the manufacture's protocol. Sections were dehydrated by dipping them into graded ethanol series (70%-80%-99%), isopropanol and xylol. Slides were mounted with Histomount and whole area bright field images were acquired with the Zeiss Axio ScanZ.1.

6.3.4.3 Sirius Red

Paraffin sections were dewaxed and rehydrated by consecutive incubations in a graded ethanol series. Afterwards, slides were washed two times in VE-water and incubated in freshly filtered hemalaun for 8 min, washed with running tap water for 10 min, washed in VE-water and stained with sirius red for 1 h. Following two times of washing with 0.5% Acetic acid in distilled water, sections were dehydrated by dipping them into graded ethanol series (70%-80%-99%), isopropanol and xylol. Slides were mounted with Histomount and whole area bright field images were acquired with the Zeiss Axio ScanZ.1.

6.3.5 Pathologist analysis

H&E, Masson's trichrome and Sirius red-stained sections were blindly analyzed by a board-certified pathologist (C. Mogler, TUM,Munich, Germany).

6.3.6 Image acquisition and analysis

Fluorescent imaged were acquired via Zeiss Axio Scan at the imaging core facility of the DFKZ. Image analysis was performed with Fiji.

6.4 Biochemistry methods

6.4.1 Fluorescence activated cell sorting (FACS)

To isolate ECs, tissue and tumors were enzymatically digested using the reagents concentrations listed on the table 21 in DMEM/F12 media at 37°C for 30min. Tissue lysates were passed through an 18G cannula syringes and incubated another 15 min at 37°C. Tissue lysates were passed through a 19G cannula syringes and further filtered through 100µM filters. To lyse erythrocytes, the tissue lysates were incubated with ammonium chloride potassium (ACK) lysis buffer for 5min and the cell suspension was subsequently washed with PBS/5% FCS. Next, positive selection using CD31 microbeads (Miltenyi Biotec) was performed to enrich the EC according to the manufacturer's protocol. Endothelial cells were further FACS-sorted for the surface marker profile CD45-/LYVE1-/PDPN-/TER-119-/CD31+/CD34+ using the antibodies listed in table 7. To exclude dead cells, the cells were stained with Propidium Iodide (PI). Cell populations were sorted using FACS Aria cell sorter and FACS Fusion cell sorter. Single stained and unstained controls were used for compensation and correct gating strategy. Cells were pre-gated to distinguish debris and doublets using FSC and SSC. FACS-sorted endothelial cells were centrifuged at 500 x g for 9min at 4°C and the pellet was stored at -80°C.

Table 21 Digestion mix for FACS

	Lung	Heart	Tumor
	1x	1x	1x
CaCl (1M)	7.4 µL	-	-
Collagenase I	2.5 mg	-	-
Dispase	11 mg	6.6 mg	0.5 mL
2% DNAseI	5 µL	3 µL	3 µL
DMEM/F12	5 mL	3 mL	-
Liberase	-	-	4.5 mL

6.4.2 ELISA

Methylated and hydroxymethyalted DNA levels in DNA isolated from FACS-sorted lung and heart ECs were determined using either global DNA methylation (Abcam, ab233486) or global DNA hydroxymethylation (Abcam, ab233487) ELISA kits, according to the manufacture's protocol. DNA was isolated as previously described in section 6.2.5. The Absorbance at 450 nm was recorded on an iMark™ Microplate Reader.

6.4.3. Serum collection

Blood was collected into 1.5ml Eppendorf tubes from the heart of anesthetized mice. The tubes were left undisturbed for 30min at RT and then centrifuged at 1.500 x g for 10min at 4^{o}C. The resulting supernatant was removed and stored at -20^{o}C until used for the serum analysis.

6.5 Statistical analysis

Statistical analysis was carried out via GraphPad Prism 8 (GraphPad Software). Data are illustrated as mean ±SD. Statistical significance between experimental groups was determined using two-tailed Student's t-test, Mann-Whitney test or Two way ANOVA, Multiple comparisons as indicated in figure legends. T-test values ≤0.05 were considered statistically significant. *=P<0.05, **= P<0.01 and ***= P<0.001.

7. Abbreviations

5-Hmc	5-hydroxymethylcytosine
5-mC	5-methylcytosine
aCap	Aerocytes
AF	Alexa-Fluor
AML	Acute myeloid leukemia
Ang	Angiopoietin
C	Celsius
C57BL/6	C57 Black 6
CAFs	Cancer associated fibroblasts
cCas3	Cleaved caspase 3
CCL2	Chemokine ligand 2
CD31	Cluster of differentiation 31
Cdh5	Cadherin 5
cDNA	Complementary DNA
CDVs	Cardiovascular diseases
CIF	Cardiac interstitial fibrosis
CM	Cardiomyocyte
CRS	Chronic restrain stress
CSF1	Colony stimulating factor 1
CT	Threshold Cycle
DMSO	Dimethylsulfoxide
DNA	Desoxyribonucleic acid
DNase	Deoxyribonuclease
$Dnmt3a^{iECKO}$	Dnmt3a inducible endothelial cells knock out
DNMTs	DNA methyltransferases
EC	Endothelial cell
ECM	Extrcellular matrix
ELISA	Enzyme-linked Immunosorbent Assay
EndMT	Endothelial-Mesenchymal transition
eNOS	endothelial nitric oxide synthase
EVs	Extracellular vesicles
FACS	Fluorescent activated cell sorting
FCS	Fetal Calf Serum

FGF	Fibroblast growth factor
FITC	Fluorescein thioisocyanate
FFA	Free fatty acids
g	Gram
g	Gravity (centrifugation context)
gCap	General capillary
γH2AX	H2A histone family member X
GLS	Global longitudinal strain
GLU1	Glucose transporter 1
GSEA	Gene set enrichment analysis
h	Hour(s)
H&E	Hematoxylin/Eosin
H_2O	Water
H3K27me3	Tri-methylation of lysine 27 on histone H3
HFD	High fat diet
HIF1α	Hypoxia Inducible Factor 1a
HSCs	Hematopoietic stem cells
i.p	Intraperitoneally
ICAM	Intercellular adhesion molecule
iECKO	Inducible endothelial cell knock-out
IHC	Immunohistochemistry
IL	Interleukin
l	Liter
LLC	Lewis Lung Carcinoma
M	Molar
mRNAs	microRNAs
mAb	Monoclonal antibody
MAPK	Mitogen-activated protein kinase
MCP-1	Monocyte chemoattractant protein-1
MDS	Myelodysplastic syndromes
min	Minute(s)
mm	Millimeter
MMP	Matrix metalloproteinase
ms	Mouse

NFKB	Nuclear Factor kappa-light chain enhancer of activated B cells
nm	Nanometer
NO	Nitric oxide
ORA	Over representation analysis
PBS	Phosphate buffered saline
PCR	Polymerase chain reaction
PDGF	Platelet derived growth factor
PFA	Paraformaldehyde
pH	Power of hydrogen
PRC2	Polycomb repressive complex 2
qRT-PCR	Quantitative real time polymerase chain reaction
rev	Reverse
RNA	Ribonucleic acid
RNase	Ribonuclease
ROS	Reactive oxygen species
RPKM	Reads Per Kilobase of transcript, per Million mapped reads
rpm	Rounds per minute
RT	Room temperature
SD	Standard deviation
SMC	Smooth muscle cells
TAM	Tamoxifen
TAMs	Tumor associated macrophages
TBS-T	Tris buffered saline with Tween
TGFβ	Transforming growth factor β
THBS1	Thrombospondin 1
Tie	Tyrosin kinase with immunoglobulin-like and EGF-like domain
TIMPs	Tissue inhibitors of metalloproteinases
TLR	Toll like receptor
TNF-α	Tumor necrosis factor α
TUNEL	Terminal deoxynucleotidyl transferase dUTP nick end labeling
U	Unit
v/v	Volume/Volume
VCAM	Vascular cell adhesion molecule
VE-Cadherin	Vascular endothelial cadherin

VEGF	Vascular endothelial growth factor
VSMC	Vascular smooth muscle cells
WB	Western blot
WHO	World health organization
WR	Working reagent
WT	Wildtype
WGA	Wheat germ agglutinin

8. References

1 Augustin, H. G. & Koh, G. Y. Organotypic vasculature: From descriptive heterogeneity to functional pathophysiology. *Science* **357**, eaal2379, doi:10.1126/science.aal2379 (2017).

2 Psaltis, P. J. *et al.* Resident vascular progenitor cells--diverse origins, phenotype, and function. *J Cardiovasc Transl Res* **4**, 161-176, doi:10.1007/s12265-010-9248-9 (2011).

3 Aird, W. C. Phenotypic heterogeneity of the endothelium: I. Structure, function, and mechanisms. *Circ Res* **100**, 158-173, doi:10.1161/01.RES.0000255691.76142.4a (2007).

4 Carmeliet, P. & Jain, R. K. Molecular mechanisms and clinical applications of angiogenesis. *Nature* **473**, 298-307, doi:10.1038/nature10144 (2011).

5 Herbert, S. P. & Stainier, D. Y. Molecular control of endothelial cell behaviour during blood vessel morphogenesis. *Nat Rev* **12**, 551-564, doi:10.1038/nrm3176 (2011).

6 Risau, W. & Flamme, I. Vasculogenesis. *Annu Rev Cell Dev Biol* **11**, 73-91, doi:10.1146/annurev.cb.11.110195.000445 (1995).

7 Deanfield, J. E. *et al.* Endothelial function and dysfunction: testing and clinical relevance. *Circ* **115**, 1285-1295, doi:10.1161/CIRCULATIONAHA.106.652859 (2007).

8 Marescal, O. & Cheeseman, I. M. Cellular Mechanisms and Regulation of Quiescence. *Dev Cell* **55**, 259-271, doi:10.1016/j.devcel.2020.09.029 (2020).

9 Ricard, N. *et al.* The quiescent endothelium: signalling pathways regulating organ-specific endothelial normalcy. *Nat Rev Cardiol* **18**, 565-580, doi:10.1038/s41569-021-00517-4 (2021).

10 Chen, P. Y. *et al.* Endothelial TGF-beta signalling drives vascular inflammation and atherosclerosis. *Nat Metab* **1**, 912-926, doi:10.1038/s42255-019-0102-3 (2019).

11 Lee, S. *et al.* Autocrine VEGF signaling is required for vascular homeostasis. *Cell* **130**, 691-703, doi:10.1016/j.cell.2007.06.054 (2007).

12 Thomas, M. & Augustin, H. G. The role of the Angiopoietins in vascular morphogenesis. *Angiogenesis* **12**, 125-137, doi:10.1007/s10456-009-9147-3 (2009).

13 Augustin, H. G. *et al.* Control of vascular morphogenesis and homeostasis through the angiopoietin-Tie system. *Nat Rev Molecular cell biology* **10**, 165-177, doi:10.1038/nrm2639 (2009).

14 Felcht, M. *et al.* Angiopoietin-2 differentially regulates angiogenesis through TIE2 and integrin signaling. *J Clin Invest* **122**, 1991-2005, doi:10.1172/JCI58832 (2012).

15 Korhonen, E. A. *et al.* Tie1 controls angiopoietin function in vascular remodeling and inflammation. *J Clin Invest* **126**, 3495-3510, doi:10.1172/JCI84923 (2016).

16 Melo, L. G. *et al.* in *Cardiovascular Medicine* (eds James T. Willerson *et al.*) Ch. Chapter 74, 1541-1565 (Springer London, 2007).

17 Yu, H. *et al.* Smooth muscle cell apoptosis promotes vessel remodeling and repair via activation of cell migration, proliferation, and collagen synthesis. *Arterioscler Thromb Vasc Biol* **31**, 2402-2409, doi:10.1161/ATVBAHA.111.235622 (2011).

18 Pober, J. S. & Sessa, W. C. Evolving functions of endothelial cells in inflammation. *Nat Rev Immunology* **7**, 803-815, doi:10.1038/nri2171 (2007).

19 Jansen, F. *et al.* Endothelial- and Immune Cell-Derived Extracellular Vesicles in the Regulation of Cardiovascular Health and Disease. *JACC. Basic to translational science* **2**, 790-807, doi:10.1016/j.jacbts.2017.08.004 (2017).

20 Zhang, Y. *et al.* Secreted monocytic miR-150 enhances targeted endothelial cell migration. *Mol Cell* **39**, 133-144, doi:10.1016/j.molcel.2010.06.010 (2010).

21 Hergenreider, E. *et al.* Atheroprotective communication between endothelial cells and smooth muscle cells through miRNAs. *Nat Cell Biol* **14**, 249-256, doi:10.1038/ncb2441 (2012).

22 Nelson, P. R. *et al.* Platelet-derived growth factor and extracellular matrix proteins provide a synergistic stimulus for human vascular smooth muscle cell migration. *J Vasc Surg* **26**, 104-112, doi:10.1016/s0741-5214(97)70153-8 (1997).

23 Ruiz-Ortega, M. *et al.* TGF-beta signaling in vascular fibrosis. *Cardiovasc Res* **74**, 196-206, doi:10.1016/j.cardiores.2007.02.008 (2007).

24 World Health Organization. Cardiovascular diseases (CVDs). *Retrieved from https://www.who.int/news-room/fact-sheets/detail/cardiovascular-diseases-(cvds)* (2021).

25 World Health Organization. Cancer. *Retrieved from https://www.who.int/news-room/fact-sheets/detail/cancer* (2022).

26 Lugano, R. *et al.* Tumor angiogenesis: causes, consequences, challenges and opportunities. *Cell Mol Life Sci* **77**, 1745-1770, doi:10.1007/s00018-019-03351-7 (2020).

27 Oettgen, P. Regulation of vascular inflammation and remodeling by ETS factors. *Circ Res* **99**, 1159-1166, doi:10.1161/01.RES.0000251056.85990.db (2006).

28 Foulquier, S. & Paulis, L. in *The Protective Arm of the Renin Angiotensin System (RAS)* (eds Thomas Unger *et al.*) 89-95 (Academic Press, 2015).

29 Folkman, J. Tumor angiogenesis: therapeutic implications. *NEJM* **285**, 1182-1186, doi:10.1056/NEJM197111182852108 (1971).

30 Buchler, P. *et al.* Hypoxia-inducible factor 1 regulates vascular endothelial growth factor expression in human pancreatic cancer. *Pancreas* **26**, 56-64, doi:10.1097/00006676-200301000-00010 (2003).

31 Fons, P. *et al.* Tumor vasculature is regulated by FGF/FGFR signaling-mediated angiogenesis and bone marrow-derived cell recruitment: this mechanism is inhibited by SSR128129E, the first allosteric antagonist of FGFRs. *J Cell Physiol* **230**, 43-51, doi:10.1002/jcp.24656 (2015).

32 Lambert, A. W. *et al.* Emerging Biological Principles of Metastasis. *Cell* **168**, 670-691, doi:10.1016/j.cell.2016.11.037 (2017).

33 Rankin, E. B. & Giaccia, A. J. Hypoxic control of metastasis. *Science* **352**, 175-180, doi:10.1126/science.aaf4405 (2016).

34 Lin, C. *et al.* Hypoxia induces HIF-1alpha and VEGF expression in chondrosarcoma cells and chondrocytes. *J Orthop Res* **22**, 1175-1181, doi:10.1016/j.orthres.2004.03.002 (2004).

35 Ruffell, B. & Coussens, L. M. Macrophages and therapeutic resistance in cancer. *Cancer cell* **27**, 462-472, doi:10.1016/j.ccell.2015.02.015 (2015).

36 Sewell-Loftin, M. K. *et al.* Cancer-associated fibroblasts support vascular growth through mechanical force. *Sci Rep* **7**, 12574, doi:10.1038/s41598-017-13006-x (2017).

37 Hu, H. *et al.* The Research Progress of Antiangiogenic Therapy, Immune Therapy and Tumor Microenvironment. *Front Immunol* **13**, 802846, doi:10.3389/fimmu.2022.802846 (2022).

38 Flora, G. D. & Nayak, M. K. A Brief Review of Cardiovascular Diseases, Associated Risk Factors and Current Treatment Regimes. *Curr Pharm Des* **25**, 4063-4084, doi:10.2174/1381612825666190925163827 (2019).

39 Allende-Vigo, M. Z. Pathophysiologic mechanisms linking adipose tissue and cardiometabolic risk. *Endocr Pract* **16**, 692-698, doi:10.4158/EP09340.RA (2010).

40 Carter, A. M. Complement activation: an emerging player in the pathogenesis of cardiovascular disease. *Scientifica* **2012**, 402783, doi:10.6064/2012/402783 (2012).

41 Woywodt, A. *et al.* Circulating endothelial cells: life, death, detachment and repair of the endothelial cell layer. *Nephrol Dial Transplant* **17**, 1728-1730, doi:10.1093/ndt/17.10.1728 (2002).

42 Sun, H. J. *et al.* Endothelial dysfunction and cardiometabolic diseases: Role of long non-coding RNAs. *Life Sci* **167**, 6-11, doi:10.1016/j.lfs.2016.11.005 (2016).

43 Charakida, M. *et al.* Endothelial dysfunction in childhood infection. *Circ* **111**, 1660-1665, doi:10.1161/01.CIR.0000160365.18879.1C (2005).

44 Celermajer, D. S. *et al.* Endothelium-dependent dilation in the systemic arteries of asymptomatic subjects relates to coronary risk factors and their interaction. *J Am Coll Cardiol* **24**, 1468-1474, doi:10.1016/0735-1097(94)90141-4 (1994).

45 Lin, L. & Knowlton, A. A. Innate immunity and cardiomyocytes in ischemic heart disease. *Life Sci* **100**, 1-8, doi:10.1016/j.lfs.2014.01.062 (2014).

46 Sharma, S. *et al.* TLR signalling and association of TLR polymorphism with cardiovascular diseases. *Vascul Pharmacol* **87**, 30-37, doi:10.1016/j.vph.2016.10.008 (2016).

47 Zhang, Y. X. *et al.* Insights into innate immune signalling in controlling cardiac remodelling. *Cardiovasc Res* **113**, 1538-1550, doi:10.1093/cvr/cvx130 (2017).

48 Libby, P. The changing landscape of atherosclerosis. *Nature* **592**, 524-533, doi:10.1038/s41586-021-03392-8 (2021).

49 Frangogiannis, N. G. Cardiac fibrosis: Cell biological mechanisms, molecular pathways and therapeutic opportunities. *Mol Aspects Med* **65**, 70-99, doi:10.1016/j.mam.2018.07.001 (2019).

50 Nikpay, M. *et al.* A comprehensive 1,000 Genomes-based genome-wide association meta-analysis of coronary artery disease. *Nat Genet* **47**, 1121-1130, doi:10.1038/ng.3396 (2015).

51 Howson, J. M. M. *et al.* Fifteen new risk loci for coronary artery disease highlight arterial-wall-specific mechanisms. *Nat Genet* **49**, 1113-1119, doi:10.1038/ng.3874 (2017).

52 Shi, Y. *et al.* Epigenetic regulation in cardiovascular disease: mechanisms and advances in clinical trials. *Signal Transduct Target Ther* **7**, 200, doi:10.1038/s41392-022-01055-2 (2022).

53 Mai, J. *et al.* An evolving new paradigm: endothelial cells--conditional innate immune cells. *J Hematol Oncol* **6**, 61, doi:10.1186/1756-8722-6-61 (2013).

54 McCoy, M. G. *et al.* Endothelial TLR2 promotes proangiogenic immune cell recruitment and tumor angiogenesis. *Sci Signal* **14**, doi:10.1126/scisignal.abc5371 (2021).

55 Salvador, B. *et al.* Modulation of endothelial function by Toll like receptors. *Pharmacol Res* **108**, 46-56, doi:10.1016/j.phrs.2016.03.038 (2016).

56 Teijaro, J. R. *et al.* Endothelial cells are central orchestrators of cytokine amplification during influenza virus infection. *Cell* **146**, 980-991, doi:10.1016/j.cell.2011.08.015 (2011).

57 Baghai, T. C. *et al.* Classical Risk Factors and Inflammatory Biomarkers: One of the Missing Biological Links between Cardiovascular Disease and Major Depressive Disorder. *Int J Mol Sci* **19**, doi:10.3390/ijms19061740 (2018).

58 Pober, J. S. & Cotran, R. S. Cytokines and endothelial cell biology. *Physiol Rev* **70**, 427-451, doi:10.1152/physrev.1990.70.2.427 (1990).

59 Nottebaum, A. F. *et al.* VE-PTP maintains the endothelial barrier via plakoglobin and becomes dissociated from VE-cadherin by leukocytes and by VEGF. *J Exp Med* **205**, 2929-2945, doi:10.1084/jem.20080406 (2008).

60 Broermann, A. *et al.* Dissociation of VE-PTP from VE-cadherin is required for leukocyte extravasation and for VEGF-induced vascular permeability in vivo. *J Exp Med* **208**, 2393-2401, doi:10.1084/jem.20110525 (2011).

61 Ouyang, W. *et al.* Regulation and functions of the IL-10 family of cytokines in inflammation and disease. *Annu Rev Immunol* **29**, 71-109, doi:10.1146/annurev-immunol-031210-101312 (2011).

62 Tedgui, A. & Mallat, Z. Anti-inflammatory mechanisms in the vascular wall. *Circ Res* **88**, 877-887, doi:10.1161/hh0901.090440 (2001).

63 Sun, X. *et al.* Endothelium-mediated contributions to fibrosis. *Semin Cell Dev Biol* **101**, 78-86, doi:10.1016/j.semcdb.2019.10.015 (2020).

64 Yin, Q. *et al.* Pulmonary microvascular endothelial cells from bleomycin-induced rats promote the transformation and collagen synthesis of fibroblasts. *J Cell Physiol* **226**, 2091-2102, doi:10.1002/jcp.22545 (2011).

65 Ellulu, M. S. *et al.* Obesity and inflammation: the linking mechanism and the complications. *Arch Med Sci* **13**, 851-863, doi:10.5114/aoms.2016.58928 (2017).

66 Halberg, N. *et al.* The adipocyte as an endocrine cell. *Endocrinol Metab Clin N Am* **37**, 753-768, x-xi, doi:10.1016/j.ecl.2008.07.002 (2008).

67 Roberts, A. C. & Porter, K. E. Cellular and molecular mechanisms of endothelial dysfunction in diabetes. *Diab Vasc Dis Res* **10**, 472-482, doi:10.1177/1479164113500680 (2013).

68 Caer, C. *et al.* Immune cell-derived cytokines contribute to obesity-related inflammation, fibrogenesis and metabolic deregulation in human adipose tissue. *Sci Rep* **7**, 3000, doi:10.1038/s41598-017-02660-w (2017).

69 Awan, Z. & Genest, J. Inflammation modulation and cardiovascular disease prevention. *EJPC* **22**, 719-733, doi:10.1177/2047487314529350 (2015).

70 Abel, E. D. *et al.* Cardiac remodeling in obesity. *Physiol Rev* **88**, 389-419, doi:10.1152/physrev.00017.2007 (2008).

71 Maffei, M. *et al.* Leptin levels in human and rodent: measurement of plasma leptin and ob RNA in obese and weight-reduced subjects. *Nat Med* **1**, 1155-1161, doi:10.1038/nm1195-1155 (1995).

72 Pischon, T. & Rimm, E. B. Adiponectin: a promising marker for cardiovascular disease. *Clin Chem* **52**, 797-799, doi:10.1373/clinchem.2006.067819 (2006).

73 Lu, J. *et al.* Adipose Tissue-Resident Immune Cells in Obesity and Type 2 Diabetes. *Front Immunol* **10**, 1173, doi:10.3389/fimmu.2019.01173 (2019).

74 Lumeng, C. N. *et al.* Obesity induces a phenotypic switch in adipose tissue macrophage polarization. *J Clin Invest* **117**, 175-184, doi:10.1172/JCI29881 (2007).

75 Hevener, A. L. *et al.* Macrophage PPAR gamma is required for normal skeletal muscle and hepatic insulin sensitivity and full antidiabetic effects of thiazolidinediones. *J Clin Invest* **117**, 1658-1669, doi:10.1172/JCI31561 (2007).

76 Azzu, V. *et al.* Adipose Tissue-Liver Cross Talk in the Control of Whole-Body Metabolism: Implications in Nonalcoholic Fatty Liver Disease. *Gastroenterology* **158**, 1899-1912, doi:10.1053/j.gastro.2019.12.054 (2020).

77 Ghosh, A. *et al.* Role of free fatty acids in endothelial dysfunction. *J Biomed Sci* **24**, 50, doi:10.1186/s12929-017-0357-5 (2017).

78 Kim, F. *et al.* Toll-like receptor-4 mediates vascular inflammation and insulin resistance in diet-induced obesity. *Circ Res* **100**, 1589-1596, doi:10.1161/CIRCRESAHA.106.142851 (2007).

79 Huang, P. L. Endothelial nitric oxide synthase and endothelial dysfunction. *Curr Hypertens Rep* **5**, 473-480, doi:10.1007/s11906-003-0055-4 (2003).

80 Herold, J. & Kalucka, J. Angiogenesis in Adipose Tissue: The Interplay Between Adipose and Endothelial Cells. *Front Physiol* **11**, 624903, doi:10.3389/fphys.2020.624903 (2020).

81 Siddiqi, S. *et al.* Epigenetic remodeling of chromatin architecture: exploring tumor differentiation therapies in mesenchymal stem cells and sarcomas. *Curr Stem Cell Res Ther* **5**, 63-73, doi:10.2174/157488810790442859 (2010).

82 Tahiliani, M. *et al.* Conversion of 5-methylcytosine to 5-hydroxymethylcytosine in mammalian DNA by MLL partner TET1. *Science* **324**, 930-935, doi:10.1126/science.1170116 (2009).

83 Wu, X. & Zhang, Y. TET-mediated active DNA demethylation: mechanism, function and beyond. *Nat Rev Genet* **18**, 517-534, doi:10.1038/nrg.2017.33 (2017).

84 Cheng, Y. *et al.* Targeting epigenetic regulators for cancer therapy: mechanisms and advances in clinical trials. *Signal Transduct Target Ther* **4**, 62, doi:10.1038/s41392-019-0095-0 (2019).

85 Shirodkar, A. V. *et al.* A mechanistic role for DNA methylation in endothelial cell (EC)-enriched gene expression: relationship with DNA replication timing. *Blood* **121**, 3531-3540, doi:10.1182/blood-2013-01-479170 (2013).

86 Chan, Y. *et al.* The cell-specific expression of endothelial nitric-oxide synthase: a role for DNA methylation. *Journal Biol Chem* **279**, 35087-35100, doi:10.1074/jbc.M405063200 (2004).

87 Tran, N. *et al.* Endothelial Nitric Oxide Synthase (eNOS) and the Cardiovascular System: in Physiology and in Disease States. *Am J Biomed Sci Res* **15**, 153-177 (2022).

88 Lindner, D. J. *et al.* Thrombospondin-1 expression in melanoma is blocked by methylation and targeted reversal by 5-Aza-deoxycytidine suppresses angiogenesis. *Matrix Biol* **32**, 123-132, doi:10.1016/j.matbio.2012.11.010 (2013).

89 Lui, E. L. *et al.* DNA hypermethylation of TIMP3 gene in invasive breast ductal carcinoma. *Biomed Pharmacother* **59 Suppl 2**, S363-365, doi:10.1016/s0753-3322(05)80079-4 (2005).

90 Sundrani, D. P. *et al.* Differential placental methylation and expression of VEGF, FLT-1 and KDR genes in human term and preterm preeclampsia. *Clin Epigenetics* **5**, 6, doi:10.1186/1868-7083-5-6 (2013).

91 Yan, M. S. & Marsden, P. A. Epigenetics in the Vascular Endothelium: Looking From a Different Perspective in the Epigenomics Era. *Arterioscler Thromb Vasc Biol* **35**, 2297-2306, doi:10.1161/ATVBAHA.115.305043 (2015).

92 Park, J. *et al.* The role of histone modifications: from neurodevelopment to neurodiseases. *Signal Transduct Target Ther* **7**, 217, doi:10.1038/s41392-022-01078-9 (2022).

93 Bedenbender, K. *et al.* Inflammation-mediated deacetylation of the ribonuclease 1 promoter via histone deacetylase 2 in endothelial cells. *FASEB J* **33**, 9017-9029, doi:10.1096/fj.201900451R (2019).

94 Liu, O. H. *et al.* Hypoxia-Mediated Regulation of Histone Demethylases Affects Angiogenesis-Associated Functions in Endothelial Cells. *Arterioscler Thromb Vasc Biol* **40**, 2665-2677, doi:10.1161/ATVBAHA.120.315214 (2020).

95 Ling, C. & Groop, L. Epigenetics: A Molecular Link Between Environmental Factors and Type 2 Diabetes. *Diabetes* **58**, 2718-2725, doi:10.2337/db09-1003 (2009).

96 Schlereth, K. *et al.* The transcriptomic and epigenetic map of vascular quiescence in the continuous lung endothelium. *Elife* **7**, e34423, doi:10.7554/eLife.34423 (2018).

97 Berezin, A. Epigenetics in heart failure phenotypes. *BBA Clinical* **6**, 31-37, doi:10.1016/j.bbacli.2016.05.005 (2016).

98 Haas, J. *et al.* Alterations in cardiac DNA methylation in human dilated cardiomyopathy. *EMBO molecular medicine* **5**, 413-429, doi:10.1002/emmm.201201553 (2013).

99 Zhang, L. *et al.* in *Epigenetics in Allergy and Autoimmunity* (eds Christopher Chang & Qianjin Lu) 3-55 (Springer Singapore, 2020).

100 Medzhitov, R. & Horng, T. Transcriptional control of the inflammatory response. *Nat Rev. Immunology* **9**, 692-703, doi:10.1038/nri2634 (2009).

101 Sullivan, K. E. *et al.* Epigenetic regulation of tumor necrosis factor alpha. *Mol Cell Biol* **27**, 5147-5160, doi:10.1128/MCB.02429-06 (2007).

102 Kao, Y. H. *et al.* Tumor necrosis factor-alpha decreases sarcoplasmic reticulum Ca2+-ATPase expressions via the promoter methylation in cardiomyocytes. *Crit Care Med* **38**, 217-222, doi:10.1097/CCM.0b013e3181b4a854 (2010).

103 Porowski, D. *et al.* Liver Failure Impairs the Intrahepatic Elimination of Interleukin-6, Tumor Necrosis Factor-Alpha, Hepatocyte Growth Factor, and Transforming Growth Factor-Beta. *BioMed Res Int* **2015**, 934065, doi:10.1155/2015/934065 (2015).

104 Shuto, T. *et al.* Promoter hypomethylation of Toll-like receptor-2 gene is associated with increased proinflammatory response toward bacterial peptidoglycan in cystic fibrosis bronchial epithelial cells. *FASEB J* **20**, 782-784, doi:10.1096/fj.05-4934fje (2006).

105 Villagra, A. *et al.* Histone deacetylases and the immunological network: implications in cancer and inflammation. *Oncogene* **29**, 157-173, doi:10.1038/onc.2009.334 (2010).

106 Barnes, P. J. Targeting the epigenome in the treatment of asthma and chronic obstructive pulmonary disease. *Proc Am Thorac Soc* **6**, 693-696, doi:10.1513/pats.200907-071DP (2009).

107 Gonzalgo, M. L. *et al.* Low frequency of p16/CDKN2A methylation in sporadic melanoma: comparative approaches for methylation analysis of primary tumors. *Cancer Res* **57**, 5336-5347 (1997).

108 Ahuja, N. *et al.* Aging and DNA methylation in colorectal mucosa and cancer. *Cancer Res* **58**, 5489-5494 (1998).

109 Issa, J. P. *et al.* Methylation of the oestrogen receptor CpG island links ageing and neoplasia in human colon. *Nat Genet* **7**, 536-540, doi:10.1038/ng0894-536 (1994).

110 Issa, J. P. *et al.* Methylation of the estrogen receptor CpG island in lung tumors is related to the specific type of carcinogen exposure. *Cancer Res* **56**, 3655-3658 (1996).

111 Esteller, M. *et al.* MLH1 promoter hypermethylation is associated with the microsatellite instability phenotype in sporadic endometrial carcinomas. *Oncogene* **17**, 2413-2417, doi:10.1038/sj.onc.1202178 (1998).

112 Toyota, M. *et al.* Aberrant methylation in gastric cancer associated with the CpG island methylator phenotype. *Cancer Res* **59**, 5438-5442 (1999).

113 Zhang, W. & Xu, J. DNA methyltransferases and their roles in tumorigenesis. *Biomark Res* **5**, 1, doi:10.1186/s40364-017-0081-z (2017).

114 Fuks, F. *et al.* Dnmt3a binds deacetylases and is recruited by a sequence-specific repressor to silence transcription. *EMBO J* **20**, 2536-2544, doi:10.1093/emboj/20.10.2536 (2001).

115 Nilsson, E. *et al.* Altered DNA methylation and differential expression of genes influencing metabolism and inflammation in adipose tissue from subjects with type 2 diabetes. *Diabetes* **63**, 2962-2976, doi:10.2337/db13-1459 (2014).

116 Movassagh, M. *et al.* Distinct epigenomic features in end-stage failing human hearts. *Circ* **124**, 2411-2422, doi:10.1161/CIRCULATIONAHA.111.040071 (2011).

117 Baccarelli, A. & Ghosh, S. Environmental exposures, epigenetics and cardiovascular disease. *Curr Opin Clin Nutr Metab Care* **15**, 323-329, doi:10.1097/MCO.0b013e328354bf5c (2012).

118 Okano, M. *et al.* DNA methyltransferases Dnmt3a and Dnmt3b are essential for de novo methylation and mammalian development. *Cell* **99**, 247-257, doi:10.1016/s0092-8674(00)81656-6 (1999).

119 Okano, M. *et al.* Cloning and characterization of a family of novel mammalian DNA (cytosine-5) methyltransferases. *Nat Genet* **19**, 219-220, doi:10.1038/890 (1998).

120 Gowher, H. & Jeltsch, A. Enzymatic properties of recombinant Dnmt3a DNA methyltransferase from mouse: the enzyme modifies DNA in a non-processive manner and also methylates non-CpG [correction of non-CpA] sites. *J Mol Biol* **309**, 1201-1208, doi:10.1006/jmbi.2001.4710 (2001).

121 Jurkowska, R. Z. *et al.* Structure and function of mammalian DNA methyltransferases. *Chembiochem* **12**, 206-222, doi:10.1002/cbic.201000195 (2011).

122 Ley, T. J. *et al.* DNMT3A mutations in acute myeloid leukemia. *NEJM* **363**, 2424-2433, doi:10.1056/NEJMoa1005143 (2010).

123 Mayle, A. *et al.* Dnmt3a loss predisposes murine hematopoietic stem cells to malignant transformation. *Blood* **125**, 629-638, doi:10.1182/blood-2014-08-594648 (2015).

124 Yamashita, Y. *et al.* Array-based genomic resequencing of human leukemia. *Oncogene* **29**, 3723-3731, doi:10.1038/onc.2010.117 (2010).

125 Walter, M. J. *et al.* Recurrent DNMT3A mutations in patients with myelodysplastic syndromes. *Leukemia* **25**, 1153-1158, doi:10.1038/leu.2011.44 (2011).

126 Huber, A. *et al.* Abstract A008: DNA methyltransferase 3A promotes inflammation-associated gastric cancer growth and presents a therapy target for gastric cancer. *Cancer Res* **82**, A008-A008, doi:10.1158/1538-7445.CancEpi22-A008 %J Cancer Research (2022).

127 Zhou, Y. *et al.* DNMT3A facilitates colorectal cancer progression via regulating DAB2IP mediated MEK/ERK activation. *Biochim Biophys Acta Mol Basis Dis* **1868**, 166353, doi:10.1016/j.bbadis.2022.166353 (2022).

128 Fomchenko, E. I. *et al.* DNMT3A co-mutation in an IDH1-mutant glioblastoma. *Cold Spring Harb Mol Case Stud* **5**, doi:10.1101/mcs.a004119 (2019).

129 Rajavelu, A. *et al.* Chromatin-dependent allosteric regulation of DNMT3A activity by MeCP2. *Nucleic Acids Res* **46**, 9044-9056, doi:10.1093/nar/gky715 (2018).

130 Weinberg, D. N. *et al.* Two competing mechanisms of DNMT3A recruitment regulate the dynamics of de novo DNA methylation at PRC1-targeted CpG islands. *Nat Genet* **53**, 794-800, doi:10.1038/s41588-021-00856-5 (2021).

131 Deplus, R. *et al.* Regulation of DNA methylation patterns by CK2-mediated phosphorylation of Dnmt3a. *Cell Rep* **8**, 743-753, doi:10.1016/j.celrep.2014.06.048 (2014).

132 U. S. National Institutes of Health, N. C. I. Cardiovascular system. *SEER Training Modules* (2023).

133 Rodriguez, E. R. & Tan, C. D. Structure and Anatomy of the Human Pericardium. *Prog Cardiovasc Dis* **59**, 327-340, doi:10.1016/j.pcad.2016.12.010 (2017).

134 Heineke, J. & Molkentin, J. D. Regulation of cardiac hypertrophy by intracellular signalling pathways. *Nat Rev. Molecular cell biology* **7**, 589-600, doi:10.1038/nrm1983 (2006).

135 van Weerd, J. H. & Christoffels, V. M. The formation and function of the cardiac conduction system. *Development* **143**, 197-210, doi:10.1242/dev.124883 (2016).

136 Zhang, H. *et al.* Endocardial Cell Plasticity in Cardiac Development, Diseases and Regeneration. *Circ Res* **122**, 774-789, doi:10.1161/CIRCRESAHA.117.312136 (2018).

137 Ojji, D. *et al.* Circulating biomarkers in the early detection of hypertensive heart disease: usefulness in the developing world. *Cardiovasc Diagn Ther* **10**, 296-304, doi:10.21037/cdt.2019.09.10 (2020).

138 Talman, V. & Kivela, R. Cardiomyocyte-Endothelial Cell Interactions in Cardiac Remodeling and Regeneration. *Front Cardiovasc Med* **5**, 101, doi:10.3389/fcvm.2018.00101 (2018).

139 Severs, N. J. *et al.* Remodelling of gap junctions and connexin expression in diseased myocardium. *Cardiovasc Res* **80**, 9-19, doi:10.1093/cvr/cvn133 (2008).

140 Kaur, N. *et al.* Paracrine signal emanating from stressed cardiomyocytes aggravates inflammatory microenvironment in diabetic cardiomyopathy. *iScience* **25**, 103973, doi:10.1016/j.isci.2022.103973 (2022).

141 Humeres, C. & Frangogiannis, N. G. Fibroblasts in the Infarcted, Remodeling, and Failing Heart. *JACC. Basic Transl Sci* **4**, 449-467, doi:10.1016/j.jacbts.2019.02.006 (2019).

142 Musicante, M. *et al.* Regulation of endothelial nitric oxide synthase in cardiac remodeling. *Int J Cardio* **364**, 96-101, doi:10.1016/j.ijcard.2022.05.013 (2022).

143 Lavine, K. J. *et al.* Distinct macrophage lineages contribute to disparate patterns of cardiac recovery and remodeling in the neonatal and adult heart. *PNAS* **111**, 16029-16034, doi:10.1073/pnas.1406508111 (2014).

144 Ninh, V. K. & Brown, J. H. The contribution of the cardiomyocyte to tissue inflammation in cardiomyopathies. *Curr Opin Physiol* **19**, 129-134, doi:10.1016/j.cophys.2020.10.003 (2021).

145 Farbehi, N. *et al.* Single-cell expression profiling reveals dynamic flux of cardiac stromal, vascular and immune cells in health and injury. *Elife* **8**, e43882, doi:10.7554/eLife.43882 (2019).

146 Kaneda, M. *et al.* Essential role for de novo DNA methyltransferase Dnmt3a in paternal and maternal imprinting. *Nature* **429**, 900-903, doi:10.1038/nature02633 (2004).

147 Sorensen, I. *et al.* DLL1-mediated Notch activation regulates endothelial identity in mouse fetal arteries. *Blood* **113**, 5680-5688, doi:10.1182/blood-2008-08-174508 (2009).

148 Fabbrini, E. *et al.* Obesity and nonalcoholic fatty liver disease: biochemical, metabolic, and clinical implications. *Hepatology* **51**, 679-689, doi:10.1002/hep.23280 (2010).

149 Gillich, A. *et al.* Capillary cell-type specialization in the alveolus. *Nature* **586**, 785-789, doi:10.1038/s41586-020-2822-7 (2020).

150 Ribatti, D. *et al.* Limitations of Anti-Angiogenic Treatment of Tumors. *Transl Oncol* **12**, 981-986, doi:10.1016/j.tranon.2019.04.022 (2019).

151 Zhu, J. *et al.* Targeting PELP1 Attenuates Angiogenesis and Enhances Chemotherapy Efficiency in Colorectal Cancer. *Cancers* **14**, doi:10.3390/cancers14020383 (2022).

152 Ahuja, N. *et al.* Epigenetic Therapeutics: A New Weapon in the War Against Cancer. *Annu Rev Med* **67**, 73-89, doi:10.1146/annurev-med-111314-035900 (2016).

153 Passalidou, E. *et al.* Vascular phenotype in angiogenic and non-angiogenic lung non-small cell carcinomas. *Br J Cancer* **86**, 244-249, doi:10.1038/sj.bjc.6600015 (2002).

154 Pezzella, F. *et al.* Non-small-cell lung carcinoma tumor growth without morphological evidence of neo-angiogenesis. *Am J Pathol* **151**, 1417-1423 (1997).

155 Kuczynski, E. A. *et al.* Co-option of Liver Vessels and Not Sprouting Angiogenesis Drives Acquired Sorafenib Resistance in Hepatocellular Carcinoma. *JNCI* **108**, doi:10.1093/jnci/djw030 (2016).

156 Krishna Priya, S. *et al.* Tumour angiogenesis-Origin of blood vessels. *Int J Cancer* **139**, 729-735, doi:10.1002/ijc.30067 (2016).

157 Maniotis, A. J. *et al.* Vascular channel formation by human melanoma cells in vivo and in vitro: vasculogenic mimicry. *Am J Pathol* **155**, 739-752, doi:10.1016/S0002-9440(10)65173-5 (1999).

158 Folberg, R. *et al.* Vasculogenic mimicry and tumor angiogenesis. *Am J Pathol* **156**, 361-381, doi:10.1016/S0002-9440(10)64739-6 (2000).

159 Wagenblast, E. *et al.* A model of breast cancer heterogeneity reveals vascular mimicry as a driver of metastasis. *Nature* **520**, 358-362, doi:10.1038/nature14403 (2015).

160 Zheng, Y. *et al.* Angiomotin like-1 is a novel component of the N-cadherin complex affecting endothelial/pericyte interaction in normal and tumor angiogenesis. *Sci Rep* **6**, 30622, doi:10.1038/srep30622 (2016).

161 Hu, J. *et al.* Gene expression signature for angiogenic and nonangiogenic non-small-cell lung cancer. *Oncogene* **24**, 1212-1219, doi:10.1038/sj.onc.1208242 (2005).

162 Jeong, H. S. *et al.* Investigation of the Lack of Angiogenesis in the Formation of Lymph Node Metastases. *JNCI* **107**, doi:10.1093/jnci/djv155 (2015).

163 Pezzella, F. & Gatter, K. C. Evidence Showing That Tumors Can Grow Without Angiogenesis and Can Switch Between Angiogenic and Nonangiogenic Phenotypes. *JNCI* **108**, doi:10.1093/jnci/djw032 (2016).

164 Powell-Wiley, T. M. *et al.* Obesity and Cardiovascular Disease: A Scientific Statement From the American Heart Association. *Circulation* **143**, e984-e1010, doi:10.1161/CIR.0000000000000973 (2021).

165 Zeidan, A. *et al.* Essential role of Rho/ROCK-dependent processes and actin dynamics in mediating leptin-induced hypertrophy in rat neonatal ventricular myocytes. *Cardiovasc Res* **72**, 101-111, doi:10.1016/j.cardiores.2006.06.024 (2006).

166 Gabrielli, L. *et al.* Increased rho-kinase activity in hypertensive patients with left ventricular hypertrophy. *Am J Hypertens* **27**, 838-845, doi:10.1093/ajh/hpt234 (2014).

167 Pietrocola, F. & Bravo-San Pedro, J. M. Targeting Autophagy to Counteract Obesity-Associated Oxidative Stress. *Antioxidants* **10**, doi:10.3390/antiox10010102 (2021).

168 Liu, C. F. & Tang, W. H. W. Epigenetics in Cardiac Hypertrophy and Heart Failure. *JACC. Basic Transl Sci* **4**, 976-993, doi:10.1016/j.jacbts.2019.05.011 (2019).

169 Gilsbach, R. *et al.* Distinct epigenetic programs regulate cardiac myocyte development and disease in the human heart in vivo. *Nat Commun* **9**, 391, doi:10.1038/s41467-017-02762-z (2018).

170 Huang, Z. P. *et al.* MicroRNA-22 regulates cardiac hypertrophy and remodeling in response to stress. *Circ Res* **112**, 1234-1243, doi:10.1161/CIRCRESAHA.112.300682 (2013).

171 Koh, W. K. *et al.* DNMT3A Regulates Hematopoietic Stem Cell Function Via DNA Methylation-Independent Functions. *Blood* **138**, 24-24, doi:10.1182/blood-2021-153759 (2021).

172 Vire, E. *et al.* The Polycomb group protein EZH2 directly controls DNA methylation. *Nature* **439**, 871-874, doi:10.1038/nature04431 (2006).

173 Mohammad, H. P. *et al.* Polycomb CBX7 promotes initiation of heritable repression of genes frequently silenced with cancer-specific DNA hypermethylation. *Cancer Res* **69**, 6322-6330, doi:10.1158/0008-5472.CAN-09-0065 (2009).

174 Zhao, Q. *et al.* PRMT5-mediated methylation of histone H4R3 recruits DNMT3A, coupling histone and DNA methylation in gene silencing. *Nat Struct Mol Biol* **16**, 304-311, doi:10.1038/nsmb.1568 (2009).

175 Luxán, G. & Dimmeler, S. The vasculature: a therapeutic target in heart failure? *Cardiovasc Res* **118**, 53-64, doi:10.1093/cvr/cvab047 (2021).

176 Brady, T. M. The Role of Obesity in the Development of Left Ventricular Hypertrophy Among Children and Adolescents. *Curr Hypertens Rep* **18**, 3, doi:10.1007/s11906-015-0608-3 (2016).

177 Gurtl, B. *et al.* Apoptosis and fibrosis are early features of heart failure in an animal model of metabolic cardiomyopathy. *Int J Exp Pathol* **90**, 338-346, doi:10.1111/j.1365-2613.2009.00647.x (2009).

178 Krolevets, M. *et al.* DNA methylation and cardiovascular disease in humans: a systematic review and database of known CpG methylation sites. *Clin Epigenetics* **15**, 56, doi:10.1186/s13148-023-01468-y (2023).

179 Xiao, D. *et al.* Inhibition of DNA methylation reverses norepinephrine-induced cardiac hypertrophy in rats. *Cardiovasc Res* **101**, 373-382, doi:10.1093/cvr/cvt264 (2014).

180 Zhang, P. *et al.* Contribution of DNA methylation in chronic stress-induced cardiac remodeling and arrhythmias in mice. *FASEB J* **33**, 12240-12252, doi:10.1096/fj.201900100R (2019).

181 Horvath, S. *et al.* Aging effects on DNA methylation modules in human brain and blood tissue. *Genome Biol* **13**, R97, doi:10.1186/gb-2012-13-10-r97 (2012).

182 Talens, R. P. *et al.* Epigenetic variation during the adult lifespan: cross-sectional and longitudinal data on monozygotic twin pairs. *Aging cell* **11**, 694-703, doi:10.1111/j.1474-9726.2012.00835.x (2012).

183 Lister, R. *et al.* Global epigenomic reconfiguration during mammalian brain development. *Science* **341**, 1237905, doi:10.1126/science.1237905 (2013).

184 Johansson, A. *et al.* Continuous Aging of the Human DNA Methylome Throughout the Human Lifespan. *PloS one* **8**, e67378, doi:10.1371/journal.pone.0067378 (2013).

185 Florath, I. *et al.* Cross-sectional and longitudinal changes in DNA methylation with age: an epigenome-wide analysis revealing over 60 novel age-associated CpG sites. *Hum Mol Genet* **23**, 1186-1201, doi:10.1093/hmg/ddt531 (2014).

186 Moore, L. D. *et al.* DNA methylation and its basic function. *Neuropsychopharmacology* **38**, 23-38, doi:10.1038/npp.2012.112 (2013).

187 Yilmaz, A. & Grotewold, E. in *Computational Biology of Transcription Factor Binding* (ed Istvan Ladunga) 23-32 (Humana Press, 2010).

188 Spitz, F. & Furlong, E. E. Transcription factors: from enhancer binding to developmental control. *Nat Rev Genet* **13**, 613-626, doi:10.1038/nrg3207 (2012).

189 Livak, K. J. & Schmittgen, T. D. Analysis of relative gene expression data using real-time quantitative PCR and the 2(-Delta Delta C(T)) Method. *Methods* **25**, 402-408, doi:10.1006/meth.2001.1262 (2001).